

**FLUOREN-9-YLIDENE HYDRAZINE
INHIBITORS OF HIV-1 RIBONUCLEASE H**

by

Krystal Marion LaBarge

B.Sc. (Honors) Chemistry, Worcester State College, 2007

Submitted to the Graduate Faculty of

School of Medicine in partial fulfillment

of the requirements for the degree of Masters of Science

University of Pittsburgh

2011

UNIVERSITY OF PITTSBURGH

SCHOOL OF MEDICINE

This thesis was presented

by

Krystal Marion LaBarge

It was defended on

July 07, 2011

and approved by

Michael A. Parniak, Ph.D

Thesis Advisor, Professor

Department of Molecular Genetics and Biochemistry, University of Pittsburgh

Rieko Ishima, Ph.D

Thesis Advisor, Assistant Professor

Department of Structural Biology, University of Pittsburgh

Gorden Rule, Ph.D

Professor

Department of Biological Sciences, Carnegie Mellon University

Pei Tang, Ph.D

Professor

Department of Anesthesiology, University of Pittsburgh

**FLUOREN-9-YLIDENE HYDRAZINE
INHIBITORS OF HIV-1 RIBONUCLEASE H**

Krystal Marion LaBarge, M.Sc.

University of Pittsburgh, 2011

Screening a library of 5,292 hydrazone/hydrazine compounds for inhibition of HIV reverse transcriptase-associated ribonuclease H (RNH) activity identified fluoren-9-ylidene hydrazines as highly active inhibitors. The 33 fluoren-9-ylidene hydrazines in this library were expanded to 118 compounds, 65 (55%) of which showed validated inhibition of RT RNH activity (IC_{50} values $< 10 \mu M$). These inhibitors were mainly monofunctional for RNH activity, since only 25 (21%) also inhibited RT RNA-dependent DNA polymerase activity. The two most potent RNH inhibitors (RNHIs) were compounds **15** and **25**, which inhibited wild type RT-RNH activity with IC_{50} values of $0.34 \pm 0.07 \mu M$ and $0.4 \pm 0.03 \mu M$, respectively. Similar inhibition was noted with two clinically relevant NNRTI resistant mutants, Y181C and K103N/L100V. Biochemical studies showed that these compounds preferentially inhibited non-directed and DNA 3'-end directed RNH cleavages. These compounds also inhibited the activity of the p15-EC RT RNH domain fragment with IC_{50} values of $0.43 \pm 0.04 \mu M$ and $0.032 \pm 0.004 \mu M$, respectively. Furthermore, both compounds had antiviral activity against HIV-1 with EC_{50} values of $10 \pm 3 \mu M$ and $1.4 \pm 0.6 \mu M$ for compounds **15** and **25**, respectively. Order of addition experiments showed that potent inhibition required pre-incubation of the enzyme with the inhibitor; inhibitory

potency substantially decreased if the RNA/DNA substrate was present prior to inhibitor addition. Furthermore, inhibition was competitive with respect to the RNA/DNA substrate, suggesting an active site binding mode. ^1H - ^{15}N HSQC protein NMR studies with the p15-EC RT RNH domain fragment further suggested that the inhibitor binds to the RNH active site. Molecular docking studies with compound **25** were consistent with an active site binding mode in which the hydrazine functionality hydrogen bonds with essential catalytic metal coordinating residues E52 (RT: 478) and D72 (RT: 498). A sulfonamido-phenyl ring substituent on compound **25** makes edge on- π interactions with H127 (RT: 539), another residue essential for RNH catalysis. We therefore propose that the fluoren-9-ylidene hydrazine RNHIs act by preventing access of RNH essential catalytic residues to the RNA/DNA substrate.

TABLE OF CONTENTS

ACKNOWLEDGEMENTS	xi
CHAPTER 1: INTRODUCTION.....	1
1.1 Human Immunodeficiency virus.....	1
1.1.1 Brief overview of HIV-1 infectivity and the composition of its genome.....	1
1.2 HIV-1 Reverse Transcriptase	2
1.2.1 Significance of HIV-1 RT polymerase and RNH activities in viral replication.....	2
1.2.2 Structure of HIV-1 RT.....	4
1.3 HIV-1 Reverse Transcriptase Ribonuclease H Domain.....	6
1.3.1 Structure of HIV-1 RT-RNH domain.....	6
1.3.2 Hydrolysis by RT-RNH.....	7
1.3.3 Modes of RT-RNH cleavages.....	9
1.4 Current Progress in HIV-1 RT-RNH Inhibitors.....	10
1.4.1 RNHIs with an undefined binding site.....	11
1.4.1.1 Illimaquinone.....	11
1.4.1.2 Naphthalenesulfonic Acids.....	14
1.4.1.3 4-chlorophenylhydrazone of mesoxalic acid (CPHM).....	15
1.4.1.4 <i>N</i> -Hydroxymides and <i>N</i> -hydroxyisoquinolines.....	16
1.4.1.5 Diketo Acids (DKA).....	18
1.4.1.6 Vinylogous Ureas.....	21
1.4.1.7 5-nitro-furan-2-carboxylic carbamoylmethyl ester (NACME).....	23
1.4.1.8 Alizarines.....	25
1.4.2 RNHIs with a Known binding site.....	26
1.4.2.1 Tropolones.....	26
1.4.2.2 Pyrimidinol Carboxylic Acids.....	28
1.4.2.3 <i>N</i> -hydroxy naphthyridinones.....	29
1.4.2.4 <i>N</i> -Acylhydrazones.....	32
1.4.3 Summary.....	38
1.5 Rational and statement of hypothesis.....	40

**CHAPTER 2: IDENTIFICATION AND CHARACTERIZATION OF THE
FLUOREN-9-YILDENE HYDRAZINE PHARMACOPHORE.....41**

2.1	ABSTRACT.....	41
2.2	INTRODUCTION.....	44
2.3	MATERIALS AND METHODS.....	45
2.3.1	Reagents.....	45
2.3.2	Protein expression and purification.....	46
2.3.2.1	Expression and purification of HIV-1 RT.....	46
2.3.2.2	Expression and purification of the p15-EC RT RNH domain fragment.....	46
2.3.3	RT polymerase enzyme assay.....	46
2.3.4	High-throughput screening substrates for RNH activity.....	47
2.3.5	RNH FRET high-throughput enzyme assay.....	48
2.3.6	Gel based dual labeled RNH cleavage assay.....	50
2.3.7	RNH order of addition studies.....	51
2.3.8	HIV-1 antiviral studies.....	52
2.4	RESULTS.....	54
2.4.1	Initial identification and expansion of the fluorene-9-yildene hydrazine library.....	54
2.4.2	Characterization of the expanded fluorene-9-yildene hydrazine library for RNH inhibition with HIV-1 wild type RT.....	55
2.4.3	Four structural subgroups of the Fluoren-9-yildene hydrazine library.....	57
2.4.4	Structural moieties significant for RT-RNH inhibition.....	61
2.4.5	Fluorene-9-yildene hydrazine library RNH inhibition of the p15-EC RNH domain fragment.....	63
2.4.6	Fluoren-9-yildene hydrazine compounds preferentially inhibit non-directed and DNA 3'-end directed modes of RNH cleavages.....	66
2.4.7	Fluoren-9-yildene hydrazine type of RNH inhibition is competitive with respect to the RNA/DNA substrate.....	69
2.4.8	Fluoren-9-yildene hydrazine activity against NNRTI resistant mutants.....	73
2.4.9	Fluoren-9-yildene hydrazine HIV-1 antiviral activity.....	74
2.5	DISCUSSION.....	76

**CHAPTER 3: POTENTIAL BINDING SITE OF THE FLUOREN-9-YILDENE
HYDRAZINE COMPOUNDS WITH the p15-EC RT RNH
DOMAIN FRAGMENT.....79**

3.1	ABSTRACT.....	79
3.2	INTRODUCTION.....	80
3.3	MATERIALS AND METHODS.....	81
3.3.1	Reagents.....	81

3.3.2	Isotropic labeling of the p15-EC RT RNH domain fragment	81
3.3.3	Solution NMR ^1H - ^{15}N HSQC.....	82
3.3.4	Molecular docking with Schrödinger suit software.....	83
3.4	RESULTS.....	85
3.4.1	Influence of DMSO on the ^1H - ^{15}N HSQC spectrum of p15-EC.....	85
3.4.2	Influence of compound 25 on the ^1H - ^{15}N HSQC spectrum of p15-EC.....	86
3.4.3	Influence of compound 117 on the ^1H - ^{15}N HSQC spectrum of p15-EC.....	90
3.4.4	Molecular docking of compound 25 with the p15-EC RT RNH domain fragment.....	91
3.5	DISCUSSION.....	95
 CHAPTER 4: SUMMARY AND CONCLUSIONS.....		98
4.1	Major Findings and Conclusions.....	98
4.1.1	Chapter 2: Identification and characterization of the fluoren-9-ylidene hydrazine pharmacophore.....	98
4.1.2	Chapter 3: Potential Binding site of the fluoren-9-ylidene hydrazine compounds with the p15-EC RT RNH domain fragment.....	99
4.2	Significance and Future Studies.....	100
 APPENDIX A: SUPPLEMENTARY TABLE 1.....		101
 APPENDIX B: SUPPLEMENTARY FIGURES.....		119
<i>Supplementary Figure 1:</i> Overlay of ^1H - ^{15}N HSQC of p15-EC RT RNH domain fragment with compound 117 and DMSO spectra.....		119
<i>Supplementary Figure 2:</i> Overlay of ^1H - ^{15}N HSQC of p15-EC RT RNH domain fragment with compound 25 and DMSO spectra.....		120
APPENDIX C: ABBREVIATIONS.....		121
 BIBLIOGRAPHY.....		123

LIST OF TABLES

Table 1. List of Natural Products HIV-1 RT RNHIs.....	13
Table 2. Nucleic acid substrates for RNH FRET high-throughput enzyme assay.....	47
Table 3. Nucleic Acid Substrates for the Gel Based Dual Labeled RNH Assay.....	50
Table 4. Most active RNHIs from each subgroup.....	56
Table 5. Subgroups of Fluoren-9-ylidene hydrazine library.....	58
Table 6. 9 <i>H</i> -(fluoren-9-ylidene)-2-hydropranolcarbonylhydrazines compounds.....	61
Table 7. Subgroup RNH inhibition with the p15-EC RT RNH domain fragment.....	65
Table 8. Fluoren-9-ylidene hydrazine inhibition with different HTS substrates.....	66
Table 9. Inhibition of NNRTI resistant mutants.....	73
Table 10. HIV-1 antiviral activity of select fluoren-9-ylidene hydrazine compounds.....	74

LIST OF FIGURES

Figure 1. HIV-1 (+) RNA genome.....	1
Figure 2. HIV-1 reverse transcription.....	3
Figure 3. Structure of HIV-1 RT.....	5
Figure 4. Structure of HIV-1 RT-RNH domain.....	6
Figure 5. Mechanism of HIV-1 RT-RNH hydrolysis.....	8
Figure 6. Modes of RT-RNH cleavages.....	9
Figure 7. Structure of natural product RNHI, illimaquinone.....	11
Figure 8. Structures of naphthalenesulfonic acid RNHIs.....	14
Figure 9. Structure of CPHM.....	15
Figure 10. Structures of <i>N</i> -Hydroxymide and <i>N</i> -hydroxyisoquinolines RNHIs.....	16
Figure 11. Structures of DKA RNHIs.....	18
Figure 12. Structures of vinylogous urea RNHIs.....	21
Figure 13. Structures of NACME RNHIs.....	23
Figure 14. Structures of Alizarines RNHIs.....	25
Figure 15. Structures of tropolones RNHIs.....	26
Figure 16. Structures of pyrimidinol carboxylic acid RNHIs.....	28
Figure 17. Structure of <i>N</i> -hydroxy naphthyridinone RNHIs.....	29
Figure 18. Structure of <i>N</i> -acylhydrazone RNHIs.....	32
Figure 19. Fluoren-9-ylidene hydrazine pharmacophore.....	54

Figure 20. Correlation between RT-RNH and pol inhibition.....	55
Figure 21. RT-RNH and polymerase inhibition per subgroup.....	57
Figure 22. RNH inhibition of the p15-EC RT RNH domain fragment.....	65
Figure 23. Correlation between RT-RNH inhibition with non-directed and DNA 3'-end directed cleavage substrates.....	66
Figure 24. RT-RNH inhibition of DNA 3'-end and RNA 5'-end directed RNH cleavages.....	68
Figure 25. Dixon plot of compound 25 with non-directed cleavage substrate.....	69
Figure 26. Order of addition influence on RNH inhibition with full length RT and the p15-EC RT RNH domain fragment using the high-throughput FRET RNH enzyme assay.....	70
Figure 27. Order of addition influence on RT-RNH inhibition with full length RT using the gel based dual labeled RNH assay.....	72
Figure 28. Amid backbone chemical shift perturbations of the p15-EC RT RNH domain fragment induced by DMSO	85
Figure 29. Amide backbone chemical shift perturbations of p15-EC induced by compound 25	88
Figure 30. Amide backbone peak intensity changes of p15-EC induced by compound 25	89
Figure 31. Amid backbone chemical shift perturbations of p15-EC induced by compound 117	90
Figure 32. 3D representation of the molecular docking with compound 25 and p15-EC.....	91
Figure 33. 2D representation of the molecular docking with compound 25 and p15-EC.....	92

ACKNOWLEDGEMENTS

First and foremost, I would like to convey a message of complete gratitude to both of my mentors, Dr. Micheal A. Parniak and Dr. Rieko Ishima for their continuous guidance and support over the past few years, the intellectual growth I have gained would have not been possible without either one of them. I would also like to thank Dr. Lena G. Miller, Eva Nagy, Dr. Lakshmi Menon and Dr. Nataliya Sergeevna Myshakina for their assistance with various parts of my research. Lastly, I would like to extend a special thank you to both of my dear friends, Dr. Tatiana Ilina and Wazo Myint for always providing me with unconditional encouragement and guidance over the past years, without either of them, many of my accomplishments would have not been possible.

CHAPTER 1: INTRODUCTION

1.1 HUMAN IMMUNODEFICIENCY VIRUS

1.1.1 Brief Overview of HIV Infectivity and the Composition of its Genome

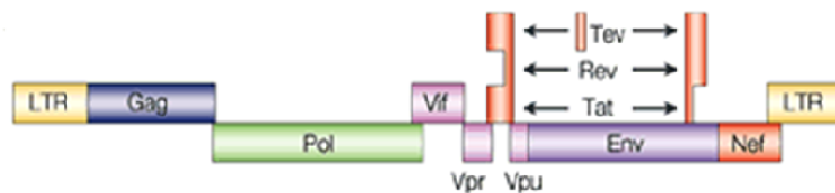


Figure 1. HIV-1 (+) RNA Genome. The *gag* and *env* genes encode for the structural and envelope proteins, while the *pol* gene encodes the viral enzymes RT, IN and PR. The remaining six genes (*vif*, *vpr*, *tev*, *rev*, *tat*, *nef*) encode for the accessory proteins, while the long terminal repeats (LTR) are essential for viral replication and integration. Figure was adapted from wikipedia.

Human immunodeficiency virus (HIV) is a lentivirus, a member of the Retroviridae family. HIV infection is a worldwide pandemic that affects approximately 33 million people (98) and is the causative agent for acquired immunodeficiency syndrome (AIDS). HIV primarily infects vital cells in the human immune system such as helper T-cells (to be specific, CD4 T-cells), macrophages, and dendritic cells. HIV infection leads to low levels of CD4 T-cells through three main mechanisms: first, direct viral killing of infected cells; second, increased rates of apoptosis

in infected cells; and third, killing of infected CD4 T-cells by CD8 cytotoxic lymphocytes that recognize infected cells. When CD4 T-cell numbers decline below a critical level, cell-mediated immunity is lost, and the body becomes progressively more susceptible to opportunistic infections. HIV has an (+) RNA genome (*Figure 1*), that consists of nine genes (*gag*, *pol*, *env*, *tat*, *rev*, *nef*, *vif*, *vpr* and *vpu*) encoding 19 proteins. The six genes *tat*, *rev*, *nef*, *vif*, *vpr*, and *vpu* (or *vpx* in the case of HIV-2), are regulatory genes for proteins that control the ability of HIV to infect cells, produce new copies of virus (replicate), or cause disease. The *gag* gene encodes the viral structural proteins, while the *env* gene encodes for the envelope proteins essential for cellular attachment and entry. Lastly the *pol* gene, encodes for essential enzymes, including reverse transcription (RT), integrase (IN) and protease (PR) that are responsible for viral transcription, integration and cleavage, respectively.

1.2 HIV-1 Reverse Transcriptase

1.2.1 Significance of HIV-1 RT Polymerase and RNH Activities in Viral Replication

HIV-1 reverse transcriptase is an essential multifunctional enzyme of HIV-1 replication. RT has both RNA and DNA dependent polymerase activity, along with an essential ribonuclease H (RNH) activity. All three functions associated with RT are equivalently indispensable for viral replication; since the RT enzyme is required to reverse transcribe the viral (+) RNA genome into a double stranded DNA (dsDNA) genome. Upon absorption of the virus by the host cell and release of two (+) RNA viral genomes into the host cytoplasm, the activities of HIV-1 RT are

initiated from a host tRNA^{lys3} that is annealed to the primer binding site (PBS) of the (+) RNA genome and catalyzed by the RNA dependent polymerase (RDDP) activity of RT. The RDDP activity of RT transcribes the (+) RNA genome to synthesize the complementary (-) DNA strand, which undergoes strand transfer of the terminal repeat regions to the same or another co-packaged viral (+) RNA strand. This strand transfer process requires RT-RNH activity to degrade the (+) RNA component complementary to the newly synthesized (-) strong stop DNA. RT DNA dependent DNA polymerase (DDDP) activity then forms the complimentary (+) DNA strand to complete synthesis of the viral duplex DNA (*Figure 2*).

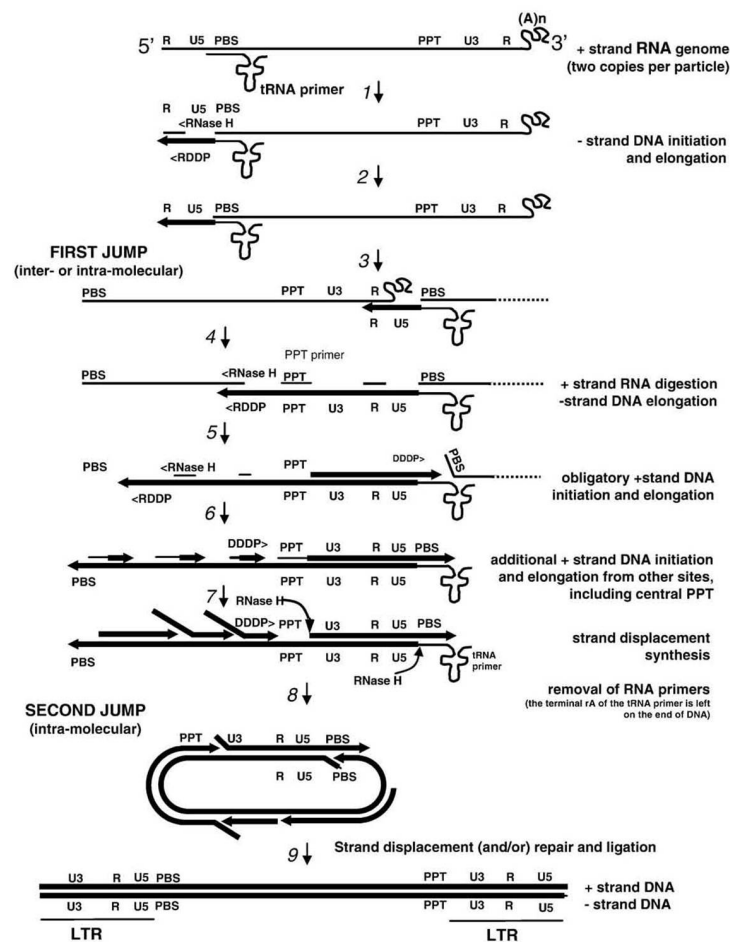


Figure 2. HIV-1 Reverse Transcription. Figure acquired from Sarafianos, S.G. et al. 2009 (76).

1.2.2 Structure of HIV-1 RT

HIV-1 RT is a heterodimer composed of both a 51 kDa (p51) and 66 kDa (p66) subunits that have identical primary sequence and secondary components, but differ in tertiary orientation (*Figure 3*). The p51 subunit is formed by proteolytic removal of the 15 kDa RNH domain during viral maturation. The cleavage occurs between residues F440/Y441 (13, 23, 46, 96), thereby creating the catalytically active p51/p66 heterodimer of RT (73) that is optimal for viral replication (1). The intact p66 subunit contains both the polymerase and RNH active sites, spatially separated by about 40 Å, corresponding to a distance of approximately 17 nucleotides on a DNA/DNA substrate (48, 49) or 18 nucleotides apart with an RNA/DNA substrate (75). The polymerase domain of the p66 subunit of RT can be broken down into four subdomains containing the fingers (residues 1-85 and 118-155), palm (residues 86-117 and 156-236), thumb (residues 237-318) and connection (residues 319-426) subdomains (76), with a tertiary structure similar to a right hand. The polymerase active site is located within the palm subdomain between the thumb and finger subdomains, with catalytic residues D110, D185 and D186 (*Figure 3*). The p51 subunit, without any catalytically active sites, contains identical subdomains as seen with the p66's polymerase domain, where the thumb subdomain of p51 is oriented in such a manner that it makes direct contact with the base of p66's RNH domain, near the RNH active site. The connection domain of the p66 subunit is responsible for linking both the RNH and polymerase domains and has significant contacts with the substrate's DNA strand (75). Furthermore, mutational studies has indicated residue H361 of the connection subdomain to be highly significant for *in vitro* RNH activity and during *in vivo* experiments causes a depletion in viral titers, indicating the significance of the connection subdomain for RNH activity (52). Even though the p51 subunit is catalytically inactive, it does act as a structural scaffold for the p66

subunit during both polymerization and RNH catalysis (2), while maintaining significant contact with the substrate. The significance of the p51 subunit is further supported by the fact that the isolated RNH domain is catalytically inactive. The activity of the isolated domain can be restored by introducing the p51 subunit or adding various *N*-terminal fusions to the RNH domain that take on the substrate interacting roles of the p51 subunit, including an extended *C*-helix loop found with *E. coli* RNH (p15-EC) (22, 47, 54, 85, 86, 87, 88, 89).

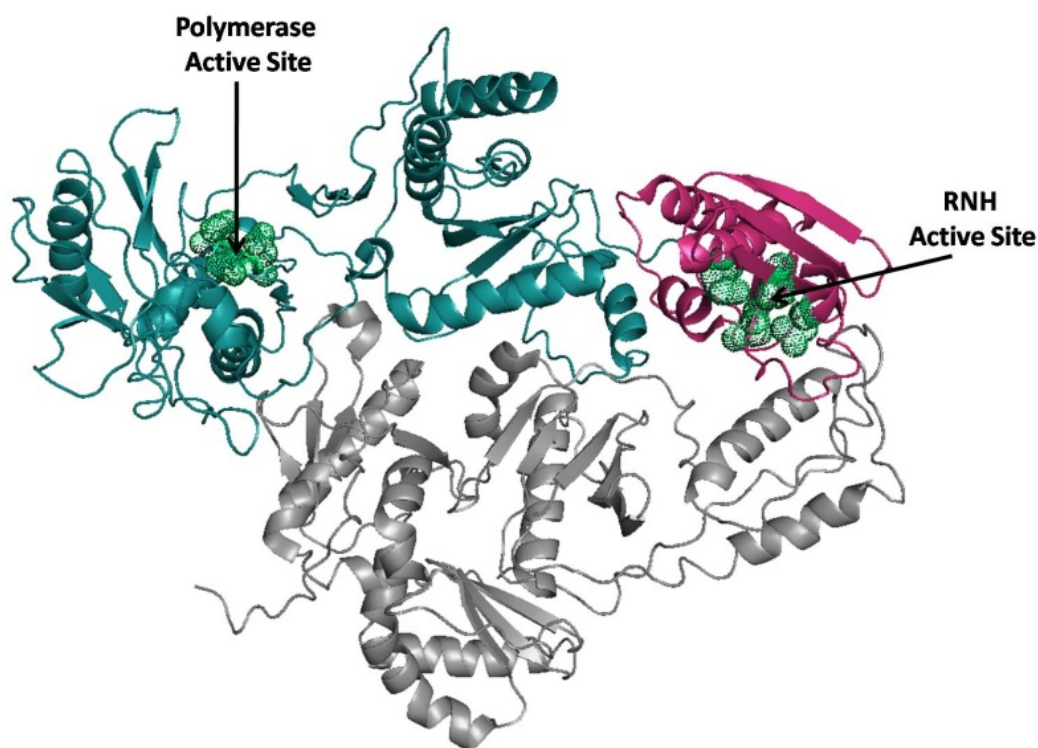


Figure 3. Structure of HIV-1 RT. The p66 subunit is denoted in teal with the c-terminal RNH domain denoted in pink, while green dotted spheres represent both the polymerase and RNH active site residues. Light gray indicates the p51 subunit. HIV-1 RT structure was obtained from PDB file 2I5J (43) and rendered using Pymol software (DeLano Scientific LLC, San Carlos, California).

1.3 HIV-1 REVERSE TRANSCRIPTASE RIBONUCLEASE H DOMAIN

1.3.1 Structure of HIV-1 RT-RNH Domain

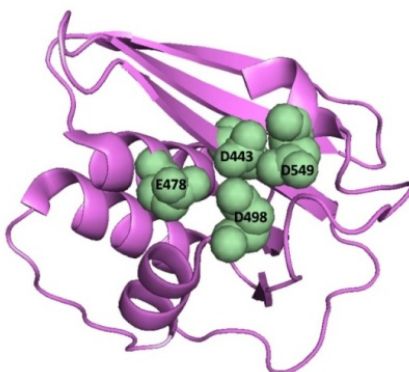


Figure 4. Structure of HIV-1 RT-RNH Domain. The RNH domain is depicted in violet and green spheres represent the active site residues D443, E478, D98 and D549. The HIV-1 RT-RNH domain structure is rendered using pymol software (DeLano Scientific LLC, San Carlos, California) with the PBD file 2I5J (43).

Numerous X-ray crystal structures of RT-RNH have been solved either as the isolated domain or as the intact RT molecule (16, 48, 58). Co-crystal structures have also been determined with the RT and its DNA/DNA (4, 49) or RNA/DNA (75) substrates. The RNH domain (*Figure 4*) contains p66 subunit C-terminal residues 427-560 and has a fold similar to *E. coli* RNH. HIV-1 RNH is an α - β protein, folded into a five-stranded mixed β -sheet with four flanking asymmetric α -helices. The RNH active site resides within a defined pocket containing four conserved catalytic acidic residues (D443, E478, D498 and D549) coordinate to two metal cations (16). Co-crystal structure of HIV-1 RT with an RNA/DNA hybrid substrate demonstrates that the RNH domain binds the minor groove of the nucleic acid and has direct interaction with both the RNA and DNA strands. A region adjacent to the RNH active site, the RNH primer grip is

responsible for interacting with the DNA primer strand at the complementary base paired RNA nucleotides, at positions -4 and -9, relative to the scissile phosphate. RNH protein substrate contacts are made with residues K395 and E396 (p51 subunit), G359, A360, and H361 (p66 subunit), along with residues T473, N474, Q475, K476, Y501 and I505 (RNH domain of p66) (75). The RNH primer grip is essential for proper binding and positioning of the substrate, extending from both the polymerase and RNH active sites and has been shown to have an influence on both DNA polymerization and RNH catalysis through point mutational studies (3, 51, 52, 66, 72, 104). RNH primer grip residues Y501 and Q475 are highly significant for RNH activity. Residue Y501 has direct contact with the DNA phosphate backbone (66, 75) and has a substantial influence on the efficiency and specificity of RNH cleavages, where any substitutions at this position either completely abrogates RNH activity or substantially reduces it (3, 66, 72). Residue Q475 has direct contact with the DNA deoxyribose rings (75) and mutational studies have also shown this residue to be significant for RNH cleavage specificity (72).

1.3.2 Hydrolysis by RT-RNH

HIV-1 RT-RNH is an endonuclease that hydrolyzes the RNA strand of an RNA/DNA hybrid duplex, thereby generating RNA fragments with 5'-phosphate and 3'-hydroxyl ends (12, 19, 59). The mechanism of HIV-1 RT-RNH hydrolysis has been described as a two metal cleavage event (*Figure 5*) (16, 48, 61), where the metal ions have been shown to be essential for RNH activity (14). The first metal ion A is responsible for activating a nucleophilic water molecule hydroxyl ion (-OH) and along with the second metal ion B helps stabilizing the transition state intermediate. Metal ion B has further been associated with lowering the activation energy barrier

of the transition state by destabilizing the enzyme-substrate ground state through its direct interaction with the leaving group from RNH hydrolysis (103). The four catalytic residues coordinate both metal ions, where metal ion A hydrogen bonds with carboxyl oxygens of D443 and D549, along with the carboxyl oxygen of D498 through a water molecule intermediate, while metal ion B hydrogen bonds with the carboxyl oxygens of D443, D498 and E478. The mechanism of RNH hydrolysis begins with metal ion A activating a nucleophilic water molecule with the assistance of residue H539. This causes the hydroxyl ion (OH^-) of the water molecule to attack, by an $\text{S}_\text{N}2$ reaction, the 5'-scissile phosphate of the RNA backbone. While both metal ions A and B stabilize the transition state, whereas metal ion B also interacts with the leaving group from hydrolysis, therefore destabilizing the enzyme-substrate ground state and lowering the activation energy barrier of the transition state. The phosphorus then attacks the distal oxygen, relative to the 5'-oxygen of the phosphate intermediate causing cleavage of the phosphodiester bond, leaving behind a free 5'-phosphate and 3'-hydroxyl ends.

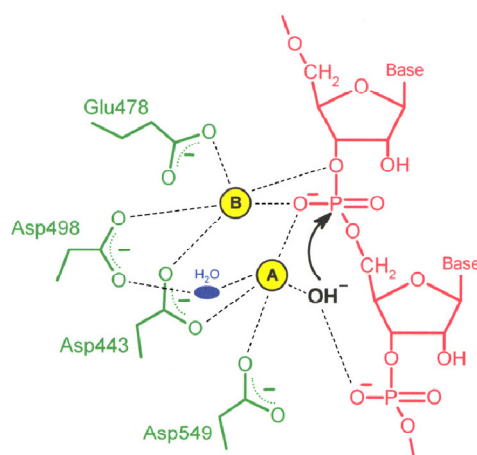


Figure 5. Mechanism of HIV-1 RT-RNH Hydrolysis. The RNH active site residues (D443, E478, D98 and 549) are indicated in green, metal cations are indicated by yellow spears and the RNA strand of the RNA/DNA substrate is depicted in pink. Acquired from Schultz, J. et al. 2008 (82).

1.3.3 Modes of RT-RNH Cleavages

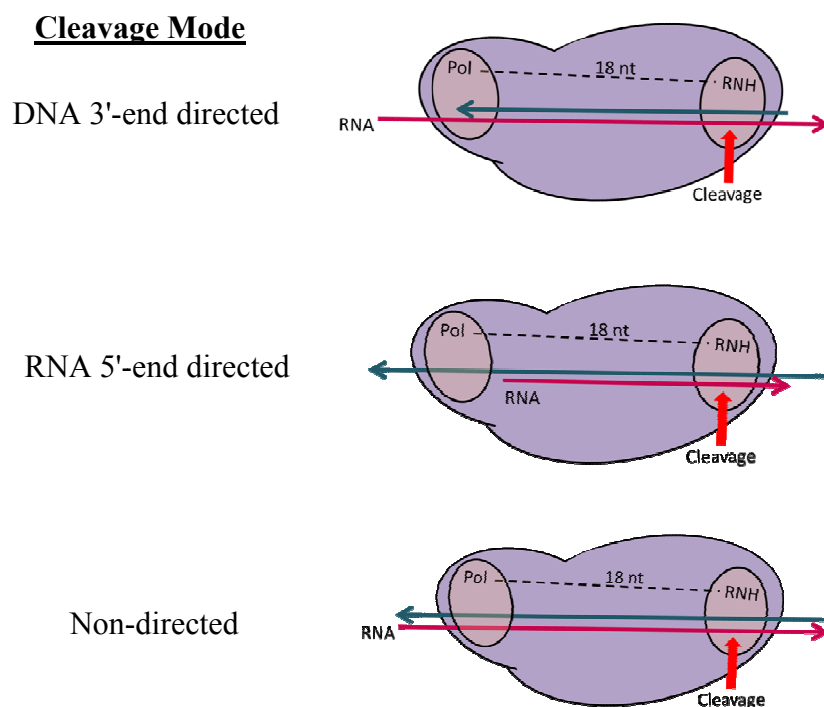


Figure 6. Modes of RT-RNH Cleavages. Heterodimer of HIV-1 RT is represented by purple spears and the RNH and pol active sites are highlighted by pink spears, while the RNA/DNA substrate is represented by extended arrows. A pink arrow represents the RNA strand and a teal arrow represents the DNA strand. Adapted from Schultz, J. et al. 2008 (82).

There are three distinct modes of HIV-1 RT-RNH cleavages (*Figure 6*) that are based on the interactions between RT and its substrate. These modes are DNA 3'-end directed cleavages, RNA 5'-end directed cleavages and non-directed cleavages. DNA 3'-end directed cleavages occur when the polymerase domain preferentially associates with a recessed 3'-end of the DNA strand, causing the RNH domain to be oriented and cleave the RNA strand at the 15-20th nucleotide positions from the 3'-DNA recessed end (21, 30, 36, 53). This mode of RNA cleavage occurs during active RNA dependent DNA polymerization and during the absence of

polymerization, such as during pausing events (91, 92). The polymerase domain can also preferentially bind a 5'-recessed end of the RNA strand, resulting in RNA 5'-end directed cleavages. During this mode of RNH cleavages the RNH domain will bind and cleave the RNA strand at the 13-19th nucleotide position, relative to the 5'-RNA end (20, 33, 34, 36, 37, 71, 77, 101). This mode of RNH cleavage represents a polymerase independent form of RNH cleavage and is dependent on the distance of the recessed end (20) and the nucleotide sequence near the cleavage site as seen with DNA 3'-end directed mode of cleavages (20, 30, 31, 81). Furthermore the RNA 5'-end directed mode is also dependent on the accessibility of the recessed end, whereas this is not seen with the DNA 3'-end directed RNH cleavage mode (80, 81). The third mode of RT-RNH cleavages, non-directed cleavages, results in cleavages internally on the RNA/DNA substrate (25, 28, 78, 79, 80). This mode of cleavage has been shown to depend on the substrate sequence (80). The non-directed mode of cleavage is independent of RT polymerase activity as it does not require recessed DNA 3'-end or RNA 5'-end recessing (25, 28, 78, 79, 80) as seen with the other two modes.

1.4 CURRENT PROGRESS IN HIV-1 RT-RNH INHIBITORS

The critical role of RT in HIV-1 replication makes this enzyme an appealing target for HIV-1 antiretroviral development. In fact most of the current clinically approved therapeutics of HIV-1 are antivirals that target RT but only the DNA polymerase activity of the enzyme (98). These antivirals are plagued with inevitable drug resistance due to the virus' high mutation rate and the fact that treatment is lifelong. Therefore, there is a necessity for new antivirals that remain active towards current resistant variants of the virus. HIV RT-RNH is essential for HIV replication

(95), yet no therapeutics target RT-RNH activity. Such therapeutics would certainly remain active against current HIV resistant. However, some progress has been made in the identification of small molecules that inhibit the RNH activity of HIV-1 RT, including natural products and synthetic compounds. Binding sites for a few of these inhibitors has been determined.

1.4.1 RNHIs with an Undefined Binding Site

1.4.1.1 Illimaquinone

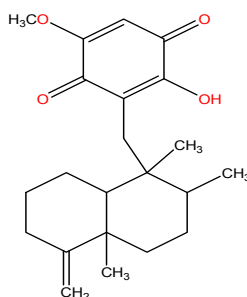


Figure 7. Structure of Natural Product RNHI, Illimaquinone

The first HIV-1 RNHI identified was in 1990, with the natural marine substance, *illimaquinone* (Figure 7) (62). *Illimaquinone* is a secondary metabolite isolated from the red sea sponge *Smenospongia SP* and that has an HIV-1 RT-RNH IC_{50} within the 15-50 μM range (62, 67) and to a lesser extent inhibits RT-polymerase activity with an IC_{50} of approximately 140 μM . Combination studies with *N*-ethylmaleimide (NEM, a thiol reactive agent that has been

shown to modify residue C280 of HIV-1 RT (64)) showed the two compounds to be mutually exclusive and antagonistic, further subunit independent C280S mutational studies indicates that binding occurs specific with the p66 subunit C280 residue, since inhibition with *illimaquinone* was only affected with the p66 C280S mutant. This suggests that *illimaquinone* acts as an allosteric inhibitor of HIV-1 RT-RNH activity by binding with the p66 thumb subdomain near or at residue C280 (63). Though *illimaquinone* is not a potent inhibitor of HIV-1 RT-RNH activity, it was the first RNHI to be identified and showed that specific inhibition of RT-RNH activity is possible. These discoveries lead to the identification of a cascade of small molecule inhibitors, from natural products to specifically synthesized small molecules, as inhibitors of HIV-1 RT-RNH activity with and without a defined binding site. A few other natural products have been identified as RNHIs, these compounds tend to lack specificity for targeting RT-RNH but nonetheless they have been shown to inhibit the RNH function of RT, as seen in *Table 1*.

Table 1: List of Natural Products HIV-1 RT RNHIs

Active Compound	Source	RT-RNH IC ₅₀ (μM)	RT-Pol IC ₅₀ (μM)	HIV-1 EC ₅₀ (μM)	Reference
Illimaquinone	<i>Smenospongia Sp</i> (red sea sponge)	15-50	140	n.d. [¶]	Loya, S. et al. 1990 (62) Loya, S. et al. 1993 (63) Min, B.S. et al. 2000 (67)
HP 0.35	<i>Cephalosporin ceftazidion</i> (Bacterialactum antibiotic)	<50*	>200*	n.d. [¶]	Hafkemeyer, P. et al. 1991 (39)
Argentine Plant Extracts 2I ₄ 4I ₄	<i>Achyrocline flaccida</i> <i>Phyllanthus sellowianus</i>	3.9±0.9* 2.4±0.8*	1.0±0.1* 5.9±1.4*	0.25* 3.0*	Hnatyszyn, O. et al. 1999 (45)
Compound 14	Juglans Manshurica	39	0.04	n.d. [¶]	Min, B.S. et al. 2000 (67)
Ardimerin digallate	Ardisia japonica	1.5	>50	n.a. [^]	Tien Da, N. et al. 2007 (94)
1,3,4,5- Tetragalloylapitol	<i>Hylodendron gabunensis</i> (Fabaceae plant)	0.24	n.d. [¶]	>40	Takada, K. et al. 2007 (93)
Phenolic Gylcosides (1) hyemalosite A (3) hyemalosite C	<i>Eugenia hyemalis</i> L. Cambess (evergreen tree)	1.46±0.01 1.19±0.05	n.d. [¶]	>20*	Bokesch, H.R., et al. 2008 (8)
Madurahydroxylactones 3j 4e	<i>Nonomuraea rubra</i> (soil bacterium)	0.69±0.13 0.78±0.12	n.d. [¶]	n.d. [¶]	Marchand, C. et al. 2008 (65)

* units in μg/ml not in μM

[¶] not determined (n.d.)

[^] was evaluated for HIV-1 antiviral activity and had no activity (n.a.)

1.4.1.2 Naphthalenesulfonic Acids

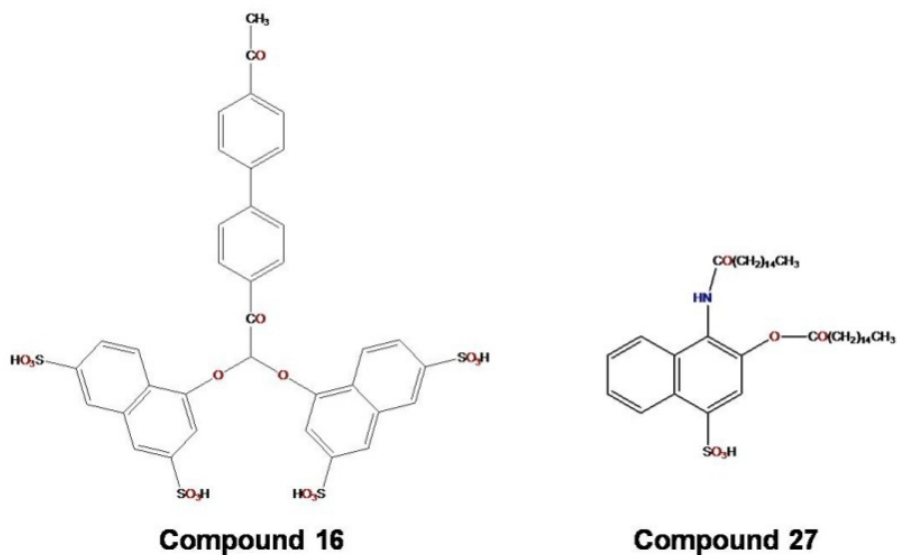


Figure 8. Structures of Naphthalenesulfonic Acid RNHIs

Two naphthalenesulfonic acid compounds (compounds **16** and **27**, *Figure 8*) from a small library of 25 naphthalenesulfonic acid derivatives have been identified as bi-functional inhibitors of HIV-1 RT-RNH and polymerase activity, with a greater potency for RT-polymerase inhibition. Both compounds had an RT-RNH IC_{50} ranging from 15-17 μM with an RT RDDP IC_{50} between 0.7-4 μM and a 7 μM IC_{50} with DDDP activity. These compounds may chelate metal ions based on the presence of the naphthalenesulfonic acid moiety. This observation suggests the inhibitors would have a preference for binding within the polymerase and/or RNH active sites. Though this assumption is plausible, there has been no attempts to prove or exclude metal chelation or identify the potential binding site. These compounds do have antiviral activity against HIV-1 but the antiviral properties are most likely the result of targeting virus attachment and/or absorption

versus RT activity, since the physiochemical properties of this inhibitor class indicates they would be highly charged molecules and unlikely to permeate the cell membrane enabling them to work at the level of HIV-1 reverse transcription (68).

1.4.1.3 4-chlorophenylhydrazone of Mesoxalic Acid (CPHM)

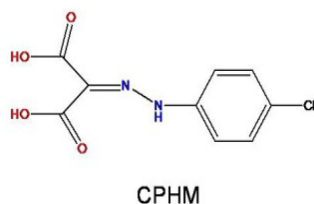


Figure 9. Structure of CPHM

The compound 4-chlorophenylhydrazone of mesoxalic acid (**CPHM** or **PD1226338**, *Figure 9*) was first identified from the screening of a library of 115 compounds for specific HIV-1 RT strand transfer inhibition properties (32). **CPHM** inhibited HIV-1 RT strand transfer with an IC_{50} of 4.5 μ M. Additional analysis of **CPHM's** ability to directly inhibit RT-RNH activity using a gel based RNH cleavage assay resulted in an IC_{50} of 3 μ M, suggesting the strand transfer inhibition is mainly the result of RT-RNH inhibition and indeed this was further supported since **CPHM** was unable to inhibit RT-polymerase activity up to 75 μ M. **CPHM's** RNH inhibition principally targets RNH polymerase independent cleavages, since experiments in the absence of dNTPs had an RT-RNH IC_{50} of 3.0 μ M, similar to the strand transfer IC_{50} of 2.2 μ M in the presence of a HIV-1 nucleocapsid. The dicarboxylic acid group of **CPHM** has been shown to be involved in metal chelation with Mg^{+2} and essential for RT-RNH inhibition, since substitution of one or two of the dicarboxylic acid group's hydroxyls with a methyl caused the RT-RNH IC_{50} to increase substantial to 30-200 μ M (17). It was further shown that **CPHM** is a moderately

specific inhibitor of HIV-1 RT since it was unable to inhibit M_{Lu}V RT, AMV RT, Klenow Fragment DNA polymerase, and T4 DNA polymerase up to 68 μ M, but was able to inhibit *E. coli* RNH activity with an IC₅₀ of 2.6 ± 0.6 μ M (17). It can be proposed but not concluded that **CPHM** inhibits by binding to the RT-RNH active site through metal chelation, since this RNHI can also inhibit the structurally similar *E. coli* RNH but in order to definitely conclude binding within the RNH active site more direct evidence is required.

1.4.1.4 *N*-Hydroxymides and *N*-Hydroxyisoquinolines

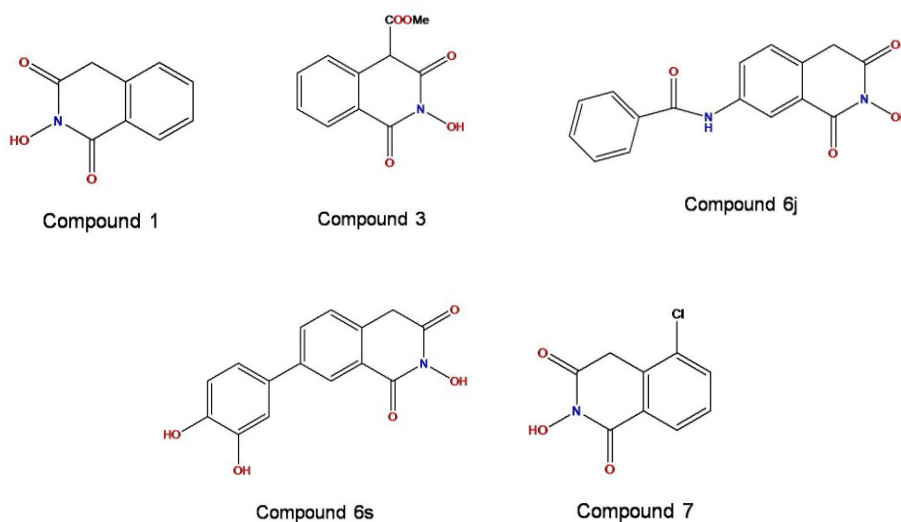


Figure 10 . Structures of *N*-Hydroxymide and *N*-Hydroxyisoquinolines RNHIs

N-hydroxymide compounds were designed to directly interact with a two metal ion active site, such as HIV-1 RT-RNH, where the three oxygen atoms would mimic the catalytic residue geometry required for metal ion interaction (57). Compound **1** (Figure 10) was the most potent compound with an RT-RNH IC₅₀ of 1 μ M and an RT-polymerase IC₅₀ of 40 μ M, while being

unable to inhibit *E. coli* RNH, influenza and T7 DNA polymerase activity. The *N*-hydroxyl functionality was essential for inhibition potency since replacing the hydroxyl with either a methoxy or an amino group resulted in a complete loss of RT-RNH inhibition. Phenyl group substituents such as chloride (-Cl) enhanced potency and selectivity for RT-RNH inhibition. Compound **7** (*Figure 10*) was the most potent compound with an RT-RNH IC₅₀ of 0.3 μM. Interestingly, NMR studies have indicated that RT-RNH inhibition by *N*-hydroxymides is metal dependent and requires the enol form of the inhibitor for binding to occur. Compounds **1** and **7** inhibited an HIV-1 RNH domain fragment with an IC₅₀ of 0.43 μM and 0.38 μM, respectively. Protein intrinsic tryptophan quench studies using the RNH domain fragment showed compound **1** to have a K_d of 2.32x10⁻⁵ M with a 1:1 binding ratio. This binding was assumed to occur near the RNH active site, since a gradual blue shift peak was seen with residue W123 near the RNH active site (40). The putative inhibition mechanism for *N*-hydroximides thus involves metal chelation with the active site metal ions.

N-Hydroxyisoquinolines are a class of metal chelating compounds that were derived from the *N*-hydroxymides pharmacophore and are bi-functional inhibitors of HIV-1 RT-RNH activity and IN. Initial IC₅₀ for IN inhibition ranged from 0.09-19 μM, while with RT-RNH the IC₅₀ ranged from 5.7-96 μM, depending on the substitutions made to the 7'-position of the *N*-hydroximide functional group (6). None of the compounds inhibited RT-polymerase activity up to 50 μM. The initial lead compound, **1** (*Figure 10*) had an RT-RNH IC₅₀ of 5.9 ± 1.4 μM and 6.3 ± 2.6 μM IC₅₀ with IN. Further structural modification of the 7'-position of compound **1** enhanced IN inhibition but had little to no effect on RT-RNH inhibition. The two best dual inhibitors of RT-RNH and IN activity were compounds **6s** and **6j** (*Figure 10*), with an RNH IC₅₀ of 6.6 ± 0.5 μM and IN IC₅₀ of 0.65 ± 0.3 μM for compound **6s**. Compound **6j** had an RNH IC₅₀

of $5.7 \pm 1.5 \mu\text{M}$ and an IN IC_{50} of $1.24 \pm 1.04 \mu\text{M}$, and was the only compound with antiviral activity against HIV (EC_{50} of $22 \mu\text{M}$ and a CC_{50} of $84 \mu\text{M}$) (6). Addition of an electron withdrawing methoxycarbonyl group to the 4'-position of compound **1** (compound **3**, *Figure 10*), intended to enhance metal chelation, substantially improved RNH inhibition ($61 \pm 5 \text{ nM}$ IC_{50}) (7). This modification had little to no effect on IN inhibition ($5 \pm 0.6 \mu\text{M}$ IC_{50}) and slightly enhancing antiviral activity with (EC_{50} of $13 \pm 5 \mu\text{M}$ and CC_{50} $61 \pm 3 \mu\text{M}$). The addition of an electron-withdrawing group at the 4'-position stabilized the enol form of the *N*-hydroximide functional group, therefore enhancing metal chelation, since the enolic form of these compounds been shown to be responsible for the ability to chelate two metal ions (6, 7). Compounds designed from *N*-hydroxyisoquinolines inhibitor class are unfavorable candidate for drug development considering the two compounds with antiviral activity had only a selectivity index around 4. However, these compounds are good examples for showing how HIV-1 RT-RNH and IN inhibition activity might be modified through metal chelation properties.

1.4.1.5 Diketo Acids (DKA)

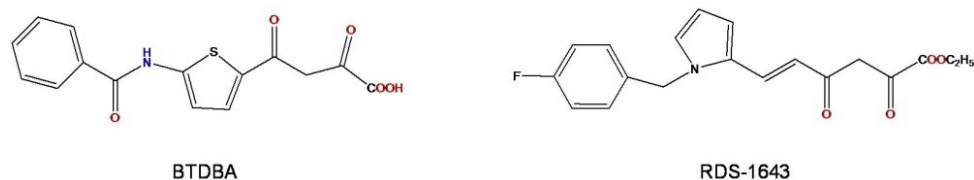


Figure 11. Structure of DKA RNHIs

The first compound from the diketo acid class of compounds to be described as an RNHI was **4-[5-(Benzoylamino)thien-2-yl]-2,4-dioxobutanoic acid (BTDBA)** (Figure 11) with an RT-RNH IC_{50} of $3.2 \pm 1.7 \mu M$ and no RT-polymerase inhibition up to $50 \mu M$. This compound has also been shown to directly inhibit and bind with a stoichiometry of 1:1 to a catalytically active RT-RNH domain fragment with a K_d of $8.9 \pm 3.5 \mu M$ and IC_{50} of $4.7 \pm 3.2 \mu M$. These binding studies also indicated that the inhibitor does not require the presence of the substrate in order to bind with the enzyme (83). **BTDBA** appears to have some specificity for RT-RNH inhibition, since it was unable to inhibit a structurally similar enzyme, *E. coli* RNH. Unfortunately, **BTDBA** does not have any HIV-1 antiviral activity. Mutational studies with a D185N-RT (a lethal polymerase active site mutation that has no effect on RNH activity) indicates that **BTDBA** does not bind within the polymerase active site, since there was no significant loss in RNH inhibition with this mutation having an (IC_{50} of $8.8 \pm 1.8 \mu M$ IC_{50}). Based on both the mutational studies with D185N-RT, the metal dependence for direct inhibition and binding with the p15-EC RT RNH domain fragment, it is plausible that **BTDBA** binds within in the RNH active site, directly interacting with the active site metal ions. The ability of **BTDBA** to inhibit HIV-1 IN activity with an IC_{50} of $1.9 \mu M$ similar to the RT-RNH IC_{50} ($3.2 \pm 1.7 \mu M$), also supports binding within the RNH active site since both enzymes have similar active sites (83). Compounds from the same structural class of **BTDBA** inhibit HIV-1 IN through a metal sequestration mechanism, suggesting **BTDBA** could inhibit through the same metal chelating mechanism as seen with the other thiophene diketo acid compounds (38, 41). However, there have been no published studies directly showing metal chelation with **BTDBA**.

A derivative of **BTDBA**, **6-[1-(4-Fluorophenyl)methyl-1H-pyrrol-2-yl]-2,4-dioxo-5-hexenoic acid ethyl ester (RDS-1643, Figure 11)** was originally designed as an HIV-1 IN

inhibitor and later evaluated as an RT RNHI (97), since both enzymes have similar active sites. This compound is much less potent as an RNHI compared to **BTDBA** with an RT-RNH IC₅₀ of $13 \pm 4 \mu\text{M}$ but it did have antiviral activity against HIV-1 with MT4 cells, unlike its predecessor **BTDBA** (EC₅₀ of $14 \pm 2 \mu\text{M}$ and a CC₅₀ of $63 \pm 4 \mu\text{M}$). Additionally, **RDS-1643** was also active against non-nucleoside reverse transcriptase inhibitor (NNRTI of RT polymerase activity) resistant strains of HIV-1, including Y181C-RT, K103N/Y181C-RT and K103R/V179D/P225H-RT indicating a potential of this inhibitor class for being able to inhibit clinically relevant resistant variants of HIV-1. Interestingly, this compound was unable to inhibit HIV-1 IN up to $\sim 95 \mu\text{M}$, while having no polymerase inhibition against HIV-1 RT and AMV-RT activities, along with no inhibition against *E. coli* RNH activity up to $100 \mu\text{M}$. These results suggest **RDS-1643** to be a more specific inhibitor targeting RT-RNH activity compared to **BTDBA**. Kinetic studies using Michaelis-Menton and Segal assumptions showed that **RDS-1643** is a non-competitive and reversible RT-RNH inhibitor with a K_i of $17 \mu\text{M}$. As with **BTDBA**, **RDS-1643**'s RT-RNH inhibition is independent of substrate binding, since time of addition experiments had no change in inhibitory properties. Although no direct studies with **BTDBA** have shown metal chelation, UV-Vis experiments in the presence of MgCl₂ with **RDS-1643** confirm DKA's are metal chelators. Combination studies with **RDS-1643** and *nevirapine* or *efavirenz* (NNRTIs) had no effect on RT-RNH and polymerase inhibition, suggesting **RDS-1643** binding is unlikely to occur in or near the non-nucleoside reverse transcriptase inhibitor binding pocket (NNRTIBP). Additional studies with NNRTI resistant mutant further supports **RDS-1643** inability to bind near or within the NNRTIBP, while the metal chelating properties of **RDS-1643** further suggest DKA binding occurs via metal chelation with the RNH active site metal ions.

1.4.1.6 Vinylogous Ureas

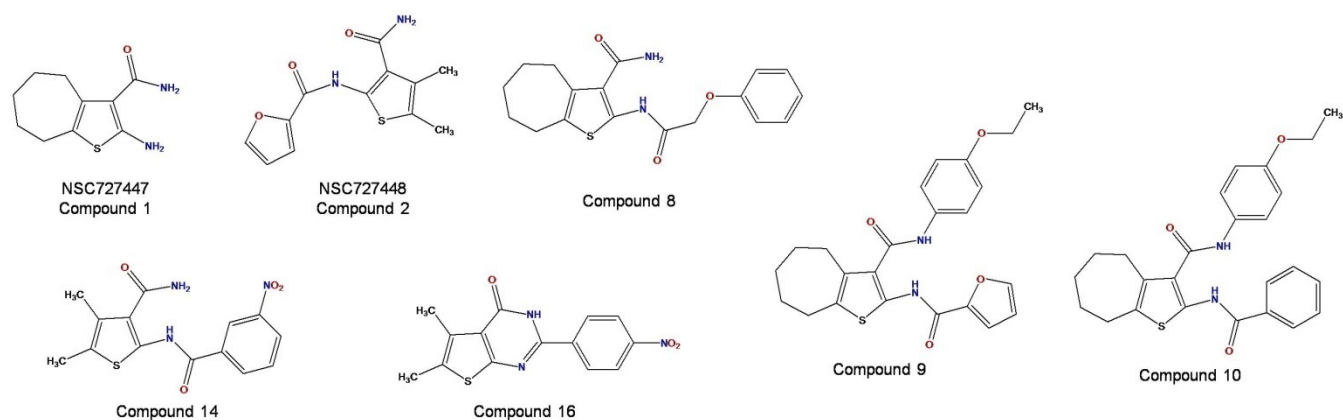


Figure 12. Structures of Vinylogous Urea RNHIs

The screening of a library containing ~230,000 natural and synthetic compounds identified vinylogous ureas as RNHIs. Two compounds (*Figure 12*), **NSC727447** (compound **1**) and **NSC727448** (compound **2**) showed the best inhibition properties. Both compounds were monofunctional inhibitors of RT-RNH activity. Compound **1** inhibited HIV-1 RT-RNH (2.0 μM IC_{50}), HIV-2 RT-RNH (2.5 μM IC_{50}), *E. coli* RNH (100 μM IC_{50}) Human RNH (10.6 μM IC_{50}) (99), and had antiviral activity against HIV-1 (4.3 μM $\text{EC}_{50}^{\text{i}}$ and 19.9 μM CC_{50}) (15). Compound **2** inhibited HIV-1 RT-RNH (3.2 μM IC_{50}), HIV-2 RT-RNH (5 μM IC_{50}), *E. coli* RNH (73 μM IC_{50}), human RNH (29 μM IC_{50}) (99) and no antiviral activity against HIV-1. Various studies suggested that vinylogous ureas bind outside of the RNH active site. MALDI-TOF and ESI-TOF MS/MS studies following *N*-hydroxysuccinimidyl-biotin treatment and

ⁱ Antiviral activity was never evaluated to be the result of directly targeting reverse transcriptase (15).

tryptic digestion experiments, suggest that compound **1** binds within or near residues K281 and C280, since compound **1** protected K281 and C280 modification by *N*-hydroxysuccinimide.

Further studies (15) involving 3'-CONH₂ and cycloalkane modification of the thiophene ring of the vinylogous urea pharmacophore resulted in an additional 22 derivatives. Evaluation of RT-RNH activity based on the structural modifications indicated that the size of the cycloalkane ring is important, where a ring size that is too small or too large negatively affects RT-RNH inhibition, suggesting that binding is dependent on hydrophobic interactions and/or pi-pi stacking between the inhibitor and protein residues. Additional modifications of compound **1**'s 2'-NH₂ functional group with a 2'-phenoxy acetylamino (6.9 μM RT-RNH IC₅₀, compound **8**) or 2'-furanoyl with a 4'-ethoxyphen (4.2 μM RT-RNH IC₅₀, compound **9**) indicates the furanoyl group is highly significant for RT-RNH inhibition, since replacement of furanoyl with a phenyl group causes a complete loss in RT-RNH inhibition (>500 μM RT-RNH IC₅₀, compound **10**). The significance of the furanoyl group suggests its oxygen may be involved in hydrogen bonding with protein residues in order to enhance RT-RNH inhibition. Structural modifications of compound **2** by introducing either a rigid or flexible bulky aryl substitutions resulted in the most active vinylogous urea RNHI, compounds **14** (1.3 μM RT-RNH IC₅₀, *Figure 12*) and **16** (0.85 μM RT-RNH IC₅₀, *Figure 12*). These results suggest that the increase in thiophene ring rigidity with the formation of a pyrimidine ring from the 2'-NH₂ and 3'-CONH₂ group largely enhances RT-RNH inhibition, whereas increasing the flexibility of the aryl had a negative effect on inhibition. Substitution of compound **16**'s 4'-NO₂ functional group with a -OCH₃ group caused a complete loss in RT-RNH inhibition (>50 μM RT-RNH IC₅₀), suggesting that the 4'-NO₂ group may be involved in hydrogen bonding (15).

Molecular modeling studies indicated the binding location of compound **1** to reside within the interface between the p51 and RNH domain, where the cycloalkane ring occupies a small binding pocket formed by G541 (RNH domain residues), C280 (p51 residue) and R284 (p51 residue). The most favorable pose had the thiophene ring making three hydrogen bonds with protein residues V276 (p51 residue), K275 (p51 residue) and H539 (RNH domain residue). In addition the carbonyl of residue V276 and side chain amine of residue K275 are hydrogen bonding with the 3'-CONH₂ functional group, along with the backbone carbonyl-oxygen of residue H539 hydrogen bonding with the thiophene ring's 2'-NH₂ functional group. Molecular modeling studies with compound **16**, resulted in the docking within the same binding pocket as compound **1** with a slightly different orientation, in which the thiophene ring's 4'-NO₂ group makes a potential 4 Å hydrogen bond with residue R284 (p51 residue) and the planar benzene ring resides within the same hydrophobic pocket of compounds **1**'s cycloalkane (15).

1.4.1.7 5-nitro-furan-2-carboxylic carbamoylmethyl ester (NACME)

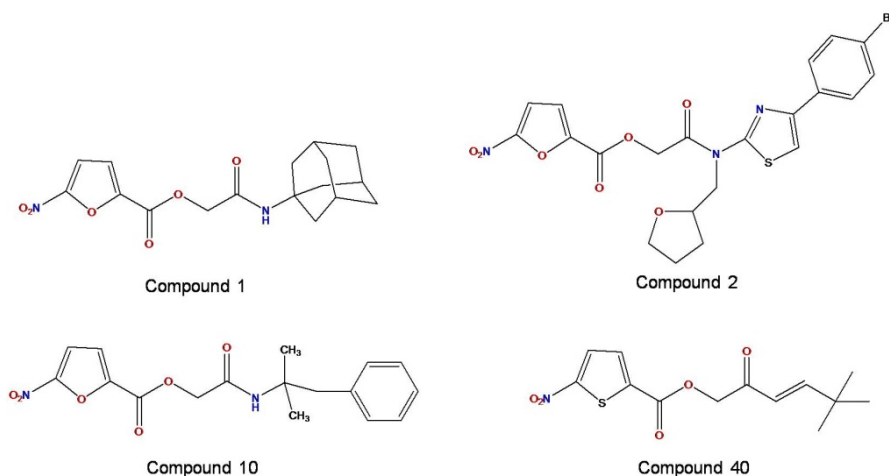


Figure 13. Structures of NACME RNHIs

5-nitro-furan-2-carboxylic carbamoylmethyl ester (NACME) RNHIs were identified during the screening of a library of 20,000 compounds for potential RT-RNH inhibitors. Of the NACME compounds in the library, 32 (35%) inhibited HIV-1 RT-RNH activity. The two most potent compounds were *5-nitro-furan-2-carboxylic acid adamantan-1-carbamoylmethylester* (compound **1**, Figure 13) and *5-nitro-furan-2-carboxylic acid [[4-(4-bromo-phenyl)-thiazol-2-yl]-(tetrahydro-furan-2-ylmethyl)-carbamoyl]-methyl ester* (compound **2**, Figure 13). Both compounds were evaluated for an ability to inhibit HIV-1 RT from different viral clades. Compound **1** inhibit RT of all three major HIV-1 clades (clade B, C and CRFO1 A-E) with IC₅₀ values of 29.6 ± 9.2 μM, 26.5 ± 15.0 μM, and 3.8 ± 1.5 μM, respectively. Compound **2** was also able to inhibit all three clades as well with an RT-RNH IC₅₀ of 26.7 ± 13.5 μM (clade B), 32.2 ± 0.5 μM (clade C), and 2.6 ± 1.8 μM (clade CRFO1 A_E). Both compounds had no effect on HIV-1 RT dependent DNA polymerase activity, HIV-1 IN activity, *E. coli* RNH activity or human RNH, but they were able to inhibit the RNH activity of MLV-RT (~9 μM IC₅₀). The reported antiviral properties seen with compounds **1** and **2** (EC₅₀ ~23-25 μM) was likely the result of compound cytotoxicity, as the *in vitro* selectivity index was low (29). Molecular modeling studies suggested that the nitro-furan group interacts with RNH active site metal cations and H539, while the amide carbonyl-oxygen interacts with residue S553.

Additional synthesis of NACME derivatives evaluated the ester linker, nitro-furan group and hydrophobic moieties for RT-RNH inhibition (102). Compounds **10** and **40** (Figure 13) were the most potent derivatives with an RT-RNH IC₅₀ of 0.9 μM and 2.8 μM, respectively. Substitution of the nitro-furan group completely eliminated inhibitor activity. It is possible that the nitro-furan oxygens are capable of metal chelation, since the nitro-furan-carboxylic acid compounds are structurally similar to active site metal chelating RNHIs, *β-thujaplicinol*

(subsection 1.4.2.1) and pyrimidinol carboxylic acid (subsection 1.4.2.2) (5, 44, 56). The ester linkage between the nitro-furan group and hydrophobic moiety was also replaced with an amide group in order to make the compounds more favorable as drug candidates, since an ester within the human body would be rapidly digested by esterase causing drug concentrations to be depleted rapidly. Unfortunately, this resulted in a loss of inhibitor potency.

1.4.1.8 Alizarines

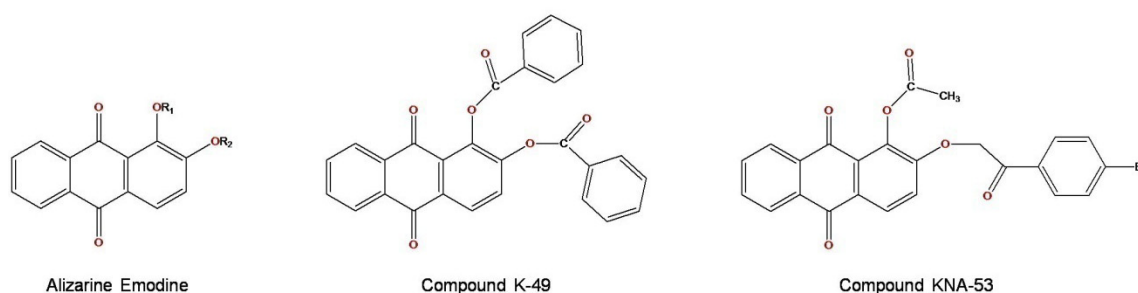


Figure 14. Structures of Alizarine RNHIs

Alizarine emodine (Figure 14) was first identified as an RT-polymerase inhibitor (IC_{50} of 79 μ M) and was unable to inhibit RNH activity (55). Alizarine emodine derivatives with substitutions at the 1' and 2'-positions of the alizarine ring were synthesized. The most potent compounds were **K-49** and **KNA-53** (Figure 14), with and RT-RNH IC_{50} of 13 ± 3 μ M and 21 ± 2 μ M, along with a RT-polymerase IC_{50} of 12 ± 3 μ M and 5 ± 2 μ M, respectively. Replacement a distal bromide (Br) of **KNA-53** with a phenyl group, resulted in a complete abrogation of RT-RNH inhibition up to 100 μ M and did not affect RT-polymerase inhibition. Addition of two

phenylketo groups at both R₁ and R₂ positions, as seen with compound **K-49**, resulted in the most potent RT-RNH inhibition from this class of RNHIs. All of the alizarine derivatives, including **K-49** and **KNA-53** had no antiviral activity against HIV-1. Michaelis-Menton kinetic studies with **K-49** showed that RT-RNH inhibition is non-competitive with respect to the substrate, having a K_I of 7 μM, K_m of 1.5 nM and a K_{cat} of 0.82 s⁻¹. **K-49** and **KNA-53** did not bind to the RNH domain fragment and showed no metal dependence for RT-RNH inhibition, suggesting the inhibitors are not RNH active site binders.

1.4.2 RNHIs with a Known Binding Site

1.4.2.1 Tropolones

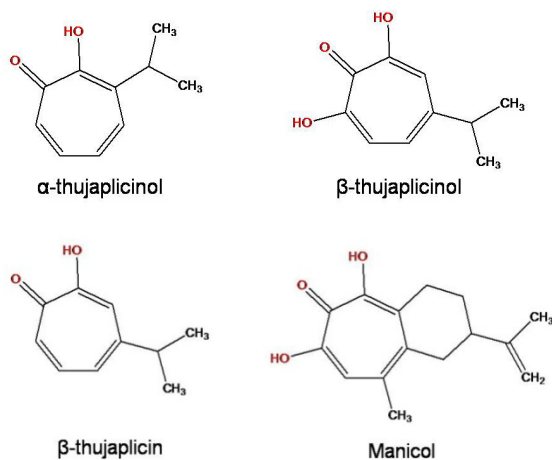


Figure 15. Structures of Tropolones RNHIs

Tropolones were first identified as an RNHI during the screening of a library of natural products (10), in which ***β-thujaplicinol*** (Figure 15) was the most active RNHI. ***β-thujaplicinol*** inhibited RNH activity with an IC₅₀ of 0.21 ± 0.03 μM (HIV-1), 0.77 ± 0.08 μM (HIV-2) and 5.7 μM (Human RNH), and was inactive against HIV-1 RT-polymerase and *E. coli* RNH activity. All of the tropolones evaluated had no antiviral activity. Tropolones, including ***β-thujaplicin*** (> 100 μM IC₅₀, Figure 14) and ***α-thujaplicinol*** (50 μM IC₅₀, Figure 14) were inactive or less potent as an HIV-1 RT-RNHI compared to ***β-thujaplicinol***. Structural comparison of ***β-thujaplicinol*** and ***β-thujaplicin*** indicated that the 7'-hydroxyl of ***β-thujaplicinol*** is essential for potent RT-RNH inhibition, while comparison with ***α-thujaplicinol*** indicates an α-hydroxyl substituent is less active than a compound with a β-hydroxyl (***β-thujaplicinol***). Michaelis-Menton kinetic studies suggested the type of inhibition was mixed, in which non-linear fitting confirmed these results with both ***β-thujaplicinol*** and ***manicol*** (Figure 15). These results indicate that the tropolone inhibitors can bind the free enzyme or binary complex of RT with the substrate near an active site (10). Recent X-ray crystal structure with HIV-1 RT (2.80Å) and a His-tag RNH domain fragment (2.04Å) revealed that ***β-thujaplicinol*** does indeed bind within the RNH active site and chelates both metal cations. All three oxygens of tropolone ring of ***β-thujaplicinol*** coordinates both metal cations (Mn⁺²) in both co-crystal structures. Ionic or hydrogen bonds are made with metal cation B and residues E478, D498, H539, while metal cation A interacts with residue D549 and the hydroxyl group of the inhibitor forms a salt bridge with residue R557. The active site binding is perhaps inconsistent with the non-competitive inhibition. However, it has been proposed that the nucleic acid substrate may sterically restrict the inhibitor within the bound state and hinder dissociation of the inhibitor (44), rather than the inhibitor binding to the substrate, as previous studies showed the inhibitors are unable to bind to an RNA/DNA substrate (10).

1.4.2.2 Pyrimidinol Carboxylic Acids

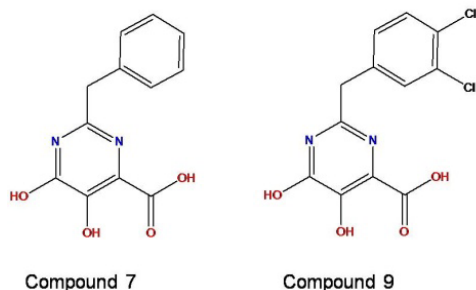


Figure 16. Structures of Pyrimidinol Carboxylic Acid RNHIs

The pyrimidinol carboxylic acid compounds were identified as RNHIs while designing a compound based on the diketo acid compound **BTDBA** (subsection 1.4.1.4) with a more stable tautomeric scaffold (56). The 2'-phenyl with a methylene linker, as seen with compound **7** (2.5 μ M RT-RNH IC_{50} , *Figure 16*) was shown to be highly significant for RT-RNH inhibition, since 2'-modifications reduced RT-RNH inhibition. Substitutions added to the phenyl ring of compound **7**, such as the addition of two chloro groups (compound **9**), enhanced RT-RNH inhibition (IC_{50} of 1.45 ± 0.4 μ M, *Figure 16*). During pre-steady state RNH cleavages kinetic analysis, compound **9** was shown to be metal dependent for RT-RNH inhibition, since the initial burst rate of catalysis was significantly inhibited under conditions of pre-incubation with the enzyme-inhibitor in the presence of metals; enzyme-inhibitor pre-incubation in the absence of metals was unable to inhibit RNH catalysis. These observations further support the metal dependent behavior of compound **9**. The compounds were further unable to inhibit human-RNH and had no HIV-1 antiviral activity with MT-4 cells. An X-ray crystal structure of compound **9** with the p15-EC RT RNH domain fragment (1.7Å), showed the inhibitor chelating RNH active

site metal cations. The carboxylate oxygen of compound **9** coordinates with metal ion B, while the oxygens of the two phenolic groups coordinate metal ion A. In addition, the 2'-phenyl substitution interacts with the imidazole ring of H539, consistent with the improved potency seen with the methylene linker. The center of the phenyl ring is 3.8 Å from the imidazole ring of H539 and makes an edge-on- π interaction with H539 (56). The X-ray structure of compound **9** chelating active site metal ions and its metal dependent behavior, suggest that pyrimidinol carboxylic acids mechanism of inhibition is the result of RNH active site metal chelation.

1.4.2.3 *N*-hydroxy Naphthyridinones

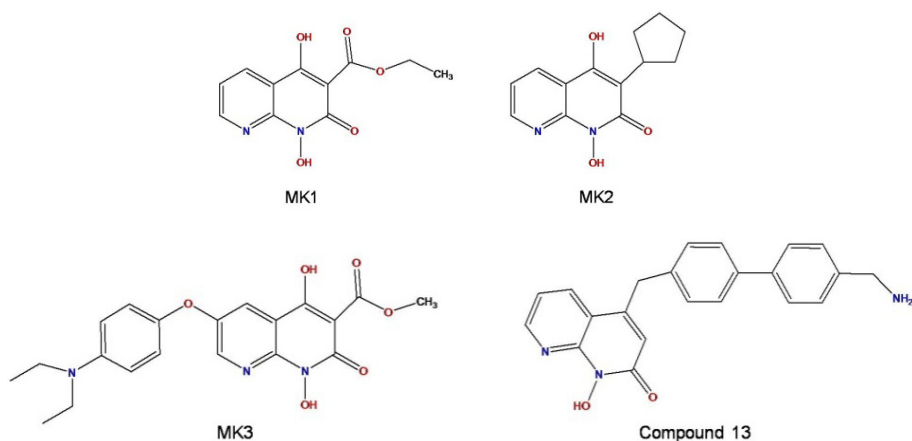


Figure 17. Structure of *N*-hydroxy Naphthyridinone RNHIs

N-hydroxy naphthyridinone RNHIs were first developed as HIV-1 IN inhibitors (42). A recent study showed three *N*-hydroxy naphthyridinone RNHIs, **MK1** (IC₅₀ of 0.11 μ M and EC₅₀ of 2.7 \pm 0.2 μ M), **MK2** (IC₅₀ of 0.12 μ M and EC₅₀ of 3 μ M) and **MK3** (IC₅₀ of 0.22 μ M and EC₅₀ of 9 μ M) (*Figure 17*) bound to the RNH active site and the *N*-hydroxy naphthyridinone core

chelates the metal ions (90, 100). These specific compounds were chosen for X-ray crystallography studies since previous studies indicated no preference for binding within either the RNH or IN active sites (42), suggesting they have the greatest probability for metal chelation. All three compounds were unable to inhibit RT-polymerase activity and though they have antiviral activity against HIV-1 no evidence has been shown to prove the antiviral activity is the result of targeting reverse transcription during *in vivo* studies.

MK1 and **MK2** x-ray crystal structures with full length RT at 2.80 Å and 2.23 Å shows that the RNH active site residues D443, E478, D498 and D549 form the binding site, in which both compounds have the same orientations with the hydroxyl group coordinating with the active site metal ions and the oxygens of the naphthyridinone nitrogen providing support. Metal ion A is coordinated by the carboxyl oxygens of D443, E478, D498 and the central hydroxyl and flanking nitrogen of compounds **MK1** and **MK2**, while metal ion B is coordinated by the residue-carbonyls of D443, D549 and the central hydroxyl of both compounds. Residues H539 is within 2.7 Å of hydrogen bonding distance from the naphthyridinone-oxygen, along with 3.2 Å and 3.3 Å of the two carboxylate-oxygen's of D549, while also within 3.0 Å from both compound's carboxylate-oxygen. Overlaying of the co-crystal structure of **MK2** with both co-crystal structures of *β-thujaplicinol* (subsection 1.4.2.1) or pyrimidinol carboxylic acid (subsection 1.4.2.2) with full length RT shows all three RNHs have similar orientations within the same binding site and have group extensions pointing towards residues H539, indicating the significance of interactions with H539 for RT-RNH inhibition when bound to the RT-RNH active site (90). The co-crystal structure of **MK3** and full length RT resulted in the RNHI binding near the NNRTIBP as opposed to binding within the RNH domain. **MK3** bound within the polymerase domain's hydrophobic binding pocket (adjacent to the NNRTIBP) was formed by

residues L100, V108, Y181, Y183, D186, L187, K223, F227, L228, W229 and L234. The diethylamiophenoxy group of **MK3** seems to lead binding within the site as opposed to the naphthyridinone core, as seen with **MK1** and **MK2**. The two different binding locations of **MK1** and **MK2** versus **MK3**'s polymerase binding site suggest that the *N*-hydroxy naphthyridinone class of compounds can bind two different locations. The binding site of **MK3** near the NNRTIBP is very similar the binding of **DHBNH** (an *N*-acylhydrazone, subsection 1.4.2.4) within the polymerase domain (43). It is plausible that **MK3** can also bind within the RNH active site, considering the compound has been shown to be metal dependent for RT-RNH inhibition. It is possible that crystal packing with full length RT and the larger size of **MK3**, prevented binding within the RNH domain. **MK3** was able to bind and chelate metal ions within the RNH domain of an isolated RNH domain fragment in a similar manner to **MK1** and **MK2** (90). **MK3** bound the active site of the isolated RNH domain fragment has a slight difference in orientation compared to **MK1** and **MK2**, in which the phenyl ring of **MK3** also packs against residue Q500 (90).

Derivatives of **MK1** were created with the intention of enhancing ligand contacts with the RNH active site, through lipophilic modification of the 4'-position of the naphthyridinone core (100). The most potent compound was compound **13** (*Figure 17*), with an homologation of the benzene linker and a meta bi-phenyl group, containing a substituted para aminomethyl group on the distal phenyl ring with the intention of enhancing inhibitor-protein contacts and solubility. Compound **13** had and RT-RNH IC₅₀ of 45 ± 20 nM and was able to inhibit RT-polymerase activity with a 13 ± 1.3 μM IC₅₀, unlike its predecessor. Compound **13** had an enhancement in antiviral activity against HIV-1 with an EC₅₀ of 190 ± 120 nM and a CC₅₀ of 3.3 ± 2.3 μM, resulting in a favorable selectivity index of 57.5. However, the antiviral activity has not been

identified to work at the level of HIV-1 reverse transcription. Attempts were made to obtain x-ray crystal structure of compound **13** with full length RT, along with molecular docking studies but these attempts were unsuccessful (100).

1.4.2.4 *N*-Acylhydrazones

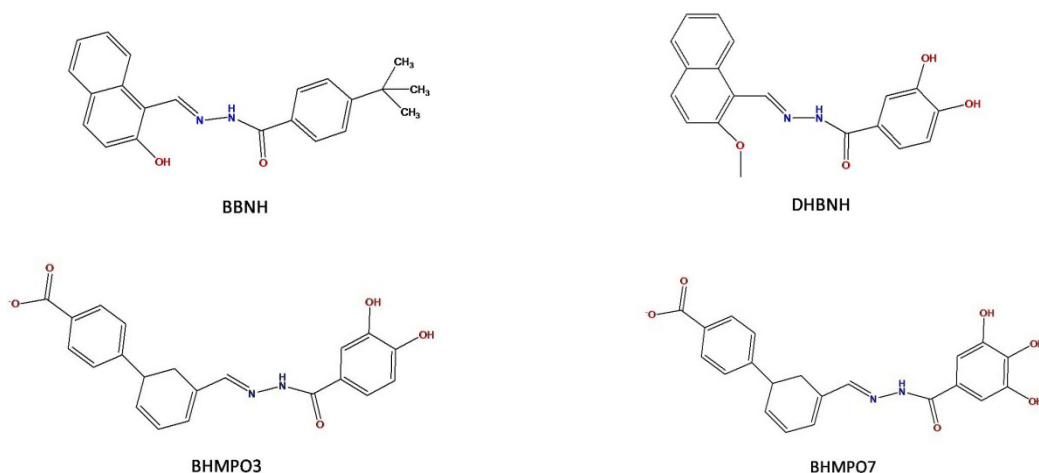


Figure 18. Structure of *N*-acylhydrazone RNHIs

N-acylhydrazones were the first RNHIs with antiviral activity (9). The first *N*-acylhydrazone compound described was *N*-(4-tert-Butylbenzoyl)-2-hydroxy-1-naphthaldehyde hydrazone (**BBNH**), Figure 18. **BBNH** is a bi-functional inhibitor of HIV-1 RT RNH and polymerase activity with a 3.5 μM and 0.8-34 μM IC_{50} (depending on template/primer), respectively. HIV-1 antiviral activity of **BBNH** with PBMC and MT4 cells had an EC_{50} of 1.5 μM and 5 μM , respectively. RT-RNH inhibition was time dependent according to the length of enzyme-

inhibitor pre-incubation and required the presence of metal ions. RT-RNH inhibition was reversible and competitive with respect to the RNA/DNA substrate during kinetic studies, while also being moderately specific for HIV-1 RT-RNH inhibition. **BBNH** was able to inhibit *E. coli* RNH ($2.7 \pm 0.9 \mu\text{M}$) and MLV RT-RNH activity ($0.8 \pm 0.2 \mu\text{M}$), while being unable to inhibit RNH activity of HIV-2, AMV and bovine pancreatic RNase A. RT-polymerase inhibition was reversible and mixed-type with both the substrate and dNTP. In fact, the polymerase kinetic inhibition profile was identical to the polymerase kinetic inhibition profile of known NNRTIs. The polymerase inhibition of **BBNH** was specific to HIV-1 RT, since it was unable to inhibit HIV-2, AMV, MLV, Taq DNA Polymerase, Klenow DNA polymerase, HeLa cell nuclear extracts and DNA polymerase activities up to $50 \mu\text{M}$. **BBNH** retained *in vitro* RT-RNH and polymerase inhibition potency with clinically relevant RT resistant mutants, including K103N, Y181C, Y181I, Y188H and Y188L. Combination studies with known NNRTIs and photo-labeling 9-ANⁱⁱ had no affect on RT-RNH inhibition by **BBNH**, suggesting that **BBNH** has a potential for binding a location separate from the NNRTIBP. This is further reinforced by the fact that RT-RNH inhibition of **BBNH** is metal dependent and therefore suggesting binding within the an active site involving metal chelation. In addition, the ability to protect RT-polymerase activity dose dependently from being deactivated during 9-AN photo-labeling studies, while also being unable to inhibit the polymerase activity of other enzymes that lack the NNRTIBP, such as HIV-2 (9), suggest that **BBNH** is able to bind an additional site independent of an active site. These observations suggest that **BBNH** binds two spatially distinct sites, within an active site by metal chelation and at or near the NNRTIBP.

ⁱⁱ A photoactive analogue of nevirapine that permanently blocks the NNRTIBP (9).

Molecular modeling studies showed **BBNH** docked within the RNH active site, in which the naphthyl benzene ring of the compound makes pi-pi stacking interaction with residue Y501 (3). The hydrazone amide and carbonyl groups are making further hydrogen bonds with the active site metal ions. A derivative compound of **BBNH** lacking a second naphthyl benzene ring, **BBSH** indicated the second naphthyl benzene ring for pi-pi stacking is significant for RT-RNH inhibition. This was evident, since **BBSH** had a loss in RT-RNH inhibition ($2.5 \pm 0.4 \mu\text{M}$ IC_{50}) while retaining its RT-polymerase inhibition. Additional mutational studies with Y501x (W and R) confirm that **BBNH** must have significant contact with residue Y501, since RT-RNH inhibition was reduced or completely abrogated and RT-polymerase inhibition was unaffected by these mutations (3). **BBNH** was the first compound to display bi-functional inhibition against RT-RNH and polymerase activities through a mechanism that suggests binding within two spatially distinct sites within the polymerase and RNH domains. An extended study with **BBNH** showed that its binding with HIV-1 RT impacts heterodimer stability and causes dimer dissociation (84), suggesting its mechanism of inhibition is the result of the heterodimer dissociation of RT.

A **BBNH** derivative, *dihydroxy benzoyl naphthyl hydrazone* (**DHBNH**, Figure 18) has been described in the literature (43). **DHBNH** was created to prevent metal cation chelation, since the hydroxyl of the naphthyl ring was replaced with a methoxy group. **DHBNH** is a monofunctional inhibitor of RT-RNH activity (IC_{50} of $0.5 \pm 0.2 \mu\text{M}$) and is unable to inhibit RT-polymerase activity, unlike its predecessor **BBNH**. **DHBNH** is a much weaker inhibitor of the p15-EC RT RNH domain fragment (IC_{50} of $18.5 \pm 3.4 \mu\text{M}$), suggesting that the compound may not bind to the RNH active site. An X-ray crystal structure of **DHBNH** with full length RT (3.15 Å) shows the inhibitor bound within a site ~ 3.5 Å away from the polymerase active site near the

NNRTIBP. The benzyl ring partially enters the NNRTIBP and interacts with NNRTIBP residue W229, while the naphthyl ring is oriented near the polymerase active site and primer grip region. The binding site of the inhibitor is formed by residues V108, L187, Y188, K223, F227, and L228, in which residue-inhibitor contacts occur through main chain β -carbons, suggesting that **DHBNH** may retain activity against HIV-1 NNRTI resistant strains. Additional studies have shown that the inhibitor remains active against common NNRTI resistant RT mutants, including Y188L. **DHBNH** also retains antiviral activity against NNRTI resistant strains of HIV-1, including RT mutant strains such as Y181C (nevirapine resistant), Y106A/Y181C (UC781 resistant), L100I/K103N (efavirenz resistant) and D67N/K70R/T215F/K219Q (AZT resistant). Real time PCR experiments showed that the antiviral activity of **DHBNH** ($5.5 \pm 1.7 \mu\text{M}$ EC₅₀ with HIV-1, CC₅₀ > 100 μM) works at the level of reverse transcription by inhibiting the initiation of HIV-1 reverse transcription. In addition, comparison of DHBNH-RT with the co-crystal structure of CP-94-07-RT, have a very similar protein conformation, therefore supporting these PCR results since inhibitor **CP-94-07** inhibits the initiation of transfer-RNA primed DNA synthesis. The co-crystal structure of **DHBNH** led to the proposal that the bound inhibitor would cause structural changes in the polymerase primer grip and thumb domain and would alter the trajectory of the P/T and prevent proper orientation of the substrate with the RNH active site, thereby inhibiting RNH hydrolysis. Superposing of RT-DHBNH crystal structure with and RT-RNA/DNA co-crystal structure further suggest that **DHBNH** cannot prevent substrate or dNTP from binding, and in fact kinetic studies with **DHBNH** indicates the type of RT-RNH inhibition is non-competitive with the substrate. Though the crystal structure of **DHBNH** bound to RT results in a binding site within the polymerase domain, there is still a possibility of a second binding site within the RNH domain. The potential for a second binding site of **DHBNH** is

supported by the fact that its RT-RNH inhibition is unaffected in a presence of excess of (20 μM) *nevirapine* (43). Furthermore, superposition of DHBNH-RT and nevirapine-RT crystal structures, suggest that *nevirapine* (NNRTI) would cause residue Y188 to rotate and clash with the benzyl ring of **DHBNH** and prevent the inhibitor from binding. Therefore, it is plausible that **DHBNH** was unable to bind within the RNH domain due to crystal packing, causing the inhibitor to be sterically excluding from binding within the RNH domain, as seen with *N*-hydroxy naphthyridinone compound (**MK3**, subsection 1.4.2.3) with full length RT (90).

Recently, two derivatives of **DHBNH** have been described (35), in which the fused naphthyl ring of **DHBNH** was replaced with a flexible extended biphenyl system that has a carboxylate group in the distal phenyl ring with either a dihydroxy (**BHMP03**) or trihydroxy (**BHMP07**) benzyl substituents (*Figure 18*). The carboxylate group was added in order to make ionic interactions with the polymerase domain residue K223 and therefore enhancing inhibitor-protein contacts and subsequently enhancing inhibitor potency. **BHMP03** and **BHMP07** are identical in structure except for an added third hydroxyl to the distal phenyl ring with **BHMP07**, which seems to be responsible for the added ability to inhibit RT-polymerase activity as well as RT-RNH activity, unlike the RT-RNH monofunctional inhibitor **BHMP03**. Indeed **BHMP07** is able to inhibit RT-RNH activity with an IC_{50} of $0.2 \pm 0.1 \mu\text{M}$ and RT-polymerase activity with an IC_{50} of $0.3 \pm 0.2 \mu\text{M}$, along with inhibiting the p15-EC RT RNH domain fragment (IC_{50} of $0.8 \pm 0.06 \mu\text{M}$). **BHMP03** is unable to inhibit the RNH activity of the fragment but is able to bind with the enzyme (K_d of $23.1 \mu\text{M}$), along with inhibiting the RNH activity of full length RT (IC_{50} of $0.4 \pm 0.2 \mu\text{M}$). **BHMP07** had a greater binding affinity with the p15-EC RT RNH domain fragment with a K_d of $5.3 \mu\text{M}$. Solution NMR ^1H - ^{15}N HSQC chemical shift binding studies of the interaction of **BHMP07** with the p15-EC RT RNH domain fragment, showed that

BHMP07 causes chemical shift perturbation of residues 72-110, of which residues 81-104 are residues that make up the extended *E. coli* helix-loop to restores activity to the enzyme. Supposition of the p15-EC RT RNH domain fragment NMR chemical shift structure with the X-ray crystal structure of full length RT (PDB: 2I5J) suggest that the extended *E. coli* loop mimics the inter subunit interface between the p51 subunit and the RNH domain of the p66 subunit and therefore acting like a substrate handle. HSQC titration experiment with **BHMP07** and the p15-EC RT RNH domain fragment in a ratio of 1:4 (protein: ligand) resulted in a K_d of 142.7 ± 35.7 mM in the absence Mg^{+2} and a K_d of 392.0 ± 69.9 μ M in the presence Mg^{+2} . The NMR dissociation constants (K_d) indicates that **BHMP07** has a better binding affinity with the p15-EC RT RNH domain fragment in the absence of metal cation and suggest that the inhibitor is not metal dependent for RNH inhibition. Mutational studies with *N*-acylhydrazones (including **BHMP03**, **BHMP07** and **DHBNH**) resulted in a reduction or loss in RT-RNH inhibition with the amino acid substitutions A502G/F and A502G/F+D256G (35). **DHBNH's** loss of RT-RNH inhibition with mutated RNH residues, along with the proposed NMR binding site suggest that **DHBNH** has a second binding site within the RNH domain between the interface with the p51 subunit that is independent of the binding site near the NNRTIBP.

1.4.3 Summary

Progress in RT RNHI discovery has occurred since the discovery of the natural product *illimaquinone* as an HIV-1 RNHI, where *illimaquinone* has been indicated to bind near residue C280 of the p66 subunit (63). Since the identification of *illimaquinone* as an RNHI, a cascade of natural products (8, 39, 45, 62, 63, 65, 67, 93, 94) and synthesized small molecules (3, 5, 6, 7, 10, 15, 17, 24, 29, 32, 35, 40, 43, 44, 55, 56, 57, 68, 83, 90, 97, 99, 100, 102) as HIV-1 reverse transcriptase associated ribonuclease H inhibitors has pursued.

Current progress in RT RNHI discovery has been mainly focused on active site metal chelating small molecules, including naphthalenesulfonic acids (68), **CPHM** (17, 32), *N*-hydroxymides (40, 57), DKAs (83, 97), *N*-hydroxyisoquinolines (6, 7), NACME (29, 102), tropolones (5, 10, 44), pyrimidinol carboxylic acids (56), and *N*-hydroxy naphthyridinones (90, 100). Only three of these classes, tropolones (44), pyrimidinol carboxylic acids (56), *N*-hydroxy naphthyridinones (90) have been confirmed to bind within the RNH active site by metal chelation with co-crystallized X-ray crystal structures of full length RT. In addition, only a few of the proposed active site metal chelating small molecule RNHIs, including DKAs (97) and hydroxyisoquinolines (6), along with confirmed active site metal chelating RNHI from the *N*-hydroxy naphthyridinones class (90) have displayed antiviral activity against HIV-1 but none of them have been confirmed to work at the level of HIV-1 reverse transcription during *in vivo* studies. A few other classes of RNHIs, that are not active site metal chelating inhibitors have also been discussed within the literature, including vinylogous ureas (15, 99), alizarines (24, 55), and *N*-acylhydrazones (3, 9, 35, 43, 84). Vinylogous ureas have been proposed to bind at the interface of the RNH domain and p51 subunit and cause heterodimer dissociation (15), though no structural studies have been shown to confirm the proposed binding site. In addition, the

vinyllogous ureas do have HIV-1 antiviral activity (15), but it has never been proven that their antiviral activity works at the level of HIV-1 reverse transcription. Alizarines class of RNHIs have been suggested to bind within the NNRTIBP (24) but no structural studies have been published to prove binding within this site, while this class has no HIV-1 antiviral activity. The *N*-acylhydrazone class of RNHIs was the first class identified as an RNHI with antiviral activity and is the only class to date to confirm antiviral activity works at the level of HIV-1 reverse transcription (9). Furthermore, the *N*-acylhydrazone RNHI class has also been demonstrated by structural studies to bind two spatially distant locations, near the NNRTIBP (43) and within the interface between the RNH domain and p51 subunit (35). Though some progress with HIV-1 RT RNHI discovery has been made through the past eleven years, there is still a necessity to discovery new RNHIs that work independent of active site metal chelation and can be developed as specific inhibitors of HIV-1 RT-RNH activity, that are least likely to produce potentially fatal off-target affects within the host.

1.5 RATIONALE AND STATEMENT OF HYPOTHESIS

Approximately 33 million people worldwide are infected with HIV-1 (98). The U.S. Food and Drug Administration have approved 26 anti-HIV-1 drugs, which predominantly target the activities of protease and the polymerase activity of reverse transcriptase (74). These current antivirals are plagued by the development of drug resistance and even though current combination therapies have been successful with slowing down the rate of viral mutation, drug resistance remains a serious issue. There is a necessity for novel antivirals of HIV-1 to counteract the emergent resistant virus strains. One plausible target is the ribonuclease H activity of HIV-1 reverse transcriptase.

There has been some progress with HIV-1 RT RNHI discovery over the past eleven years, since the identification of *illimaquinone* as an RNHI (62). The area of RNHI discovery has been predominantly focused on active site metal chelating small molecules, including small molecules that have only been suggested as RNH active site inhibitors (6, 17, 29, 40, 57, 68, 83, 97, 102) and small molecules that have been confirmed as active site RNHIs (10, 44, 56, 90, 100) through biophysical structural studies. A few of the active site RNHIs have antiviral activity against HIV-1 (6, 90, 97) but none of them have been shown to directly target and inhibit the activity of reverse transcriptase during *in vivo* HIV-1 replication. Furthermore, inhibition at the level of metal chelation has a potential for off-target inhibitory effects, which could be detrimental to the host, suggesting that metal chelating RNHIs may not be a favorable direction

for HIV-1 RT RNHI discovery and for this reason it certainly should not be the only avenue for RNHI discovery.

Only one class of RNHIs, *N*-acylhydrazones has been shown to have antiviral activity against HIV-1 at the level of directly inhibiting the activity of RT (9). *N*-acylhydrazones RT-RNH inhibition is not the result of active site binding and metal chelation, but rather through an unknown inhibitory mechanism that involves binding two spatially distinct sites within the RNH and polymerase domains of RT (35, 43). The ability of the *N*-acylhydrazones to inhibit RT-RNH activity independent of metal chelation makes small molecules with the hydrazone functionality promising leads for future RNHI discovery, therefore our laboratory hypothesizes that small molecules with the hydrazone or hydrazine functionality will be a highly active class of HIV-1 RT RNHIs that can inhibit RT-RNH activity independent of active site metal chelation.

CHAPTER 2: IDENTIFICATION AND CHARACTERIZATION OF THE FLUOREN-9-YILDENE HYDRAZINE PHARMACOPHORE

2.1 ABSTRACT

Screening a library of 5,292 hydrazone/hydrazine compounds for inhibition of HIV-1 RT-RNH activity resulted in the identification of the fluoren-9-yildene hydrazine pharmacophore as highly active inhibitors. The initial 33 compounds library was expanded to an additional 118 compounds with the fluoren-9-yildene functionality. This focused library gave confirmed hit rate of 55% (65 compounds), for inhibitors of RT-RNH activity. The fluoren-9-yildene hydrazine compounds turned out to be mainly monofunctional for RNH activity, since only 21% (25 compounds) of the compounds inhibited RT-polymerase activity. The two most potent RNHIs were compounds **15** and **25**, which inhibited wild type RT-RNH activity with IC₅₀ values of $0.34 \pm 0.07 \mu\text{M}$ and $0.4 \pm 0.03 \mu\text{M}$, respectively. Similar inhibition was observed with two clinically relevant NNRTI resistant mutants, Y181C and K103N/ L100V. Biochemical studies showed that these compounds preferentially inhibited non-directed and DNA 3'-end directed RNH cleavages. Most of the compounds that were able to inhibit RT-RNH activity were also able to inhibit with a greater potency the RNH activity of the p15-EC RT RNH domain fragment, including compounds **15** and **25** having RNH IC₅₀ values of $0.43 \pm 0.04 \mu\text{M}$ and $0.032 \pm 0.004 \mu\text{M}$, respectively. Both compounds had antiviral activity against HIV-1 with EC₅₀ values of $10 \pm$

3 μ M and 1.4 ± 0.6 μ M for compounds **15** and **25**, respectively. Order of addition experiments showed that potent inhibition required pre-incubation of the enzyme with the inhibitor; inhibitory potency substantially decreased if the RNA/DNA substrate was present prior to inhibitor addition. Furthermore, inhibition was competitive with respect to the RNA/DNA substrate, suggesting an active site binding mode.

2.2 INTRODUCTION

Previous research within our laboratory (3, 9, 35, 43, 84) and other groups (17, 32, 83) have identified several hydrazone inhibitors of HIV-1 RT-RNH activity, suggesting that small molecules with the hydrazone functionality could provide great leads for new RNHI discovery. Therefore, in an attempt to investigate this promising observation a small commercial library of 5,296 hydrazone/hydrazine compounds were evaluated for HIV-1 RT RNH inhibition. The library screening yielded 1,141 confirmed hits (≤ 50 % inhibition at the 10 μ M screening concentration) with a hit rate of 22 %, indicating hydrazone/hydrazine small molecules as an important class of RNHIs. A variety of different hydrazone pharmacophore classes were identified among the actives, including the fluorene-9-ylidene hydrazine. The complete details of the screening exercise will be provided in the subsequent pages.

2.3 MATERIALS AND METHODS

2.3.1 Reagents

A library of 5,296 compounds with the hydrazone/hydrazine functionality was obtained from Life Chemicals Inc (Burlington, ON, Canada). An additional 96 fluoren-9-ylidene hydrazine compounds were obtained from Enamine Ltd. (Kiev, Ukraine). The expanded library contained 118 compounds with the fluoren-9-ylidene hydrazine functionality, a complete list of all the compound evaluated as inhibitors of RT-RNH activity can be found within appendix A: *Supplementary Table 1*. The RNA and DNA oligonucleotides for the RNH high-throughput enzyme assay (HTS-1, HTS-2 and HTS-3) and dual labeled gel based RNH assay (Duplex 2 and Duplex4) were obtained from TriLink Biotechnologies Inc. (San Diego, CA), in which RNA/DNA duplexes were annealed in a 1:1 ratios. The [³H]-TTP was obtained from Perkin-Elmer (Waltham, Ma) and template/primer (poly(rA)-oligo(dT)₁₆) was obtained from Midland Certified Reagents (Midland, Tx) for the RT polymerase enzyme assay. The 4-MUG (4-methylumbelliferyl- β -D-galactopyranoside), a β -galactosidase fluorescent substrate was obtained from Sigma-Aldrich (St. Louis, MO). P4R5 HeLa fibroblast cells were a generous gift from Dr. John Mellors (University of Pittsburgh) and originally obtained from Dr. Ned Landau (the Salk Institute for Biological Studies, La Jolla, CA). All reagents used for all biochemical and virological experiments were of the highest grade possible.

2.3.2 Protein Expression and Purification

2.3.2.1 Expression and Purification of HIV-1 RT

Plasmid p6HRT, encoding for wild-type p66/p51 heterodimeric HIV-1 RT was a gift from Dr. S. Le Grice, NCI-Fredrick, Frederick, MD, USA (60), where expression and purification of was essentially carried out as previously described (27). NNRTI resistant mutant, Y181C and K103N/ L100V were created using site directed mutagenesis.

2.3.2.2 Expression and Purification of the p15-EC RT RNH Domain Fragment

Plasmid pCSR231 encoding wild-type HIV-1 p15-EC RT RNH domain fragment containing an alpha helical substrate-binding loop derived from *E. coli* RNase HI was a generous gift from Dr. Daria Hazuda (Merck, West Point, PA, USA (54, 83, 89). The protein was over expressed in transformed *E. coli* cells, in which purification was carried out as described later.

2.3.3 RT Polymerase Enzyme Assay

Reverse transcriptase RNA-dependent DNA polymerase activity was measured as previously described (9), briefly a fixed timed assay of 20 minutes at 37°C was carried out with a reaction mixture (50µl total volume) of 50 mM Tris-HCl (8.0 pH), 60 mM KCl, 10 mM MgCl₂,

8.6 nM wild type RT, 40 nM of template/primer (poly(rA)-oligo(dT)₁₆), and 11.2 μ M of [³H]TTP substrate. Inhibitors were dissolved in 100% DMSO, while aliquots of inhibitors added to the reaction mixture were added such that the final DMSO concentrations were no more than 1% with inhibitor concentrations ranging from 0.2-25 μ M with at least six concentrations. Reactions were quenched by 200 μ l ice cold 10 % TCA containing 20 mM sodium pyrophosphate and filtered using a 1.2 μ M glass fiber filter 96-well plates (Millipore) followed by sequentially wash with 10% TCA and ethanol. The extent of radionucleotide incorporation was determined by liquid scintillation spectrometry, using a 1450 Microbeta scintillation counter (Perkin Elmer). The IC₅₀ values were determined as described below with the RNH FRET high-throughput enzyme assay using SigmaPlot software (version 11.0, Systat Software Inc., San Jose, CA).

2.3.4 High-Throughput Screening Substrates for RNH activity

Table 2: Nucleic Acid Substrates for RNH FRET High-Throughput Enzyme Assay

Substrate	Sequence	Comments
HTS-1	5'-gaucugagccugggagcu -3'-fluorescein RNA 3'-CTAGACTCGGACCCTCGA -5'-Dabcyl DNA	Non-directed substrate
HTS-2	5'-cugguagaccagaucugagccugggagcu-3'-fluorescein RNA 3'-GGTCTAGACTCGGACCCTCGA-5'-Dabcyl DNA	DNA 3'-end directed substrate
HTS-3	5'-accagaucugagccugggagcu-3'-fluorescein RNA 3'-GACCAATCTGGTCTAGACTCGGACCCTCGA-5'-Dabcyl DNA	RNA 5'-end directed substrate

Three high-throughput substrates (HTS) (*Table 2*) were used in order to probe for specific modes of RT RNH cleavages (discussed in Chapter 1, section 1.3.3) in a previously described rapid fluorescence based assay (26). A non-directed cleavage substrate (HTS-1) was designed to probe for inhibition of non-directed RNH cleavages, since the RNA/DNA hybrid is 3' and 5' blunt ended. The DNA 3'-end directed cleavage substrate (HTS-2) was designed to probe for inhibition of polymerase dependent RNH cleavages, since the 3'-end of the DNA strand of the RNA/DNA hybrid is recessed. The last substrate, HTS-3 was designed as RNA 5'-end directed cleavage substrate in order to probe for inhibition of polymerase independent cleavages, since the 5'-end of the DNA strand of the RNA/DNA hybrid is recessed.

2.3.5 RNH FRET High-Throughput Enzyme Assay

RNH activity of the RT heterodimer (wild type and NNRTI mutants, Y181C or K103N/L100V) and wild type p15-EC RT RNH domain fragment were determined using a previously described rapid fluorescence based assay (26). RT RNH high-throughput enzyme studies were conducted under both a fixed time point and kinetic time point, in which the fluorescence was monitored in real time.

The fixed time point assay was carried out using the Precision 2000 automatic pipetting system from BioTek Instruments, Inc. (Winooski, VT) at room temperature to carry out and quench the reaction after a 10 minute reaction time with 0.1 M EDTA (8.0 pH). The automatic pipetting system was not used for the kinetic studies. RT experimental reactions contained 8.5 nM enzyme to 250 nM HTS-1, HTS-2 or HTS-3 RNA/DNA substrate (50, 150 and 350 nM

for kinetic studies) in a buffer of 50 mM Tris-HCl (8.0 pH), 60 mM KCl, 1 mM MgCl₂ and 1% DMSO. The inhibitors were pre-incubated with the enzyme at room temperature for ~5 minutes, unless otherwise mentioned. Inhibitor concentrations ranged from 0.2-25 µM with at least six concentrations, in which the fluorescence intensity was quantified using BioTek Synergy4 microplate reader (BioTek Instruments, Inc., Winoosk, VT) at an excitation wavelength of 485 nm and an emission wavelength of 528 nm. The kinetic assay had a lag time of ~45 seconds, in which a time point was obtained every 60 seconds up to 15 minutes. The rate of RNH cleavages was obtained by fitting the linear portion (45-360 seconds) of the fluorescent signal with a non-linear regression equation ($y = mx + b$) using SigmaPlot software (version 11.0, Systat Software Inc., San Jose, CA) for each inhibitor and substrate concentration. A dixon plot was used to determine the type of RNH inhibition and the inhibition constant (K_I) was obtained with the equation $K_I = (IC_{50}) / (1 + S/K_m)$, being that S is the substrate concentration (250 nM) and K_m is the Michaelis-Menton constant ($K_m = 54$ nM with 8.5 nM RT and 50-350 nM HTS-1, under the same experimental conditions). The IC_{50} value used was from previously determined values during the fixed time point reactions, being 0.4 ± 0.03 µM for compound **25**.

The p15-EC RT RNH domain fragment reaction mixture contained 8 nM enzyme to 500 nM HTS-1 substrate in a buffer of 50 mM Tris-HCl (8.0 pH), 5 mM KCl and 2 mM MnCl₂ at room temperature (using the automatic pipetting system). The reactions were carried out identical to the reactions with RT heterodimer including pre-incubation and reaction times at room temperature, except reactions were initiated upon addition of substrate in the presence of Mn⁺² instead of Mg⁺². Inhibitor concentrations ranged from 0.2-25 µM with at least six concentrations, unless the IC_{50} value was determined to be less than 0.2 µM in which new dose responses range of 6.3-800 nM with at least six concentrations were used.

IC₅₀ values were determined by fitting the dose response data to a non-linear regression equation $y = (a*b)/(b+x)$, with the SigmaPlot software (version 11.0, Systat Software Inc., San Jose, CA). x is defined as the inhibitor concentration, y is the relative fluorescence units (RFU) resulting from RNH cleavage, a is defined as the maximum RFU value and b is defined as the IC₅₀ value in which $b = x*50(x,y)$. All experiments were done in at least duplicate in which each experiment was repeated at least twice, the average and standard deviations were calculate from the each individual experiments that was done in at least duplicate.

2.3.6 Gel Based Dual Labeled RNH Assay

Table 3: Nucleic Acid Substrates for the Gel Based Dual Labeled RNH Assay

Substrate	Sequence
RNA 5'-end directed substrate (<i>Duplex 2</i>)	RNA 5'- Cy3 -ccacugcuagagauuuucgacac- Cy5 DNA 3'-GTCCAGGACAAGCCCGCGGTGACGATCTCTAAAAGCTGTGACTG-5'
DNA 3'-end directed substrate (<i>Duplex 4</i>)	RNA 5'- Cy3 -gucaguguggaaaaucucuagcaguggcgcccgaacagggaccugaccag- Cy5 DNA 3'-GGCTTGTCCTGGACTGGTC-5'

Reactions were carried out at room temperature for ~10 minutes with 50 nM RNA/DNA Substrate, 10 nM wild type RT, 1 mM MgCl₂, 50 mM Tris-HCl (8.0 pH), 50 mM KCl and 0.5 mM EDTA (8.0 pH) and 1% DMSO. Two different substrates (*Table 3*) were used to probe for inhibition of specific modes of RT-RNH cleavages, including RNA 5'-end directed cleavages (duplex 2, analogous to HTS-3) and DNA 3'-end directed cleavages (duplex 4, analogous to

HTS-2), enabling probing of polymerase independent and dependent cleavages, respectively. All reactions were carried out in presence of RNase free water with 0.5 mM EDTA (8.0 pH) in order to prevent any non-specific cleavages prior to the initiation of the reaction. Inhibitor concentrations were at 5 μ M for compounds **6**, **15** and **25**. Reactions were quenched with a 1:1 mixture of 1% formamide and 10 mM EDTA (pH 8.0) at time point of 0, 0.5, 1, 1.5, 2, 2.5, 5 and 10 minutes. A 12% PAGE SDS gel with 7 M urea was used to separate the cleavage products. The Typhoon 9400 PhosphorImager, (version 3.0.0.0, Amersham Bioscience, Sunnydale, CA) with the Fluorochrome Separation application, (version 1.0.0.1) and ImageQuant application (version 1.0.01) was used to obtain an image of the gels, separate the cy3 and cy5 fluorescent signals and quantify the bands at 100 microns.

2.3.7 RNH Order of Addition Studies

Order of addition studies were carried out with both the kinetic RNH FRET high-throughput enzyme assay and the gel based dual labeled RNH assay. Four different enzyme pre-incubation conditions were evaluated, including enzyme-inhibitor, enzyme-substrate, enzyme-substrate-inhibitor and without enzyme pre-incubation. Enzyme-inhibitor pre-incubation (EI) studies were carried out as described under section 2.3.5, briefly the inhibitor was pre-incubated with the enzyme for ~5 minutes at room temperature and initiated by addition with a substrate-metal mixture. Enzyme-substrate pre-incubation (ES) experiments were carried out for ~5 minutes at room temperature and the reaction was initiated by the addition of the inhibitor-metal reaction mixture. During the enzyme-substrate-inhibitor pre-incubation (ESI) experiments, the enzyme was added to a mixture of inhibitor with the substrate and allowed to pre-incubate for ~5 minutes

at room temperature, in which the reaction was initiated with the MgCl_2 mixture. Experiments without enzyme pre-incubation (E) were carried out by initiating the reaction by adding the enzyme to a mixture of the inhibitor, substrate and Mg^{+2} . Experimental conditions for both the kinetic RNH FRET high-throughput enzyme assay and the gel based dual labeled RNH assay were carried out identical (except noted in the preceding), as stated in the above sections 2.3.6 and 2.3.7, respectively. The kinetic RNH FRET high-throughput enzyme assay was carried for a total of 10 minutes, in which the rates of RNH cleavages was obtained by fitting the linear portion of the fluorescence data from 47-347 seconds. Inhibitor concentrations for wild type RT with HTS-1 reaction ranged from 0.05-25 μM , while with the p15-EC RT RNH domain fragment with HTS-1 ranged from 0.002-5 μM . The gel based dual labeled RNH assay was carried out for 1 minute at 26°C , in order to prevent additional RNH cleavages beyond the primary cut.

2.3.8 HIV-1 Antiviral Studies

Inhibitors from the fluorene-9-ylidene hydrazine library were accessed for HIV-1 antiviral activity with the P4R5 cell line through a single-cycle viral replication fluorescence-based microplate β -galactosidase detection assay (5 or 25 ng of viral p24 per 5×10^3 cells per well). P4R5 HeLa fibroblast cells, express endogenous CXCR4, along with stably transfected CD4, CCR5 and a β -galactosidase reporter gene under the control of an HIV LTR promoter (69). The cell line was maintained in DMEM/10% FBS and supplemented with 0.5 $\mu\text{g}/\text{ml}$ puromycin. An infectious molecular clone of IIIB (HxB2) strain of HIV-1 was encoded within a pSVC21-BH10

plasmid, which carries an SV40 origin of replication for expression in 293T and COS-7 cells (26). Calcium phosphate co-precipitation transfection with 293T cells was used to prepare the HIV-1 virus particles, then 60 hours post-transfection the virus containing culture supernatant was collected and clarified by centrifugation (3000x g, 1 hour at 4°C). Viral quantification was done through quantification of the levels of HIV-1 p24 antigen, in which the virus particle infectivity was determined by using normalized quantities of HIV-1 p24 antigen contents with P4R5 cells as targets. HIV-1 virus particle stocks were then aliquoted and stored at -80°C until use.

Inhibitors were pre-incubated with the P4R5 cells 24 hours prior to HIV-1 addition with inhibitor concentration ranging from 0.5-25 μ M, in which 48 hours post-infection virus-containing culture supernatant was removed. The cells were lysed in 100 μ L lysis buffer of 60 mM Na₂HPO₄, 40 mM NaH₂PO₄ (pH 7.2), 1 mM MgSO₄, 100 mM mercaptoethanol, 2% triton [v/v] X-100 for 1 hour at 37°C, in which reactions were initiated by a final concentration of 0.5 mM 4-MUG (50 μ L) and incubated for 1 hour at 37°C. Reactions were quenched with 150 μ L of 0.2 mM Na₂CO₃ (11.2 pH). BioTek synergy multi-mode microplate reader (BioTek Instruments, Inc., Winooski, VT) was used to quantify the fluorescence intensity using an excitation wavelength of 355nm and an emission wavelength of 480nm.

2.4 RESULTS

2.4.1 Initial Identification and Expansion of the Fluoren-9-ylidene Hydrazine Library

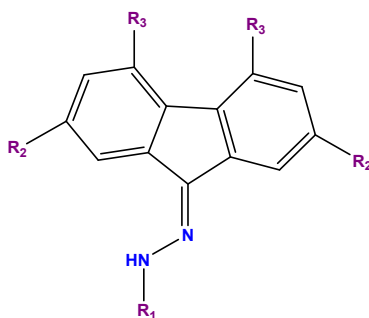


Figure 19. Fluoren-9-ylidene Hydrazine Pharmacophore

The fluoren-9-ylidene hydrazine pharmacophore (*Figure 19*) was identified from a screening of a biased library of 5,296 compounds using a high-throughput FRET RNH enzyme assay (26). This screening identified 338 compounds with an 80% or greater inhibitors of HIV-1 wild type RT-RNH activity at 10 μM . The fluorene-9-ylidene hydrazine pharmacophore was identified within this highly active subset of compounds. The potency and novelty of the fluorene-9-ylidene hydrazine inhibitor class warranted more detailed study.

Of the initial 33 fluoren-9-ylidene hydrazine compounds from the larger library, 70% inhibited RT-RNH activity with an IC_{50} range of 340 ± 0.7 nM to 13 ± 0.1 μM , where only 10 of the compounds had no RT-RNH inhibition up to 25 μM . In addition, it was also identified that these compounds inhibited the p15-EC RT RNH domain fragment with nanomolar IC_{50} range, indicating this pharmacophore class as remarkably active RNHIs that directly interact with the RNH domain, since they were also able to inhibit the RNH domain. From these promising

results, the fluorene-9-ylidene hydrazine library with an additional 96 compounds, creating a library was expanded with a total of 118 discrete fluorene-9-ylidene hydrazine analogues (there were duplicate compounds from the two sources)

2.4.2 Characterization of the Expanded Fluorene-9-ylidene Hydrazine Library for RNH Inhibition with HIV-1 Wile Type RT

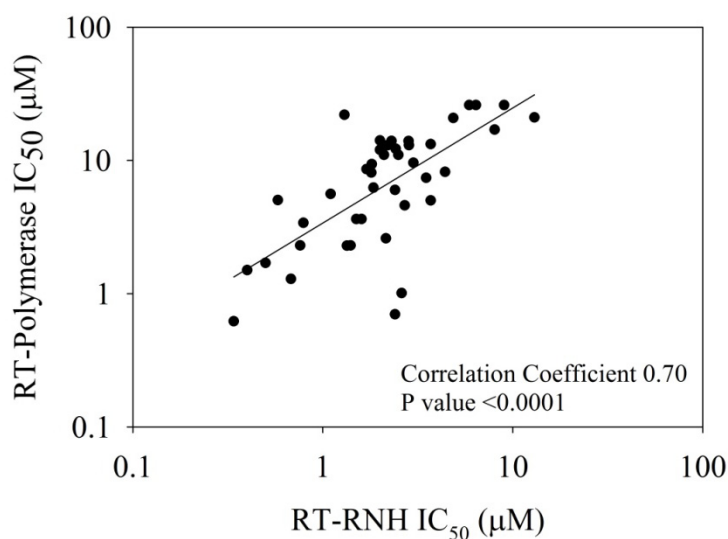
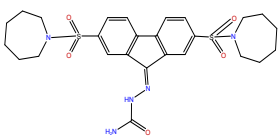
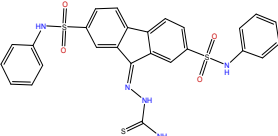
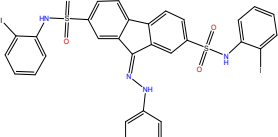
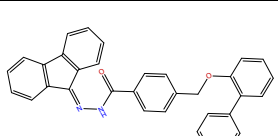


Figure 20. Correlation Between RT-RNH and Pol Inhibition.

Table 4: Most Active RNHIs from Each Subgroup

Subgroup	Compound	Structure	RT-RNH IC ₅₀ (μM)	RT-Pol IC ₅₀ (μM)
A	1		1.1 ± 0.2	5.6 ± 0.6
B	15		0.34 ± 0.07	0.62 ± 0.06
C	25		0.4 ± 0.03	1.5 ± 0.1
D	58		1.3 ± 0.2	2.3 ± 0.2

Biochemical experiments were carried out using the fixed time point high-throughput FRET RNH enzyme assay to evaluate for HIV-1 RT RNH inhibition. Screening of the expanded fluorene-9-ylidene hydrazine library for inhibitors of HIV-1 reverse transcriptase ribonuclease H activity, resulted in a hit rate of 55% (65 compounds) with IC₅₀ values < 10 μM. The library of fluorene-9-ylidene hydrazine compounds were fundamentally monofunctional for RT-RNH inhibition, since only 25 (21%) of the compounds had IC₅₀ values < 10 μM with inhibiting RT-polymerase activity. In fact the majority of the compounds, 78 (66%) were unable to inhibit RT RDDP activity at maximum tested concentration. *Figure 20*, shows that the fluorene-9-ylidene hydrazine compounds overall are better inhibitors of RT-RNH activity versus polymerase

activity, in which 58% of the RNH hit compounds had IC_{50} values within the 0.34-5 μM concentration range, while the polymerase IC_{50} values are more spread out with 90% of the hit compounds ranging from 0.62-15 μM concentration, excluding a few outliers. All of the compound's HIV-1 RT-RNH and polymerase IC_{50} values and corresponding structures for the full fluorene-9-ylidene hydrazine library can be found in appendix A: *Supplementary Table 1*. The most potent HIV-1 RT RNHIs were compounds **15** and **25** (*Table 4*), with an IC_{50} values of $0.34 \pm 0.07 \mu M$ and $0.4 \pm 0.03 \mu M$, respectively. In addition, both compounds also inhibited HIV-1 RT-polymerase activity with an IC_{50} of $0.62 \pm 0.06 \mu M$ for compound **15** and $1.5 \pm 0.1 \mu M$ for compound **25**.

2.4.3 Four Structural Subgroups of the Fluorene-9-ylidene Hydrazine Library

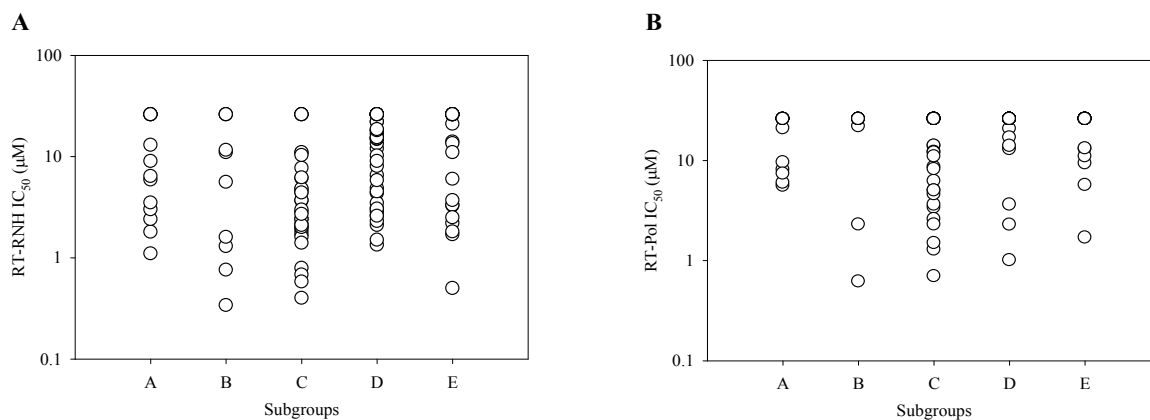


Figure 21. RT-RNH and polymerase Inhibition per Subgroup. A) RT-RNH inhibition per subgroup and B) RT-polymerase inhibition per subgroup.

Table 5: Subgroups of the Fluoren-9-ylidene Hydrazine Library

	Subgroup	# RNHIs	RT- RNH Inhibition		RT-Pol Inhibition	
			# Actives (< 10 μ M IC ₅₀)	IC ₅₀ Range (μ M)	# Actives (< 10 μ M IC ₅₀)	IC ₅₀ Range (μ M)
A	2-(9 <i>H</i> -fluoren-9-ylidene)hydrazinecarboxamids	14	8 (57%)	1.1-9	4 (29%)	5.6-8.1
B	2-(9 <i>H</i> -fluoren-9-ylidene)hydrazinecarbothioamide	10	5 (50%)	0.34-5.6	2 (20%)	0.62-2.3
C	1-(9 <i>H</i> -fluoren-9-ylidene)-2-phenylhydrazine	33	26 (79%)	0.4-7.7	13 (39%)	0.7-8.6
D	<i>N'</i> -(9 <i>H</i> -fluoren-9-ylidene)benzohydraside	38	17 (45%)	1.34-9	3 (8%)	1.0-3.6
E	Other	23	9 (39%)	0.5-6	3 (13%)	1.7-9.4

Analysis of the fluoren-9-ylidene hydrazine library as RNH inhibitors identified four primary subgroups based on the functional group directly attached to the hydrazine (R₁, Fig 20), along with an additional 23 compounds classified as other. The characteristics of each subgroup for HIV-1 RT-RNH and polymerase inhibition are found in *Table 5*.

The first subgroup (A), 2-(9*H*-fluoren-9-ylidene)hydrazinecarboxamids has a carboxamide substituent at R₁. This subgroup consists of 14 compounds and is the second to smallest subgroup. Subgroup A produced 8 (57%) compounds that inhibit RT-RNH activity with IC₅₀ values ranging from 1.1-9 μ M, making this subgroup the third most active subgroup as a fluoren-9-ylidene hydrazine RNHI. This subgroup had 4 (29%) compounds that inhibit RT-

polymerase activity with IC₅₀ values ranging from 5.6-8.1 μ M. As seen in *Figure 21A*, IC₅₀ value for RT-RNH inhibition for this subgroup is centered around 1.1-5 μ M, excluding a few outliers. The RT-polymerase inhibition for this subgroup, as seen in *Figure 21B*, is centered around IC₅₀ values of 5.6-10 μ M. The most active compound from this subgroup (compound **1**) had an RT-RNH IC₅₀ of 1.1 ± 0.2 μ M and RT-polymerase IC₅₀ of 5.6 ± 0.6 μ M (appendix A, *Supplementary Table 1*).

The second subgroup (B), 2-(9*H*-fluoren-9-ylidene)hydrazinecarbothioamide has a carbothioamide substituent at R₁. This subgroup consists of 10 compounds and is the smallest subgroup of the library. As seen in *Figure 21A*, the RT-RNH inhibition is centered around 0.34-3 μ M IC₅₀ value range, while most of the compounds from this subgroup were inactive inhibitors against RT-polymerase activity (*Figure 21B*). Of the 10 compounds, 5 (50%) inhibited RT-RNH activity with IC₅₀ values ranging from 0.34-5.6 μ M. Furthermore, the compounds within this subgroup are poor inhibitors of RT-polymerase activity, in which only 2 (20%) compounds inhibited with an IC₅₀ less than 10 μ M. This subgroup also contains one of the most active fluoren-9-ylidene hydrazine RNHIs (compound **15**). Compound **15**, inhibits RT-RNH activity with an IC₅₀ value of 0.34 ± 0.07 μ M and RT-polymerase activity with an IC₅₀ value of 0.62 ± 0.06 μ M (appendix A, *Supplementary Table 1*).

The third subgroup (C), 1-(9*H*-fluoren-9-ylidene)-2-phenylhydrazine has a phenyl group substituent at R₁. Subgroup C is the second largest subgroup with 33 compounds and the most active subgroup as an RNHI. Of the 33 compounds, 26 (79%) inhibited RT-RNH activity and 13 (39%) of the compounds inhibit RT-polymerase activity (*Table 5*), making this subgroup the most bifunctional subgroup from the whole library. The RT-RNH IC₅₀ values centered around 0.4-5 μ M IC₅₀ values (*Figure 21A*), while the polymerase IC₅₀ values were centered around 0.4-5

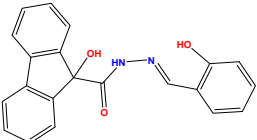
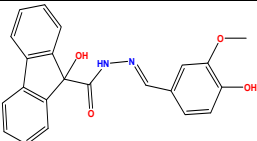
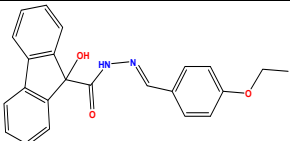
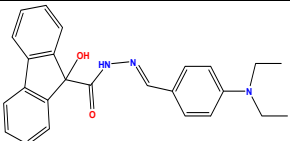
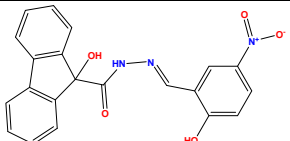
μM IC_{50} (*Figure 21B*). This subgroup also contains one of the most potent RT-RNHIs (compound **25**) with an RT-RNH IC_{50} value of $0.4 \pm 0.03 \mu\text{M}$ and a RT-polymerase IC_{50} value of $1.5 \pm 0.03 \mu\text{M}$ (appendix A: *Supplementary Table 1*).

The fourth subgroup (D), *N'*-(9*H*-fluoren-9-ylidene)benzohydrazide has an *N*-acylhydrazone substituent at R_1 . This subgroup consists of 38 compounds and is the largest subgroup for the fluoren-9-ylidene hydrazine library but it is the least active group as an RNHI. Of the 38 compounds, 17 (45%) inhibit RT-RNH activity with IC_{50} values of 1.34-9 μM (*Table 5*). As seen in *Figure 21A*, the RT-RNH inhibition was spread out and not localized around a specific IC_{50} range. This subgroup is primarily monofunctional as an RT-RNH inhibitor, since only 3 (8%) of the compounds inhibited RT-polymerase activity with IC_{50} values ranging from 1.0-3.6 μM . *Figure 21B*, further shows that for the compounds that do have RT-polymerase inhibitory activity, with IC_{50} values that are spread out. The most active compound from this subgroup was compound **58** with an RT-RNH IC_{50} of $1.3 \pm 0.2 \mu\text{M}$ and RT-polymerase IC_{50} of $2.3 \pm 0.2 \mu\text{M}$ (appendix A: *Supplementary Table 1*).

The remaining 23 compounds from the fluoren-9-ylidene hydrazine library that were not separated into any of the other four functional subgroups were clumped into a fifth subgroup, referred to as "Other " (E). Compounds within this subgroup lacked any well-defined structural similarities for substituents at R_1 . Most of the compounds within this subgroup were mainly monofunctional RNHIs, in which 9 (39%) of the compounds were active with IC_{50} values ranging from 0.5-6 μM . The few compounds that are bifunctional as RT-RNH and polymerase inhibitors, are the least active compounds against RT-polymerase activity compared to the rest of the library, with IC_{50} values ranging from 1.7-9.4 μM .

2.4.4 Structural Moieties Significant for RT-RNH Inhibition

Table 6. 9H-(fluoren-9-ylidene)-2-hydropranolcarboxylhydrazines Compounds

Compounds		RT-RNH IC ₅₀ (μM)	RT-Pol IC ₅₀ (μM)
119		>25	>25
120		>25	>25
121		>25	>25
122		>25	>25
123		11 ± 0	>25

Structure activity analysis of the fluoren-9-ylidene hydrazine library based on their inhibition of full length RT-RNH (appendix A: *Supplementary Table 1*) has resulted in the identification of some structural moieties that enhance RT-RNH inhibition. A phenyl group substituent at the R₁ position as with compound **25** or with a thioamide linker between the hydrazine and phenyl group substituent, as seen with compound **15**, enhances RNH inhibition of RT RNH activity. Comparison of compounds **20** (11 ± 0.5 μM RNH IC₅₀) and **23** (> 25 μM RNH IC₅₀) indicates

that replacement of the R₁ phenyl group with a non-aromatic ring system or aliphatic chain has a detrimental effect on RT-RNH and polymerase inhibition, in which substitution with an aliphatic group completely abrogates inhibition.

In addition, extension of the R₂ position with a sulfonamido-phenyl ring substituent results in the most potent inhibition of RT RNH and polymerase inhibition, as seen with compounds **15** and **25**. This observation is evident when comparing two compounds, **25** and **44** in which only compound **25** has a phenyl substituent added to the R₂ sulfonamido and compound **44** lacks the phenyl group. Compound **25** is a more potent RT-RNHI with an IC₅₀ of 0.4 ± 0.03 μ M, while compound **44** has an approximate ten-fold decrease in RNH inhibition with a 4.4 ± 0.3 μ M IC₅₀. Furthermore, the RT-polymerase inhibition with these two compounds has a six-fold difference, where compound **25** has a greater RT-polymerase inhibition of 1.5 ± 0.1 μ M IC₅₀ and compound **44** has an IC₅₀ of 8.2 ± 0.7 μ M. Additional observations with compounds **31** and **37** with aliphatic substitutions added to the R₂ sulfonamido-phenyl ring results in a loss in RT-RNH IC₅₀ values of 1.7 ± 0.1 μ M and 2.4 ± 0.5 μ M, respectively. These structural activity relationship observations suggest that a bulky ring system at the R₂ sulfonamido position is required for enhancement in RNH inhibition. Compounds **35** and **43** with a bulky ring system without aromaticity, as seen with the phenyl substitution at the R₂ sulfonamide position have an additional loss in RT-RNH inhibition with IC₅₀ values of 2.1 ± 0.2 μ M and 3.7 ± 0.4 μ M (respectively). These further observations suggest that it is not just a bulky ring system, which is necessary for enhancement in RT-RNH inhibition but also the aromatic functionality of the sulfonamido-phenyl ring that is necessary. The necessity of the R₂ sulfonamido-phenyl ring substitution is further supported by the fact that compound **15** from subgroup B, is the only compound from that subgroup that has the R₂ sulfonamido-phenyl ring substitution and is the

only compound within subgroup B that has significant RT-RNH inhibition. It is further seen that the ortho iodine addition to the R₂ sulfonamido-phenyl ring system (compound **25**) is responsible for the enhancement in RT-RNH inhibition versus the iodine itself; this is evident when comparing compounds **25** and **30** (RT-RNH IC₅₀ of 1.6 ± 0.2 μM) with either an ortho iodine or para chloride additions.

During initial screening of the hydrazone/hydrazine library (5,592 compounds) where the fluoren-9-ylidene hydrazine pharmacophore was first identified (*Figure 19, subsection 1.4.1*), another subset of five compounds [*9H*-(fluoren-9-ylidene)-2-hydropranolcarboxylhydrazines] having a similar structure as the fluoren-9-ylidene hydrazine pharmacophore were identified, as seen in *Table 6*. These compounds have both of the structural components of the fluoren-9-ylidene hydrazine pharmacophore, namely the fluorene and hydrazine functional groups but have an additional 2-hydropranolcarboxyl linker is between the fluorene and hydrazine functional groups. Addition of the 2-hydropranolcarboxyl linker results in a complete loss of inhibition potency. This suggests that comparison of the planar fluoren-9-ylidene hydrazone linkage to the tetrahedral geometry is detrimental to inhibition.

2.4.5 Fluoren-9-ylidene Hydrazine Library RNH Inhibition of the p15-EC RT RNH Domain Fragment

Biochemical experiments were undertaken using the fixed time high-throughput FRET RNH enzyme assay to evaluate the fluoren-9-ylidene hydrazine library for inhibiting the RNH activity of p15-EC RT RNH domain fragment. Evaluating inhibition of the p15-EC RT RNH domain fragment enables direct confirmation that the fluoren-9-ylidene hydrazine compounds directly interact with the RNH domain, since the p15-EC is a modified isolated RNH domain of HIV-1

RT in which an extended *E. coli* helix-loop was added in order to restore activity to the enzyme (54). Screening of the library (118 compounds) resulted in a hit rate of 78% (99 compounds), having IC₅₀ values < 10 µM, as inhibitors of RNH activity (complete list of the IC₅₀ values can be found under appendix A: *Supplementary Table 1*). These results suggest the RT-RNH inhibition of the fluoren-9-ylidene hydrazine compounds is the result of directly interacting with the RNH domain, in fact the compounds were more potent RNHIs with the p15-EC RT RNH domain fragment versus full length RT. As seen with *Figure 22A*, majority of the compounds are able to inhibit the RNH domain fragment with 56% of the actives localized around IC₅₀ values of 0.018-0.8 µM. A correlation is seen with being able to inhibit the p15-EC and full length RT (*Figure 22A*), excluding a few outliers. Of the 33 compounds within in subgroup C, 30 (91%) of them inhibited RNH activity (*Table 7*), with IC₅₀ values centered around 0.032-0.7 µM range (*Figure 22B*). A similar trend is seen with compounds from subgroups A and B, in which 7 (70%) compounds from subgroup B and 9 (64%) compounds from subgroup A inhibited RNH activity (*Table 7*). Subgroup D was the least potent group for RT-RNH inhibition but it was the second most potent subgroup with the p15-EC RT-RNH domain fragment, in which 30 (79%) of the compounds inhibited RNH activity with with IC₅₀ values ranging from 0.018-8.2 µM (*Table 7*). *Figure 22B*, further shows that the compounds from subgroup D were less localized and more spread out compared to the other subgroups, in which Subgroup D contains the most potent p15-EC RT RNH domain fragment inhibitor (compound **58**) with an IC₅₀ value of 0.018 µM (appendix A: *Supplementary Table 1*).

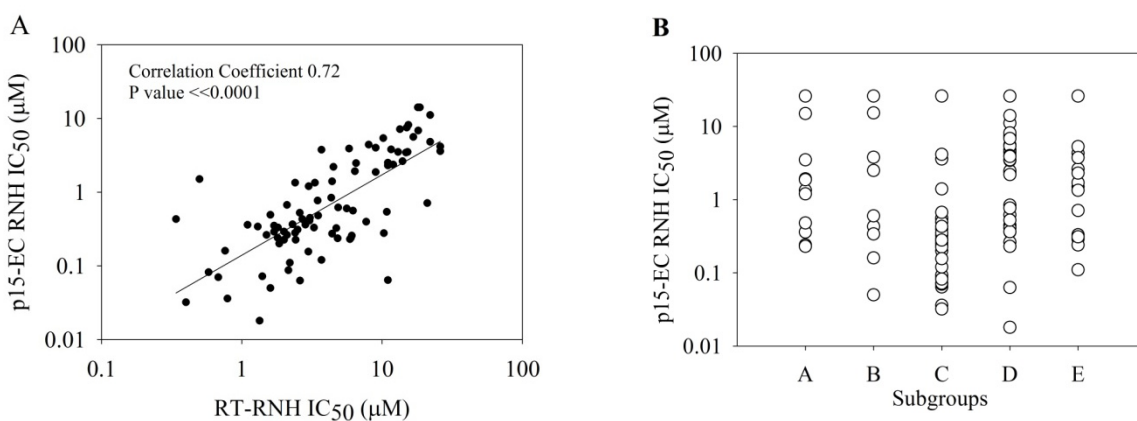


Figure 22. RNH Inhibition of the p15-EC RT RNH Domain Fragment. *A)* RNH inhibition correlation with the RNH domain fragment and length RT. *B)* RT-RNH inhibition per subgroup.

Table 7: Subgroup RNH Inhibition with the p15-EC RT RNH Domain Fragment

	Subgroup	# Compounds	p15-EC RT RNH Domain Fragment Inhibition	
			# Actives (< 10 μ M IC ₅₀)	IC ₅₀ Range (μ M)
A	2-(9H-fluoren-9-ylidene)hydrazinecarboxamids	14	9 (64%)	0.23-3.5
B	2-(9H-fluoren-9-ylidene)hydrazinecarbothioamide	10	7 (70%)	0.05-3.8
C	1-(9H-fluoren-9-ylidene)-2-phenylhydrazine	33	30 (91%)	0.032-4.2
D	N'-(9H-fluoren-9-ylidene)benzohydraside	38	30 (79%)	0.018-8.2
E	Other	23	16 (70%)	0.11-5.3

2.4.6 Fluoren-9-ylidene Hydrazine Compounds Preferentially Inhibit Non-directed and DNA 3'-end Directed Modes of RNH Cleavages

Table 8. Fluoren-9-ylidene Hydrazine Inhibition with Different HTS Substrates

Compound	RT-RNH HTS-1 IC ₅₀ (μM)	RT-RNH HTS-2 IC ₅₀ (μM)	RT-RNH HTS-3 IC ₅₀ (μM)
15	0.34 ± 0.07	0.47 ± 0.03	1.3 ± 0.3
25	0.4 ± 0.03	0.6 ± 0.1	1.9 ± 0.2

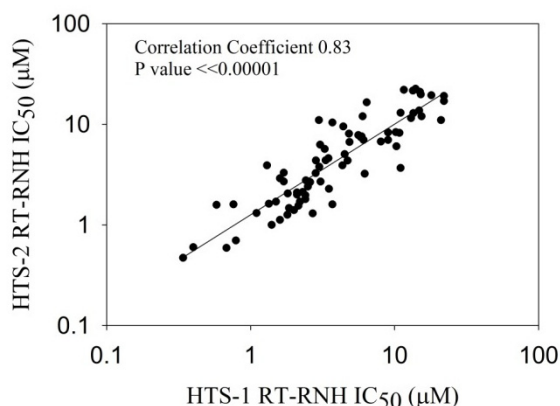


Figure 23. Correlation Between RT-RNH Inhibition with Non-directed and DNA 3'-end Directed Cleavage Substrates

The fluoren-9-ylidene hydrazine compounds were shown to be highly active inhibitors of RNH activity with full length RT, while also directly inhibiting the p15-EC RNH domain fragment, therefore the compounds were further evaluate for inhibiting specific modes of RT RNH cleavages (discussed within Chapter 1, under subsection 1.3.3). The fixed time point high-throughput FRET RNH enzyme assay was used to evaluate inhibition of specific modes of RT RNH cleavages using all three RNA/DNA substrates, HTS-1, HTS-2 and HTS-3 (*Table 2*).

The complete fluoren-9-ylidene hydrazine library was evaluated as RT-RNH inhibition with the non-directed (HTS-1) and DNA 3'-end directed (HTS-2) cleavage substrates. Screening of the library for non-directed RNH cleavages with HTS-1 resulted in a hit rate of 55% (IC_{50} values $< 10 \mu M$), while evaluation with HTS-2 resulted in a similar hit rate of 52%. A correlation was seen with the RT-RNH IC_{50} values with HTS-1 and HTS-2 substrates (*Figure 23*), such that individual IC_{50} values were insignificant for each other for the majority of the compounds, excluding a few outliers. The lack of preference for non-directed and DNA 3'-end directed RNH cleavages can further be seen with compounds **15** and **25** (*Table 8*), where compound **15** had an IC_{50} of $0.34 \pm 0.07 \mu M$ (HTS-1) and $0.47 \pm 0.03 \mu M$ (HTS-2), while compound **25** had an IC_{50} of $0.4 \pm 0.03 \mu M$ (HTS-1) and $0.6 \pm 0.1 \mu M$ (HTS-2). Neither compound **15** or **25** showed a preference for inhibiting non-directed and DNA 3'-end directed RNH cleavages, but both compounds were less potent with inhibiting RNA 5'-end directed RNH cleavages substrate (HTS-3), as seen in *Table 8*. The compounds had an approximate three-fold decrease in inhibitory potency with the RNA 5'-end directed cleavages substrate (HTS-3) compared to HTS-1 and HTS-2 cleavages, having IC_{50} values of $1.3 \pm 0.3 \mu M$ and $1.9 \pm 0.2 \mu M$ with HTS-3 substrate, respectively. These results indicate that the two most potent fluoren-9-ylidene hydrazine RT-RNH inhibitors, compounds **15** and **25** preferentially inhibit non-directed and DNA 3'-end directed cleavages over RNA 5'-end directed cleavages with the high-throughput FRET RNH enzyme assay.

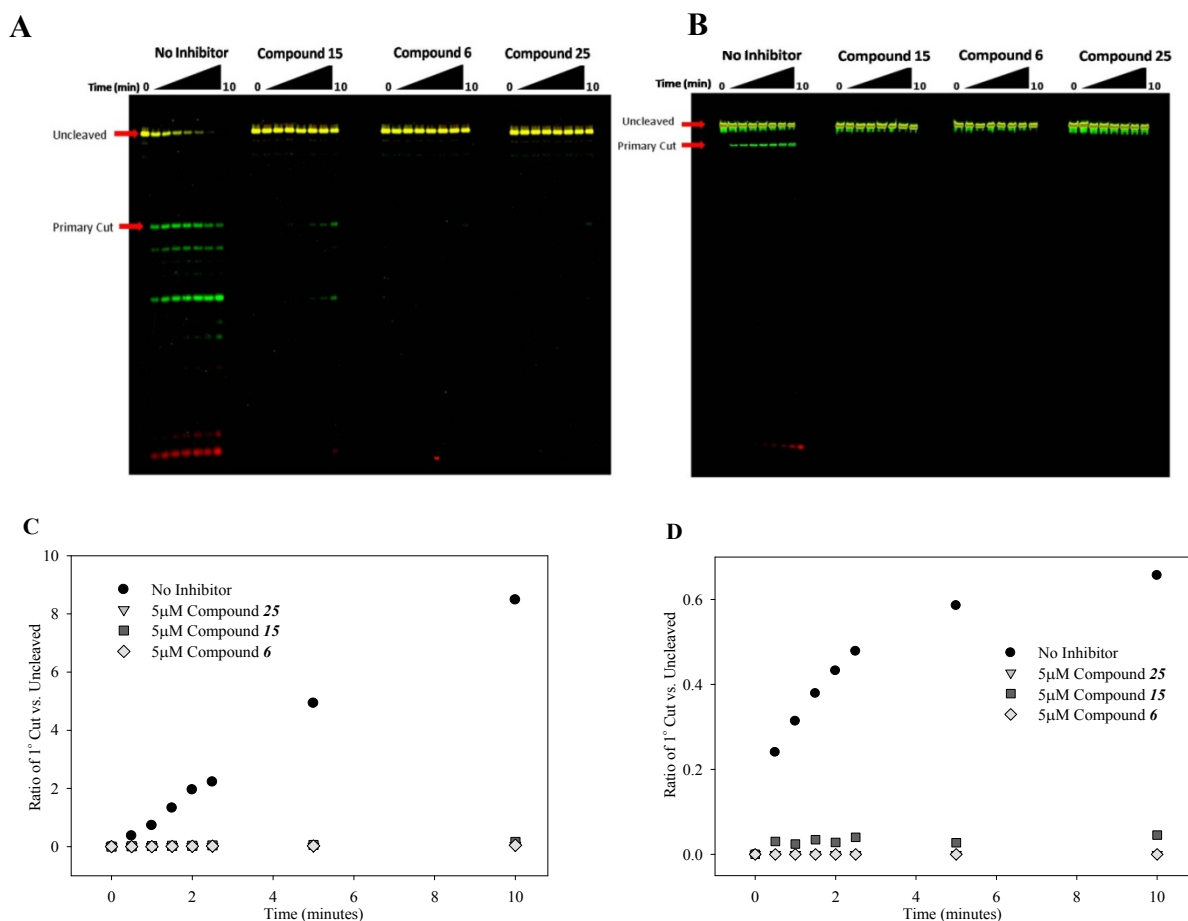


Figure 24. RT-RNH Inhibition of DNA 3'-end and RNA 5'-end directed RNH cleavages
A) RT-RNH inhibition of RNA 5'-end directed RNH cleavages (Duplex 2) and
B) RT-RNH inhibition of DNA 3'-end directed RNH cleavages (Duplex 4). **C)**
 Quantification of RNA 5'-end directed RT-RNH cleavages (Duplex 2) and **D)**
 Quantification of DNA 3'-end directed RT-RNH cleavages (Duplex 4).

A gel based dual labeled RNH assay was also used to evaluate preferential inhibition of either DNA 3'-end or RNA 5'-end directed cleavages with two different substrates, using a DNA 3'-end directed (duplex 4, analogous to HTS-2) or an RNA 5'-end directed (duplex 2, analogous to HTS-3) cleavages substrate, as seen in *Table 3*. The gel based assay was used in conjunction to the high-throughput RNH FRET enzyme assay because it can provide information on the

location of RNH cleavage and the RNA/DNA substrates are longer and perhaps more relevant to the viral RNA/DNA substrate compared to the high-throughput substrates (HTS). The most potent compounds from subgroups A (**6**), B (**15**) and C (**25**) were evaluated at 5 μM concentrations. All three compounds were able to inhibit RNA 5'-end directed cleavages (duplex 2) to various extents of inhibition potency (compounds **6** > **25** > **15**), whereas all three compounds were able to completely inhibit the DNA 3'-end directed cleavages (duplex 4) (Figure 24).

2.4.7 Fluoren-9-ylidene Hydrazine Type of RNH Inhibition is Competitive with Respect to the RNA/DNA Substrate

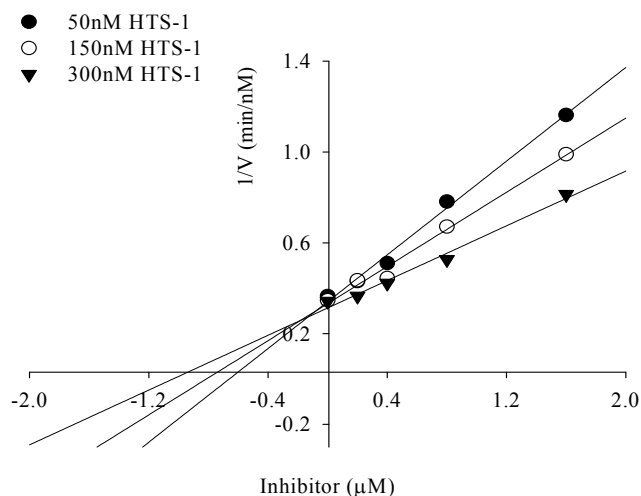


Figure 25. Dixon Plot of Compound 25 with Non-directed Cleavage Substrate

Kinetic high-throughput FRET RNH enzyme studies with compound **25** and the non-directed RT-RNH cleavage substrate (HTS-1) resulted in competitive RT-RNH inhibition with respect to the RNA/DNA substrate with a K_I of 0.14 μM , as seen in *Figure 25* with the Dixon-plot analysisⁱⁱⁱ. Competitive inhibition is evident, since linear fitting of the inhibition dose response data at three different substrate concentrations (50, 150 and 350 nM) cross and intersect beyond the y-intercept. Competitive inhibition with the substrate, suggests that the inhibitor competes with the substrate for binding within the RNH active site.

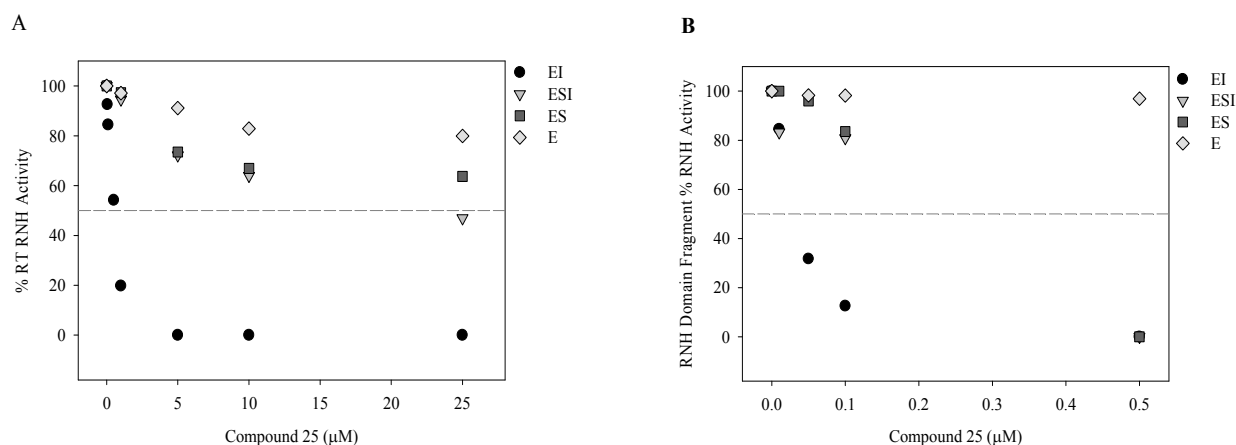


Figure 26. Order of Addition Influence on RNH Inhibition with Full Length RT and the p15-EC RT RNH Domain Fragment using the High-throughput FRET RNH Enzyme Assay. *A)* RT-RNH inhibition of non-directed RNH cleavages (HTS-1) with RT and *B)* RT-RNH inhibition of non-directed directed RNH cleavages (HTS-1) with RNH domain fragment (p15-EC). Enzyme-inhibitor pre-incubation is denoted by EI, enzyme-substrate pre-incubation (binary complex) denoted by ES, enzyme-substrate-inhibitor pre-incubation denoted by ESI and no enzyme pre-incubation denoted by E.

Additional order of addition studies were carried out to see if the inhibitors would be able to compete with the substrate and inhibit the binary complex form (RT-substrate), since previous

ⁱⁱⁱ Kinetic studies may not have been carried out under equilibrium conditions

kinetic studies discussed above showed compound **25** is competitive with respect to the RNA/DNA substrate. A kinetic high-throughput FRET RNH enzyme assay with full length RT and the p15-EC RT RNH domain fragment using the non-directed cleavage substrate (HTS-1) was carried out to evaluate RNH inhibition with four different reaction enzyme pre-incubation conditions. The first condition evaluated was pre-incubation of the inhibitor with the enzyme (denoted EI), prior to addition of the substrate and metal ions, allowing us to probe if the inhibitor could prevent essential enzyme-substrate interactions in order for RNH cleavages to occur. The second reaction condition was pre-incubation of the enzyme with a mixture of substrate and inhibitor without the metal ions (denoted ESI), allowing us to probe for competitive inhibition with respect to the substrate. The third condition evaluated was pre-incubation of the enzyme with the substrate (denoted ES), resulting in binary complex formation of the enzyme-substrate prior to addition of the inhibitor and metal ions, allowing us to probe if the inhibitor can disrupt essential pre-formed enzyme-substrate contacts. The fourth condition evaluated was without enzyme pre-incubation with the substrate or inhibitor (denoted E), such that the enzyme was added to a mixture of the substrate, inhibitor and metal ions.

Compound **25** was unable to inhibit RNH hydrolysis under conditions of pre-formed binary complexes (ES, $IC_{50} > 25 \mu M$), where the greatest RT-RNH inhibition was seen during enzyme-inhibitor pre-incubation (EI) conditions with an IC_{50} of $0.4 \mu M$, as seen in *Figure 26A*. These results suggest that compound **25** is unable to displace the enzyme-substrate contacts but is able to prevent essential enzyme-substrate contacts from occurring when the inhibitor is pre-bound to the enzyme. It was further shown that the inhibitor is able to compete with the substrate for interaction with the enzyme, since experiments with enzyme, substrate and inhibitor pre-incubation (ESI) resulted in an increased IC_{50} of $20 \mu M$, indicating that the inhibitor is only

able to weakly competes with the substrates. These results are further supported by the fact that compound **25** is unable to inhibit RNH catalysis in the absence of enzyme inhibitor pre-incubation (E, $IC_{50} > 25 \mu M$). Similar results were seen with the p15-EC RT RNH domain with compound **25** (Figure 26B), having an approximate eighteen-fold increase in RNH IC_{50} of $0.03 \mu M$ (EI) to $0.54 \mu M$ (ES). With p15-EC it is further shown that compound **25** competes with the substrate in order to inhibit RNH cleavages, since under ESI conditions the RNH inhibition has an approximate six-fold decrease in RNH inhibition (RNH IC_{50} $0.17 \mu M$) and was unable to inhibit in the absence of pre-incubation ($> 5 \mu M$ RNH IC_{50}).

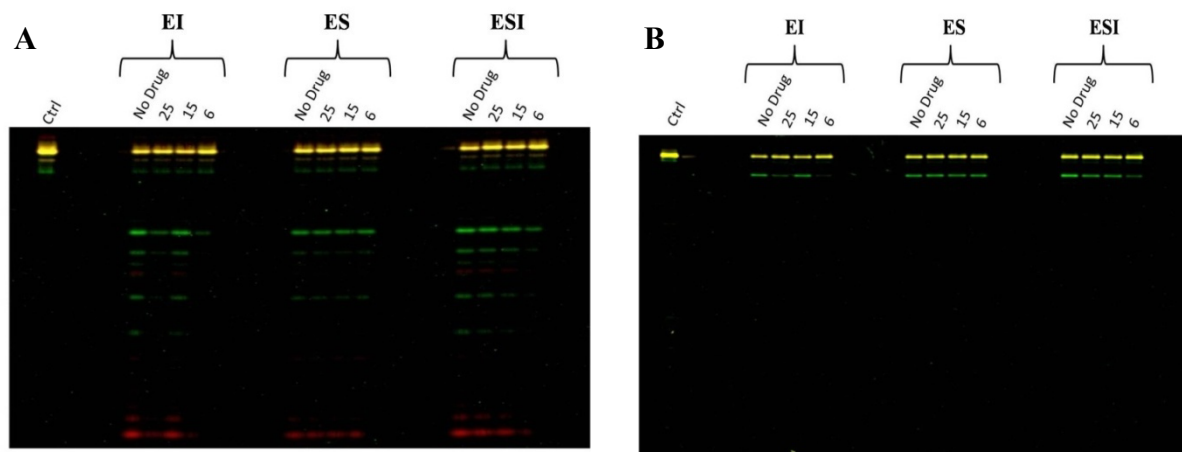


Figure 27. Order of Addition Influence on RT-RNH Inhibition with Full Length RT using the Gel Based Dual Labeled RNH Assay. *A)* RT-RNH inhibition of RNA 5'-end directed RNH cleavages (Duplex 2) and *B)* RT-RNH inhibition of DNA 3'-end directed RNH cleavages (Duplex 4). Enzyme-inhibitor pre-incubation is denoted by EI, enzyme-substrate pre-incubation (binary complex) denoted by ES and enzyme-substrate-inhibitor pre-incubation denoted by ESI.

The same order of addition studies were undertaken with the gel based dual labeled RNH assay with both the RNA 5'-end directed (duplex 2) and DNA 3'-end directed (duplex 4) cleavage

substrates. The same trend was seen with the gel based assay as seen with the kinetic high-throughput FRET RNH enzyme assay, with three of the most potent compounds **6**, **15** and **25** from subgroups A, B and C, respectively (*Figure 27*). All three compounds were unable to inhibit the binary complex (ES), while being able to completely inhibit DNA 3'-end and RNA 5'-end directed cleavages under pre-incubation conditions of enzyme-inhibitor (EI) at 5 μ M concentration. Compound **6**, the most potent compound with the gel based dual labeled RNH assay was the only inhibitor able to partly inhibit under ESI conditions with the gel based assay, suggesting the compound is able to compete with the substrate as seen in the high-throughput RNH FRET assay.

2.4.8. Fluoren-9-ylidene Hydrazine Activity Against NNRTI Resistant Mutants

Table 9. Inhibition of NNRTI Resistant Mutants

Compound	Wild Type RT-RNH IC ₅₀ (μ M)	K103N/ L100V RT-RNH IC ₅₀ (μ M)	K103N/L100V RT- Pol IC ₅₀ (μ M)	Y181C RT-RNH IC ₅₀ (μ M)	Y181C RT-Pol IC ₅₀ (μ M)
15	0.34	0.39	0.42	0.88	1.0
25	0.4	1.3	0.68	0.31	0.28

Fluoren-9-ylidene hydrazine compounds **15** and **25** were evaluated as inhibitors of HIV-1 reverse transcriptase associated ribonuclease H and polymerase activities with clinically relevant NNRTI resistant mutants, K103N/ L100V (*efavirenz* resistant) and Y181C (*nevirapine* resistant) using the fixed time high-throughput FRET RNH enzyme assay with the high-throughput non-directed

cleavage substrate (HTS-1). Both compounds were able to inhibit the RNH and polymerase activity of the NNRTI resistant mutants (*Table 9*) with similar IC₅₀ values as wild type RT. The ability of the compounds to retain similar inhibitory potency with the NNRTI resistant mutants, suggest that the fluoren-9-ylidene hydrazine compounds will be active against clinically relevant NNRTI resistant mutants that plague current patient therapy making this inhibitor class a promising class for future RNHI discovery. These results further suggest that the fluoren-9-ylidene hydrazine compounds would be unable to bind within or near the NNRTIBP, though this is only speculative and would require further studies to confirm this speculation.

2.4.9 Fluoren-9-ylidene Hydrazine HIV-1 Antiviral Activity

Table 10: HIV-1 Antiviral Activity of Select Fluoren-9-ylidene Hydrazine Compounds

Subgroup	Compound*	HIV-1 EC ₅₀ (μ M)	Toxicity* (Visual Assessment)	Compounds* (No HIV-1 Antiviral Activity)
A	3	11 \pm 0.5	~ 10-25	2, 4, 6
B	15	10 \pm 3	> 25	-
C	25	1.4 \pm 0.6	> 25	26, 29, 31, 30, 33, 35, 37, 39, 41, 43, 44

* Compounds were evaluated up to 25 μ M

HIV-1 antiviral dose response studies with P4R5 cells were carried out with 17 compounds from the fluoren-9-ylidene hydrazine library in which 3 of the compounds had antiviral activity,

compounds **3**, **15** and **25**, as seen in *Table 10*. Compound **25**, from subgroup C had the greatest antiviral activity with an EC_{50} of $1.4 \pm 0.5 \mu\text{M}$ and had no visual cytotoxic effects to $25 \mu\text{M}$. Eleven other compounds from subgroup C (**26**, **29**, **31**, **30**, **33**, **35**, **37**, **39**, **41**, **43**, **44**) were also evaluated for antiviral and cytotoxic activity up to $25 \mu\text{M}$, in which none of these compounds had antiviral activity or visual cytotoxic effects, except for compound **37** (displayed slight cytostatic activity was seen at $25 \mu\text{M}$). The second most potent antiviral compound was from subgroup B, compound **15** with an EC_{50} of $10 \pm 3 \mu\text{M}$ and had no visual cytotoxic effects to $25 \mu\text{M}$. Compound **3** from subgroup A, displayed some antiviral activity but the actual EC_{50} value is a rough estimate, since slight cytostatic activity was seen from 10- $25 \mu\text{M}$ concentrations. Three other compounds from subgroup A (**2**, **4** and **6**) were also evaluated for antiviral activity, in which they displayed no antiviral activity with HIV-1. All three compounds, except compound **4**, displayed no antiviral activity up to $25 \mu\text{M}$ concentrations. Compound **4** at the higher concentration of $25 \mu\text{M}$ displayed some cell death, in which the cells displayed no cytotoxic effects at concentrations $\leq 15 \mu\text{M}$.

2.5 DISCUSSION

Identification of the fluoren-9-ylidene hydrazines as a promising class of HIV-1 reverse transcriptase associated ribonuclease H inhibitors emerged from the screening of a library of hydrazone/hydrazine compounds. Analysis of an expanded library of the fluoren-9-ylidene hydrazines demonstrated that the pharmacophore class provides highly active RNHIs. Indeed, the expanded library of 118 compounds resulted in a hit rate of 55% ($> 10 \mu\text{M}$ IC_{50}) as HIV-1 RT RNHIs, in which the majority of the compounds were monofunctional as RNHI, since only 21% of the compounds were able to inhibit RT-polymerase activity.

Active hits from the fluoren-9-ylidene hydrazine library were subgrouped into four functional groups, based on the functional group at the R_1 , including 2-(9*H*-fluoren-9-ylidene)hydrazinecarboxamid(subgroup A), 2-(9*H*-fluoren-9-ylidene)hydrazinecarbothioamide (subgroup B), 1-(9*H*-fluoren-9-ylidene)-2-phenylhydrazine (subgroup C) and *N'*-(9*H*-fluoren-9-ylidene) benzohydraside (Subgroup D). The two most active RT RNHIs were compounds **15** and **25** from subgroups B and C, having RT-RNH IC_{50} values of $0.34 \pm 0.07 \mu\text{M}$ and $0.4 \pm 0.03 \mu\text{M}$, respectively. The other two subgroups, A and D were less potent as RT RNHIs. Preliminary analysis of the structure activity relationship based on RT-RNH inhibition suggest that the R_1 phenyl substitution with and without a thioamide linker and an R_2 sulfonamido-phenyl ring substituent significantly enhances RT-RNH inhibition, as seen with compounds **15** and **25**. Furthermore, comparison of the fluoren-9-ylidene hydrazines with the 9*H*-(fluoren-9-ylidene)-2-hydropranolcarbonylhydrazine compounds, indicates the significance of the hydrazine functionality being planar. The significance of these structural moieties seems to correlate with

antiviral activity, since both compounds **15** and **25** have antiviral activity, with EC₅₀ values of $10 \pm 3 \mu\text{M}$ and $1.4 \pm 0.6 \mu\text{M}$, respectively. Compounds **15** and **25** also preferentially inhibit non-directed and DNA 3'-end directed cleavages, suggesting they preferentially inhibit during active DNA polymerization.

The fluoren-9-ylidene hydrazine compounds were also able to directly interact and inhibit the RNH activity of the p15-EC RT RNH domain fragment, suggesting that the RNH inhibitory properties of these compounds is the result of direct interaction with the RNH domain of RT. This observation suggest that the fluoren-9-ylidene hydrazine inhibitory properties are the result of directly binding with the RNH domain. Kinetic studies with compound **25** further suggest direct binding with the RNH active, since compound the RT-RNH inhibition was competitive with respect to the RNA/DNA substrate, having a K_I of 0.14 μM . Additional order of addition studies, further supported competitive RNH inhibition with compounds **6**, **15** and **25**. Neither one of the compounds were able to inhibit the binary complex of the RNA/DNA substrate pre-bound to RT, while studies without enzyme-inhibitor pre-incubation had a complete loss or decrease in RT-RNH inhibition.

Fluoren-9-ylidene hydrazine compounds overall were much more potent RNH inhibitors of the p15-EC RT RNH domain fragment compared to the full length RT, in which compound **25** had an approximate 13-fold difference in RNH inhibition. None of the Fluoren-9-ylidene hydrazine compounds indicated any metal dependence with either Mg^{+2} or Mn^{+2} , along with no salt dependency, suggesting the difference in RNH inhibition with full length RT and the p15-EC RT RNH domain fragment must be the result of different enzyme-substrate contacts. It is expected that the smaller p15-EC RT RNH domain fragment would have a less extensive substrate contact network compared to full length RT and therefore the fluoren-9-ylidene

hydrazine should be greater inhibitors of the p15-EC RT RNH domain fragment activity versus full length RT. In fact, this was the case where all of the fluoren-9-ylidene hydrazine compounds had a greater inhibition of the p15-EC RT RNH domain fragment. Furthermore, order of addition studies with the p15-EC RT RNH domain fragment was still able to inhibit the binary complex with an eighteen-fold loss in RNH inhibitory potency. These results indicating that the enhancement in RNH inhibition with the p15-EC RT RNH domain fragment is the result of having to disrupt less enzyme-substrate contacts compared to the more expansive contact network seen with full length RT. We therefore propose that the fluoren-9-ylidene hydrazine compounds mechanism of RT-RNH inhibition is the result of competing with the substrate for the RNH active site.

CHAPTER 3: POTENTIAL BINDING SITE OF THE FLUOREN-9-YILDENE HYDRAZINE COMPOUNDS WITH THE p15-EC RT RNH DOMAIN FRAGMENT

3.1 ABSTRACT

To identify a potential binding site for the inhibitors, we performed solution NMR experiments of the p15-EC RT RNH domain fragment and molecular docking studies using the NMR results. First ^1H - ^{15}N HSQC spectra of ^{15}N -uniformly labeled p15-EC were recorded in the presence and absence of compound **25** with p15-EC, in which the inhibitor binds within the RNH active site. Second, bulk solvent effects due to DMSO and non-specific interaction were further ruled out by titrating only DMSO and a non-active compound **117** to p15-EC. The NMR experiments clearly demonstrated that a region of p15-EC that includes the RNH active site residues were perturbed upon compound **25** interactions. Molecular docking studies with compound **25** and the p15-EC, performed using these NMR results further supported a well-defined binding pocket within the RNH active site. The hydrazine functionality of compound **25** forms hydrogen bonds with catalytic essential metal coordinating residues E52 (RT: 478) and D72 (RT: 498). Along with an R_2 sulfonamido-phenyl ring substituent stacks with an essential residue for RNH catalysis, H125 (RT: 539) by making edge-on- π interactions.

3.2 INTRODUCTION

Solution NMR ^1H - ^{15}N HSQC experiments for the p15-EC RT RNH domain fragment were carried out to identify a potential binding site for the fluoren-9-ylidene hydrazine compounds. The most active RNHI, compound **25** was titrated to the protein sample to characterize residues whose chemical shifts were perturbed upon interaction. An inactive compound, **117** from the library was also evaluated in order to rule out any non-specific binding interaction. We chose NMR experiments rather than X-ray crystallography since previous X-ray crystallography studies of full-length RT complex with RNHIs did not exhibit the inhibitor in a reasonable position to reduce RNH activity (43, 90)

Biochemical experiments showed that compound **25** exhibited significant RNH inhibition on the p15-EC RT RNH domain fragment, therefore the NMR experiments were carried out with the smaller 16.7 kDa p15-EC RT RNH domain fragment versus the 117 kDa full length RT. The p15-EC enzyme is suitable to compare RNH inhibition and binding site information. As previously shown, backbone NMR signals of the p15-EC have already been assigned and have been significantly perturbed upon inhibitor interaction with the enzyme (35). Previous studies with the fluoren-9-ylidene hydrazine library and the p15-EC discussed in chapter 2, have identified these inhibitors to be more potent as RNH inhibitors with the p15-EC versus full length RT. Additionally, previous studies also indicated that compound **25** is a competitive inhibitor for RT RNH activity with respect to the substrate, suggesting this inhibitor binds within the RNH active site. Based on the observations it was of a greater advantage to use solution NMR studies with the p15-EC versus other biophysical techniques in order to deduce a potential binding site.

3.3 MATERIALS AND METHODS

3.3.1 Reagents

The M9 media consisted of 42 mM dibasic sodium phosphate, 22 mM monobasic potassium phosphate and 8.5 mM sodium chloride (7.4 pH), with added supplements of 100 mM magnesium sulfate , 10 mM calcium chloride, 1 mg/ml thiamine, 1 mg/ml d-biotin, 1.3 µg/ml kanamycin, 0.2% glucose and 0.1% ammonium chloride. All reagents used for protein expression and NMR experiments were of the highest grade available. HiTrap Q HP Sepharose ion exchange and a HiTrap SP columns and a superdex 75 26/60 size exclusion column were obtained from GE Healthcare, Piscataway, NJ, USA. 5-mm shigemi tubes were obtained from Shigemi Inc., Allison Park, PA, USA.

3.3.2 Isotropic Labeling of the p15-EC RT RNH Domain Fragment

The p15-EC RT RNH domain fragment was isotropically labeled for NMR experiments by growing pCSR231-transformed bacterial cell cultures in a modified M9 minimal media with $^{15}\text{NH}_4\text{Cl}$ as the only nitrogen source. Purification was carried out with a HiTrap Q HP Sepharose ion exchange and a HiTrap SP column, with 25 mM sodium phosphate buffer (7.0 pH), 0.02% sodium azide and 1 mM dithiothreitol (DTT) used to equilibrate the column, while a linear gradient 1 M NaCl solution was used to elude the protein. A Superdex75 26/60 size exclusion column with a 25 mM sodium phosphate buffer (7.0 pH), 0.02% sodium azide, 100 mM NaCl

and 1 mM DTT was used to further purify the RNase H fragment. Purity of the protein was assessed with 20% SDS-PAGE gel electrophoresis and all samples were stored at 70°C until use.

3.3.3 Solution NMR ^1H - ^{15}N HSQC

All spectra were recorded on a Bruker AVANCE600 spectrometers equipped with a 5-mm-triple-resonance-z-gradient cyogenic probe at 25°C. The p15-EC protein was dissolved in a 40 mM sodium phosphate buffer (6.8 pH), with 95% H_2O /5% D_2O , at 60 μM protein concentration and placed into a 5-mm shigemi tube with a total volume of $\sim 350\mu\text{l}$. A stock solution of compound **25** was prepared at 50 mM in 100% DMSO, while compound **117** was prepared at 10 mM in 100% DMSO. First, the p15-EC spectra were recorded in the absence and presence of 0.3 and 0.9% DMSO to assess the effects of DMSO on the protein. Second, the p15-EC spectra were recorded at different concentrations of compound **25**: 0, 60 and 90 μM (corresponding to 1:0, 1:1 and 1:1.5 ratio with DMSO concentrations of 0, 0.2 and 0.3% DMSO). Third, the p15-EC spectra recorded in the presence of compound **117** at 0 and 90 μM (corresponding to 1:0, and 1:1.5 ratios with DMSO concentrations of 0 and 0.9%), in order to rule out any none specific binding with the fluoren-9-ylidene hydrazine compounds. Each spectra obtained in the absence and presence of DMSO or inhibitor were carried out under the same conditions over an eight hour period per spectrum. Previously assigned Chemical shifts peaks of the backbone ^1H - ^{15}N signals (11) were used to assess changes in the resonance peak in the current experiments. Degree of chemical shift perturbations upon inhibitor titration was assess by taking the square root of the sum of squares of the ^1H and ^{15}N chemical shift peak differences. The effect of inhibitor interaction was also investigated by determining the degree of peak intensity changes

upon inhibition titration by also taking the square root of the sum of squares of the ^1H and ^{15}N peak intensity differences. Chemical shift and peak intensity perturbations were considered to significant above the cutoff line of 1.24 Hz for chemical shift data and 0.05 for peak intensity data. The cutoff lines were determined by taking the standard deviation of the chemical shift perturbation values or the change in peak intensity values for all the residues. NMR spectra of p15-EC were also recorded in the presence of DMSO and the chemical shift changes induced by the either 0.3 or 0.9% DMSO were subtracted from their corresponding inhibitor spectra. All NMR data was processed and analyzed using the NMRDraw and NMRView software packages (18, 50).

3.3.4 Molecular Docking with Schrödinger Suite Software

The Schrodinger Suite XP glide docking program (Schrödinger, LLC., New York, NY) was used for molecular docking of compound **25** to the p15-EC RT RNH domain fragment. The p15-EC RT RNH domain fragment was previously created (35) by inserting the extended E. coli loop (TQWIH NWKKR GWKTA DKKPV KNV) to the PDB file 2I5J. Molecular docking was performed in the following strategy. First, based on the NMR results, the binding region was selected and centered on residue G18 with a 12Å area. Second, the top 15 lowest energy confirmations of compound **25** at a pH 8.0 ± 0.5 using the ConfGen application were selected for docking within the defined docking area. Lastly, all 15 confirmations of compound **25** were docked within the defined binding region centering on residue G18, in which the inhibitors were allowed to be flexible while the protein was maintained at its minimized conformation. The top 5 docked structure with the greatest glide docking score and favorable protein contacts within an

4Å area were selected and analyzed. The glide docking score (gscore) is based on the energy contributions from van der Waals interactions (vdW), coulombic interactions (Coul), lipophilic-contacts with phobic-attractive interactions (Lipo), hydrogen bonding interactions (Hbond), and the polar interactions within the binding site (Site), in which the gscore is based on equation $gscore = a * vdW + b * Coul + Lipo + Hbond + Reward + Site$. The docked models were also assessed based on their Emodel score, this score takes into the account the gscore, CvdW (non-bonded internal energy between the ligand and receptor, $CvdW = Coul + VdW$) and the estimated conformational energy of the ligand. All protein and ligand preparations and hydrogenation was carried out at a pH range of 8.0 ± 0.5 , in order to correlate with biochemical data.

3.4 RESULTS

3.4.1 Influence of DMSO on the ^1H - ^{15}N HSQC Spectrum of p15-EC

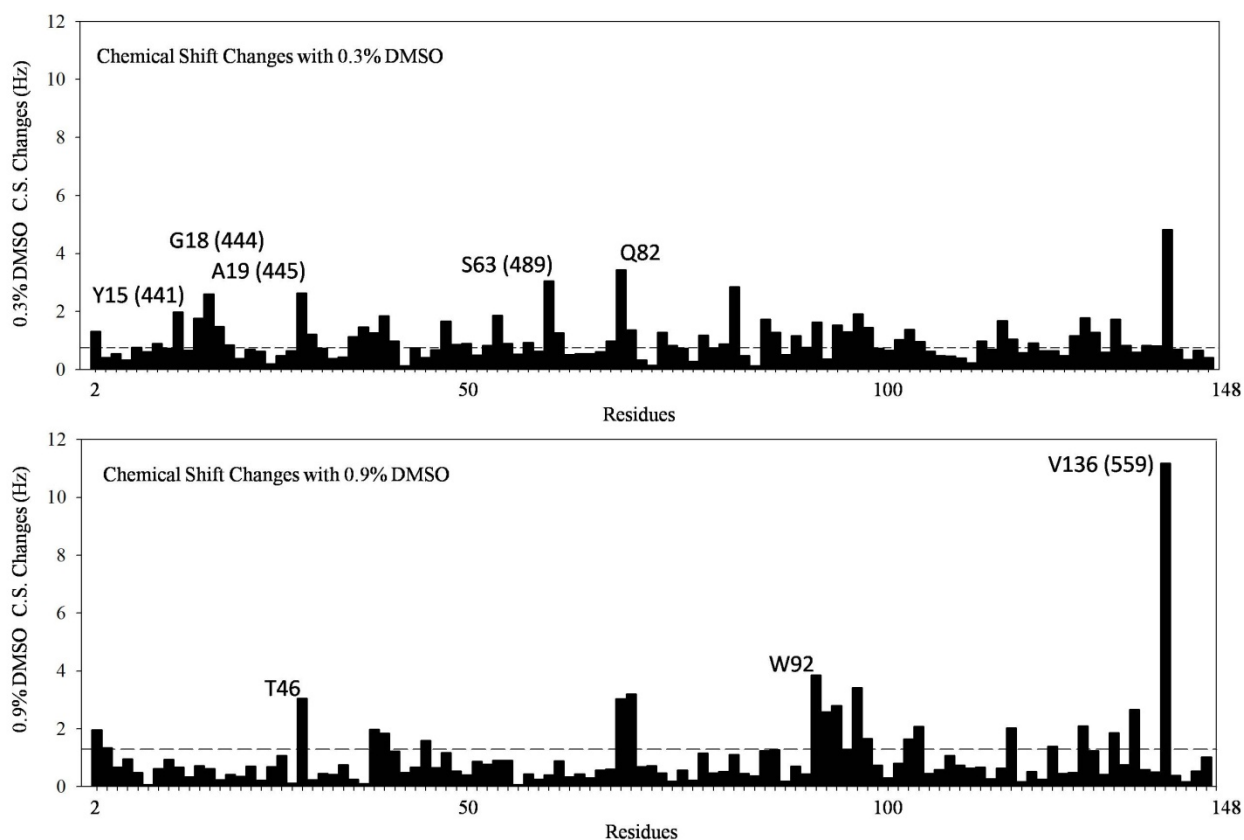


Figure 28. Amid Backbone Chemical Shift Perturbations of the p15-EC RT RNH Domain Fragment Induced by DMSO at *A*) 0.3% and *B*) 0.9% DMSO.

^1H - ^{15}N HSQC solution NMR studies of p15-EC were recorded in the presence of DMSO at 0.3 and 0.9% (both spectra are found within the appendix B: *Supplementary Figures 1* and *2*). These experiments were carried out, to identify any effects of solvent DMSO that is required to

dissolve the fluoren-9-ylidene hydrazine compounds in aqueous solution. As seen in *Figure 28*, most of the residue signals chemical shifts did not change and are primarily unaffected by the small amounts of DMSO. However, some residues (Y15, G18, A19, S63, Q82) did experience slight chemical shift changes at 0.3% DMSO. A few residues (T46, W92 and V136) exhibited more chemical shift perturbations at the higher concentration of DMSO at 0.9%. Inconsistency in the slight chemical shift changes in the presence of 0.3% and 0.9% DMSO may have arisen due to initial solution inhomogeneity of the DMSO concentration during mixing of it into the protein solution. However, as shown below, these inconsistencies were insignificant in the inhibitor titration experiments since the chemical shift differences were so small.

3.4.2 Influence of Compound 25 on the ^1H - ^{15}N HSQC Spectrum of p15-EC

In order to deduce a potential binding site for the fluoren-9-ylidene RNHIs, ^1H - ^{15}N HSQC solution NMR titration studies were carried out with compound **25** and p15-EC, since previous experiments (from chapter 2) indicated competitive RNH inhibition with the substrate and therefore suggesting direct interaction with the RNH active site. Inhibitor p15-EC spectra were collected at compound **25** concentrations of 0, 60 and 90 μM (corresponding to 1:0, 1:1 and 1:1.5 ratio with DMSO concentrations of 0, 0.2 and 0.3% DMSO). Titration studies beyond a ratio of 1:1.5 were not performed due to the limitation of the solubility of compound **25** in aqueous solution.

A few residue chemical shift perturbations were observed beyond the cutoff of 1.24 Hz for compound **25**, as seen in *Figure 29A*. The DMSO solvent affects were removed from residue chemical perturbations of compound **25**, such that the DMSO residue chemical shift

perturbations were subtracted from the residue chemical shift perturbations of compound **25** with DMSO. As seen in *Figure 29C*, residues that experienced chemical shift perturbations were G18 (RT: 444) with 6.1 Hz, T46 (RT: 472) with 1.4 Hz, Q82 (extended loop residue) with 3.5 Hz, H85 (extended loop residue) with 1.4 Hz, W123 (RT: 535) with 3.3 Hz, and V124 (RT: 536) with 1.5 Hz. G18 (RT: 444). Residue G18 (RT: 444) resides at the base of the RNH active site, neighboring catalytic active site residues D17 (RT:443) and has been shown to be significantly affected upon metal binding with p15-EC by solution NMR titration studies previously done in our laboratory (35). Furthermore residue T46 (RT: 472), is also neighboring essential residues responsible for interacting with the RNA/DNA substrate, residues T47 (RT: 473), N48 (RT: 474) and Q49 (RT: 475) (70). Residues Q82 and H85 are located in the extended *E. coli* helix-loop that is important for restoring activity to the p15-EC RT RNH domain fragment by interacting with the substrate. Alignment of the RNH domain fragment with full-length RT structure indicates the extended *E. coli* helix-loop may mimic inter-subunit interactions between the p51 and p66 subunits of RT with the RNH domain (35). Residues W123 (RT: 535) and V124 (RT: 536) are highly conserved hydrophobic residues that neighbor the active site near catalytic residue D72 (RT: 498), in which residue V124 (RT: 536) has further been implemented to experience chemical shift changes upon metal interactions of the p15-EC RT RNH domain fragment during solution NMR titration studies (35). Active site residue E52 (RT: 478), essential for protein-metal contacts has the greatest change in peak intensity of 1.6 (*Figure 30C*).

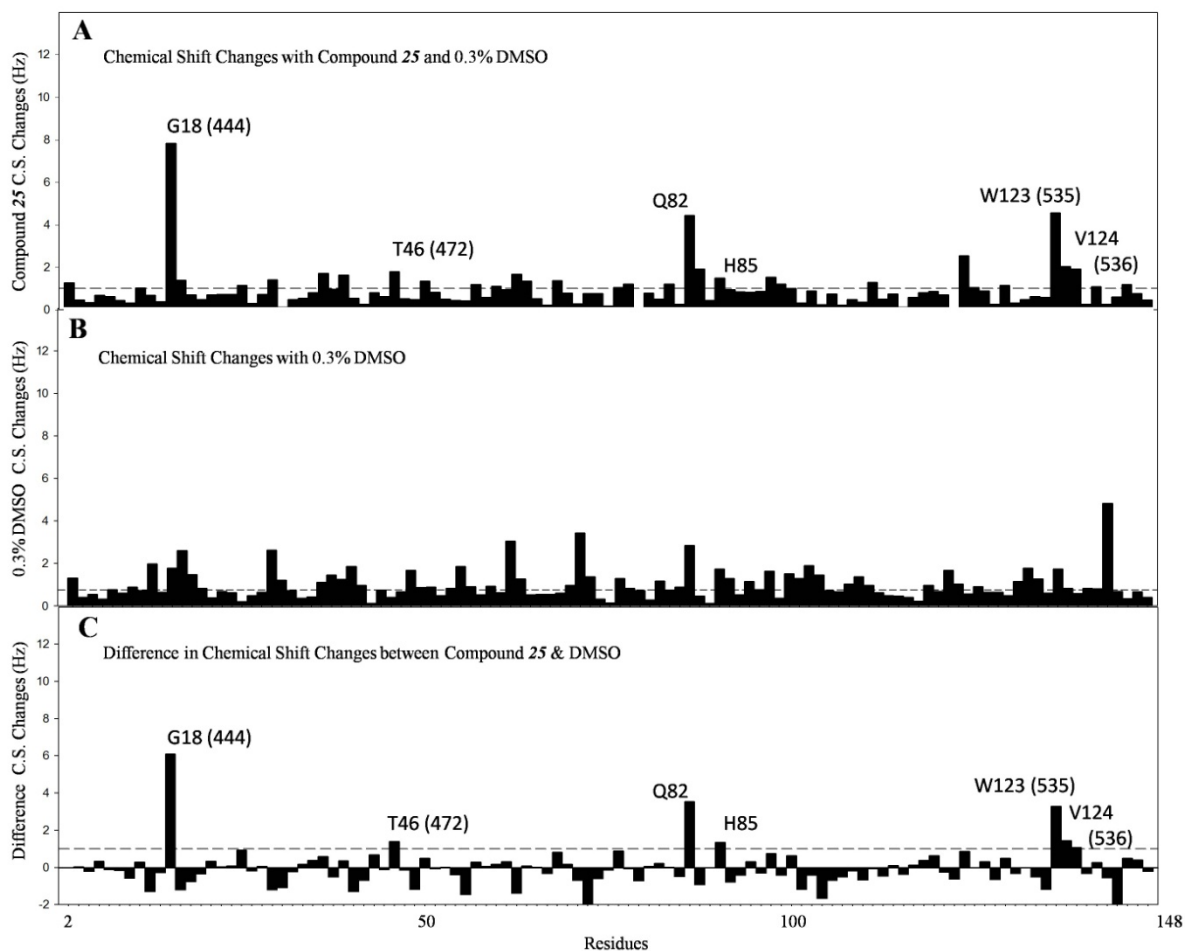


Figure 29. Amide Backbone Chemical Shift Perturbations of p15-EC Induced by Compound 25. *A*) Compound 25 in the presence of 0.3% DMSO, *B*) 0.3% DMSO and *C*) the subtraction of B from A.

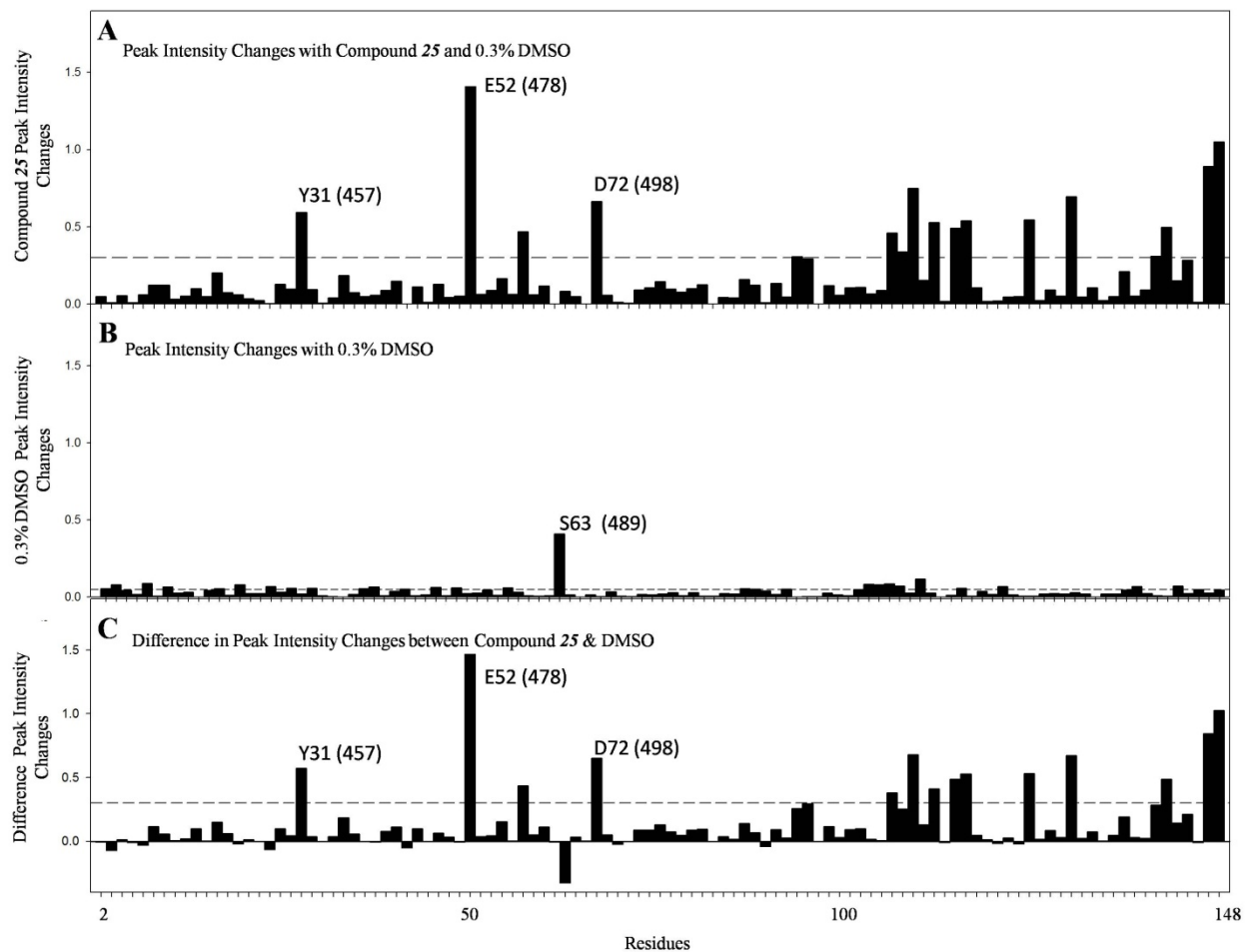


Figure 30. Amide Backbone Peak Intensity Changes of p15-EC Induced by Compound 25. *A)* Compound 25 in the presence of 0.3% DMSO, *B)* 0.3% DMSO and *C)* the subtraction of B from A.

3.4.3 Influence of Compound *117* on the ^1H - ^{15}N HSQC Spectrum of p15-EC

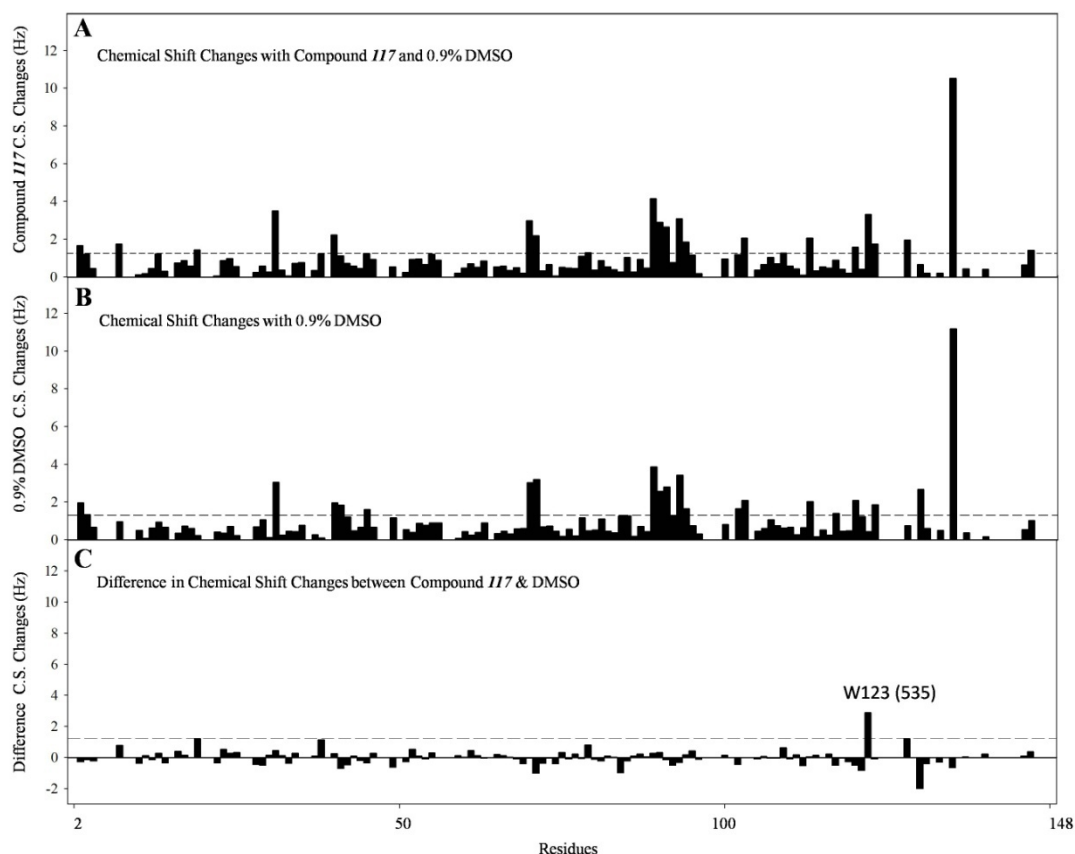


Figure 31. Amid Backbone Chemical Shift Perturbations of p15-EC Induced by Compound *117*. *A*) Compound *117* in the presence of 0.9% DMSO, and *B*) 0.3% DMSO and *C*) the subtraction of B from A.

^1H - ^{15}N HSQC solution NMR studies were carried out with compound *117* in order to rule out any amide backbone chemical shift perturbations seen upon binding of compound *25* with p15-EC was not the result of to non-specific interaction. For this purpose, the ^1H - ^{15}N HSQC spectrum was recorded in the absence and presence of compound *117* (does not inhibit p15-EC). A higher DMSO percentage was required with compound *117*, therefore a 0.9% DMSO chemical shift differences spectrum was used as a comparison and removed from compound

residue amide backbone chemical shift perturbations of compound **117**. As seen in *Figures 31A and B*, the amide backbone chemical shift perturbations for compound **117** with DMSO was almost identical to the residue chemical shift perturbation of DMSO by itself, remaining the subtraction of the two within the cut-off range (*Figure 31C*). These results suggest that the fluoren-9-ylidene hydrazine binding interaction seen by solution NMR is not the results of non-specific interactions with the p15-EC RT RNH domain fragment but rather due to specific inhibitor-residue interactions

3.4.4 Molecular Docking of Compound 25 with the p15-EC RT RNH Domain Fragment

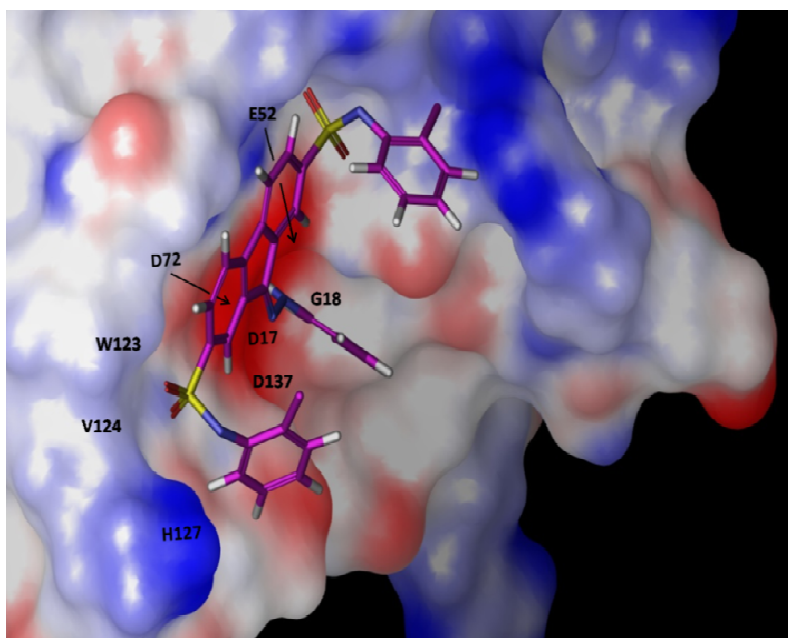


Figure 32. 3D Representation of the Molecular Docking with Compound 25 and p15-EC. Residues represented by the electrostatic potential, in which red denotes negative, blue denotes positive and white denotes neutral residues.

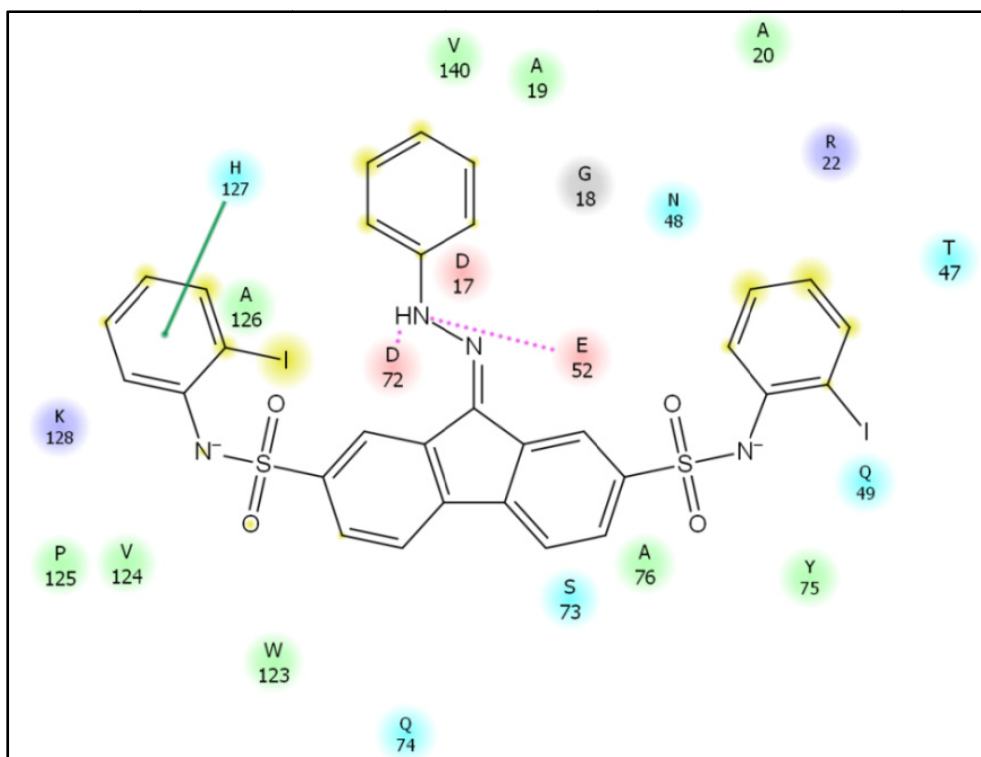


Figure 33. 2D Representations of the Molecular Docking with Compound 25 and p15-EC.

Font size corresponds to residues depth in 3D space and residues are colored according to residue type. Red highlighted residues are negative, purple are positive, cyan are polar and green are hydrophobic, while H-bonds with residue side chain atoms are represented by pink dashed lines, edge on- π interactions are denoted by green lines.

Molecular modeling studies were carried out with compound **25** and the p15-EC RT RNH domain fragment based on the above NMR results, where a biased binding site was set around residue G18 (RT: 444), incorporating the active site of an $\sim 12\text{\AA}$ area. A total of 70 docked poses were obtained, in which 15 of the models had a Emodel score > -60 . The majority of the docked models had similar gscores, along with a similar binding orientation within the RNH active site. The most favorable docked model had a gscore of -4.45, in which the greatest energy contributions was due to van der waals interactions (-35.2) versus the coulombic contributions (-

12.5). The non-bonded interaction energy between the ligand and receptor had a score of -47.7, resulting in a favorable Emodel score of -63.7. As seen in the *Figure 32*, compound **25** sets within a well-defined pocket up against the active site. The inhibitor is mainly surrounded by hydrophobic (highlighted green) and polar (highlighted cyan) residues, while the hydrazine functionality hydrogen bonds with catalytic active site residues E52 (RT: 478) and D72 (RT: 498), that are essential for metal coordination (also observed during docking studies with compound **15**) (*Figure 33*). The hydrogen bonding distance with residues E52 (RT: 478) and D72 (RT: 498) are ~ 2.4 Å with the greatest energy contributions due to van der waals interaction with scores of -3.7 and -3.2, while having a hydrogen bonding score of -0.024 and -0.032. The inhibitor is further seen to interact with residues that experienced chemical shift changes during the NMR experiments, G18 (RT: 444), W123 (RT: 535) and V124 (RT: 536). The R₂ sulfonamido-phenyl ring substituent (*Figure 33*) is located at a position to form edge-on- π interaction with residue H127 (RT: 539) that is critical for RNH catalysis. The sulfonamido-phenyl ring was 1.9 Å from H127 (RT: 539), in which the greatest interaction contribution was due to van der waals interactions with a score of -2.1, while having a slightly favorable coulombic interaction score of -0.74. The dock structure also shows that though the fluoren-9-ylidene hydrazine core is tucked into the binding pocket and is away from the solvent; the furthest ends of the R₁ and R₂ extensions are partially solvent exposed, as indicated in *Figure 33* by the yellow highlights. One of the ortho-iodine of the R₂ sulfonamido-phenyl ring substituent is also seen to be oriented towards a polar residue, Q49 (RT: 475) with a 2.8 Å distance, this residue is significant for enzyme-substrate contacts. The proximity of the inhibitor with residue Q49 (RT: 475) suggests that an ionic interaction between the negative iodine and amine of the glutamine residue may stabilize the solvent exposed phenyl ring. An additional contact is seen

with residue N48 (RT: 474), which is also a significant enzyme-substrate contact residue. The inhibitor is ~ 2.5 Å from residue N48 (RT: 474) with a favorable van der Waals interaction score of -4.6 and coulombic interaction score of -3.6.

3.5 DISCUSSION

A potential binding site for compound **25** with the p15-EC RT RNH domain fragment was defined based on amide backbone chemical shift perturbation from ^1H - ^{15}N HSQC solution NMR studies, where peak intensity changes were not used to define the pocket since the peak intensity changes above the cutoff line of 0.05 were not localized to a specific region of p15-EC. Amide backbone chemical shift perturbations were seen with residues G18 (RT: 444), T46 (RT: 472), W123 (RT: 535), and V124 (RT: 536), along with residues Q82 and H85, that are located within the extended *E. coli* helix-loop added in order to restore activity to the isolated enzyme (54). Chemical shift perturbation of the extended *E. coli* helix-loop residues, Q82 and H85 were excluded as being the result of direct inhibitor binding, since the chemical shift perturbations by compound **25** were small and were observed during the DMSO titrations. The remaining four residues G18 (RT: 444), T46 (RT: 472), W123 (RT: 535) and V124 (RT: 536) were located in or around the RNH active site, in which residue G18 (RT: 444) experienced the greatest chemical shift perturbations of 6.1 Hz. Residue G18 (RT: 444) resides within the RNH active site neighboring catalytic active residue D17 (RT: 443) and near other active site residues E52 (RT: 478) and D72 (RT: 498). The amide backbone chemical shift of residue G18 (RT: 444) has been shown to be significantly affected upon metal binding with the p15-EC RT RNH domain fragment (35). Signal intensity of one of the active site residues E52 (RT: 478) was significantly enhanced by compound **25**, suggesting that the RNHI makes specific contact with this residue upon binding to the p15-EC RT RNH domain fragment. Residues W123 (RT: 535) and V124 (RT: 536) are highly conserved hydrophobic residues that neighbor the active site near catalytic residue D72 (RT: 498), in which residue V124 (RT: 536) has been shown to experience amide

backbone chemical shift perturbations upon metal binding with the p15-EC RT RNH domain fragment (35). Residue T46 (RT: 472) neighbors residues essential for enzyme-substrate interaction, including residues T47 (RT: 473), N48 (RT: 474) and Q49 (RT: 475) (26). The ^1H - ^{15}N -HSQC NMR results suggest that compound **25** binds within the RNH active site, in which the binding pocket revolves around residue G18 (RT: 444) and involves residues T46 (RT: 472), W123 (RT: 535) and V124 (RT: 536), while interacting with active site residue E52 (RT: 478).

Compound **25** was able to be docked within a well-defined pocket within the RNH active site. Furthermore, residues deduced during the NMR studies, including G18 (RT: 444), E52 (RT: 478), W123 (RT: 535) and V124 (RT: 536), created the binding site. Indeed, the upper-back-side wall of the binding pocket consisted of residues W123 (RT: 535) and V124 (RT: 536), while the other backside of the wall contained residues T47 (RT: 473) and Q49 (RT: 475) that neighbor residue T46 (RT: 472) and have been shown to be significant for enzyme-substrate contacts (75). The third neighboring residues of T46 (RT: 472), residue N48 (RT: 474) is also a significant enzyme-substrate contact residue and resides at the base of the binding pocket near residue G18 (RT: 444). In addition, residue G18 (RT: 444) resides at the base of the active site binding pocket and contributes largely to the binding pocket floor, along with active site residues D17 (RT: 443) and D137 (RT: 549). The essential hydrazine functionality of compound **25** makes hydrogen bonds with metal coordinating active site residues E52 (RT: 478) and D72 (RT: 478). The hydrogen bonding interactions correlate with the biochemical and biophysical data, such that the hydrazine planarity and functionality is essential for RT-RNH inhibition, while residue E52 (RT: 478) has significant residue peak intensity changes indicating direct interaction with the inhibitor. The R_2 sulfonamido-phenyl ring substituent making edge-on- π contact with H127 (RT: 539), also correlates with the biochemical structure activity relationship data, such

that the R₂ sulfonamido-phenyl ring substituent has been shown to enhance RT-RNH inhibition^{iv}. These results suggest that the inhibitors interaction with H127 (RT: 539) prevents RNH catalysis from transpiring, since mutation of H127 (RT: 539) completely abrogates RNH activity. The molecular docking observations based on the NMR studies, propose that the fluoren-9-ylidene hydrazine RNHIs mechanism of inhibition involves binding within the RNH active site and preventing access of RNH essential catalytic residues to the RNA/DNA substrate. This conclusion is supported by the fact that the fluoren-9-ylidene RNHIs are competitive inhibitors with the substrate, are unable to inhibit the binary complex when enzyme-substrate contacts are pre-formed and the NMR studies identifies residue-inhibitor interactions with neighboring active site residues essential for substrate binding.

^{iv} H127 peak was not distinguished within the p15-EC RT RNH domain Fragment spectrums.

CHAPTER 4: SUMMARY AND CONCLUSIONS

4.1 Major Findings and Conclusions

4.1.1 Chapter 2: Identification and Characterization of the Fluoren-9-ylidene Hydrazine Pharmacophore

The fluoren-9-ylidene hydrazine pharmacophore was identified as a highly active inhibitor of HIV-1 reverse transcriptase associated ribonuclease H activity, having a 55% hit rate, in which 79% of the compounds were monofunctional as RNHIs ($< 10 \mu\text{M}$ IC_{50}). The most active RT-RNHIs were compounds **15** (IC_{50} of $0.34 \pm 0.07 \mu\text{M}$) and **25** (IC_{50} of $0.4 \pm 0.03 \mu\text{M}$), in which compound **25** had the greatest antiviral activity (EC_{50} of $1.4 \pm 0.6 \mu\text{M}$). Compound **25** was further able to inhibit the p15-EC RT RNH domain fragment with a ten-fold increase in potency (IC_{50} of $0.032 \pm 0.004 \mu\text{M}$). Preliminary structure-activity relationship studies with full length RT further indicate that the RNH inhibitory activity of the fluoren-9-ylidene hydrazine compounds is dependent on the planarity of the group, while also indicating that an R_1 phenyl and R_2 sulfonamido-phenyl ring substituents significantly enhances RT-RNH inhibition. Competitive inhibition with respect to the RNA/DNA substrate with both full length RT and the p15-EC RT RNH domain fragment, along with the ability to retain inhibitory activity against NNRTI resistant mutants suggest that compound **25** interaction with the RNH active site and compete with the RNA/DNA substrate.

4.1.2 Chapter 3: Potential Binding Site of the Fluoren-9-ylidene Hydrazine Compounds with the p15-EC RT RNH Domain Fragment

^1H - ^{15}N HSQC solution NMR residue amide backbone chemical shift and intensity perturbations indicate that compound **25** binds within the RNH active site of the p15-EC RT RNH domain fragment, in which the binding pocket involves residues G18 (RT: 444), T46 (RT: 472), W123 (RT: 535) and V124 (RT: 536) and has direct interaction with active site residue E52 (RT: 478). Biased molecular docking studies with compound **25** and the p15-EC RT RNH domain fragment indicate that the inhibitor is able to be docked within the RNH active site, while interacting with specific residues identified from the NMR studies. In addition the hydrazine functionality directly hydrogen bonds with active site metal coordinating residues E52 (RT: 478) and D72 (RT: 498). The R_2 sulfanamido-phenyl substituent makes edge-on- π interactions with essential RNH hydrolysis residue H127 (RT: 539), correlating with the previous observations that the R_2 sulfanamido-phenyl group substituent has an enhancement on RT-RNH inhibition. The binding pocket is further formed by significant residues for enzyme-substrate contacts, T47 (RT: 473), N48 (RT: 474) and Q49 (RT: 475) (75). This proposed binding site based on NMR and molecular modeling studies imply that the mechanism of RNH inhibition by the fluoren-9-ylidene hydrazine class of compounds involves binding within a well-defined pocket with the RNH active site. Therefore, preventing significant enzyme-substrate contacts from transpiring and possibly perturbing residues essential for RNH hydrolysis, and subsequently preventing RNH hydrolysis from transpiring.

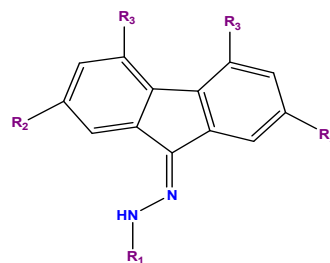
4.2 Significance and Future Studies

The current studies with the fluoren-9-ylidene hydrazine library identifies a new class of highly active HIV-1 reverse transcriptase associated ribonuclease H inhibitors with a pharmacophore that has not previously been described as an HIV-1 RNHI. Biochemical and structural biophysical studies propose a novel mechanism of HIV-1 RT-RNH inhibition, in which inhibition is the result of the inhibitor binding with RNH active site residues essential for both substrate and metal ion interactions that is independent of active site metal chelation. The binding mode of the inhibitor prevents access of essential catalytic RNH residues to the RNA/DNA substrate and subsequently inhibits RNH catalysis from being carried out. These studies suggest that compounds with the fluoren-9-ylidene hydrazine functionality as HIV-1 antivirals have a potential for less off-target interaction that could be determinate to the host. Furthermore, the lead compounds within this study have antiviral activity against HIV-1 and are able to inhibit clinically relevant NNRTI resistant mutants during *in vitro* studies, therefore identifying the fluoren-9-ylidene hydrazine class of RNHIs as a promising lead for further studies in HIV-1 RT RNHI discovery that is independent of RNH active site metal chelation.

Future studies that could be continued from this current study, would be to develop fluoren-9-ylidene hydrazine derivatives with enhanced RT-RNH inhibition based on the currently proposed binding mode. For instance, based on the molecular docking studies with compound **25**, the ortho iodine of the R₂ sulfonamido-phenyl ring substituent has a potential to make ionic interactions with residue K128 (RT: 540). Addition of a second ortho iodine substituent may enhance the inhibitor-enzyme contacts and subsequently enhance RT-RNH inhibition.

APPENDIX A

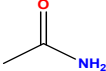
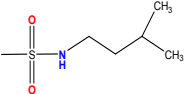
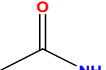
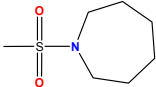

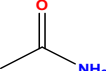
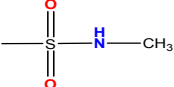

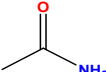
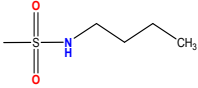
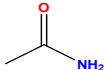
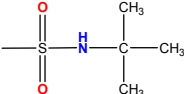
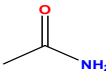
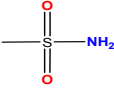
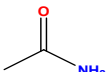
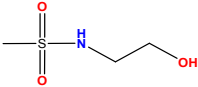
Supplementary Table 1: Screening Results of the (9H-fluoren-9-ylidene)hydrazine Library



Compound	R ₁	R ₂	R ₃	IC ₅₀ (μM)		
				HIV-1 RT-RNH	HIV-1 RT-Pol	RT-RNH Domain Fragment
A. 2-(9 <i>H</i> -fluoren-9-ylidene)hydrazinecarboxamid						
1			-H	1.1 ± 0.2	5.6 ± 0.6	0.36 ± 0.13
2			-H	1.8 ± 0.4	8.1 ± 0.9	0.24 ± 0.02
3			-H	2.4 ± 0.1	6 ± 1	1.3 ± 0.1
4			-H	3 ± 0.6	9.6 ± 0.5	1.2 ± 0.07

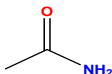
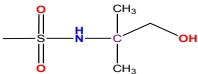
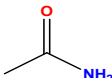
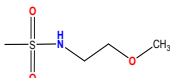
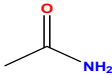
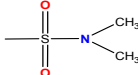
APPENDIX A

Supplementary Table 1 (continued)

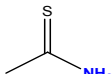
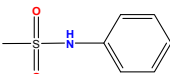
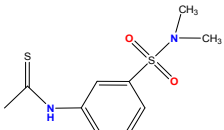
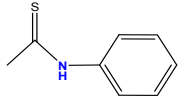
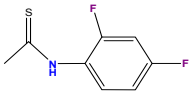
5			-H	3.5 ± 0.3	7.4 ± 1.3	0.5 ± 0.09
6				6 ± 0.1	>25	0.23 ± 0.04
7				6.4 ± 0.6	>25	1.9 ± 0.07
8			-H	9 ± 1	>25	1.9 ± 0.5
9			-H	13 ± 0.1	21 ± 1	3.5 ± 0.04
10			-H	>25	>25	15 ± 0.13
11			-H	>25	>25	>25

APPENDIX A

Supplementary Table 1 (continued)

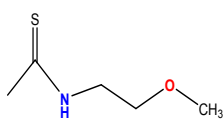
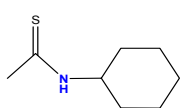
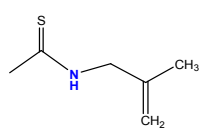
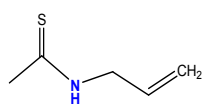
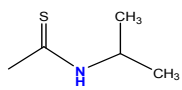
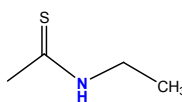
12			-H	>25	>25	>25
13			-H	>25	>25	>25
14			-H	>25	>25	>25

B. 2-(9H-fluoren-9-ylidene)hydrazinecarbothioamide

15			-H	0.34 ± 0.07	0.62 ± 0.06	0.43 ± 0.04
16		-H	-H	0.76 ± 0.1	2.3 ± 0.1	0.16 ± 0.02
17		-H	-H	1.3 ± 0.4	22 ± 2	0.34 ± 0.03
18		-H	-H	1.6 ± 0.3	>25	0.05 ± 0.02

APPENDIX A

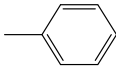
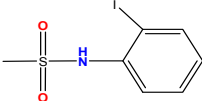
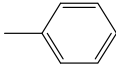
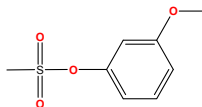
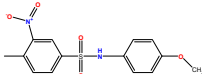
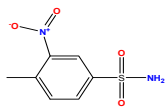
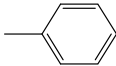
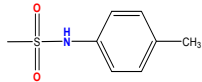
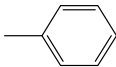
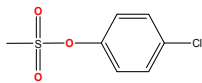
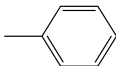
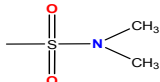
Supplementary Table 1 (continued)

19		-H	-H	5.6 ± 0.6	>25	0.6 ± 0.04
20		-H	-H	11 ± 0.5	>25	2.5 ± 0.3
21		-H	-H	12 ± 0.9	>25	3.8 ± 0.2
22		-H	-H	>25	>25	15 ± 1.3
23		-H	-H	>25	>25	>25
24		-H	-H	>25	>25	>25

APPENDIX A

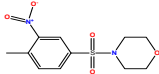
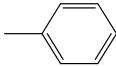
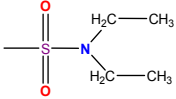
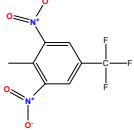
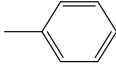
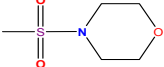
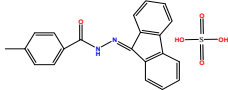
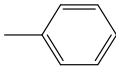
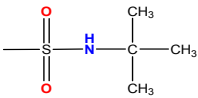
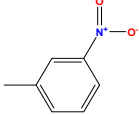
Supplementary Table 1 (continued)

C. 1-(9H-fluoren-9-ylidene)-2-phenylhydrazine

25			-H	0.4 ± 0.03	1.5 ± 0.1	0.032 ± 0.004
26			-H	0.58 ± 0.05	5 ± 0.5	0.082 ± 0.02
27		-H	-H	0.68 ± 0.1	1.3 ± 0.2	0.070 ± 0.003
28		-H	-H	0.79 ± 0.1	3.4 ± 0.7	0.036 ± 0.005
29			-H	1.4 ± 0.3	2.3 ± 0.2	0.072 ± 0.006
30			-H	1.6 ± 0.2	3.6 ± 0.8	0.49 ± 0.08
31			-H	1.7 ± 0.1	8.6 ± 0.2	0.35 ± 0.02

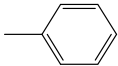
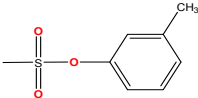
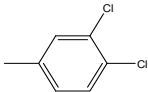
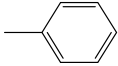
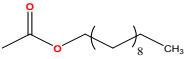
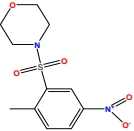
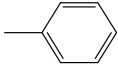
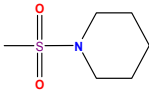
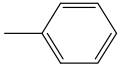
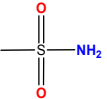
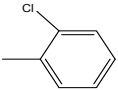
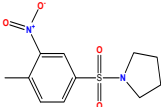
APPENDIX A

Supplementary Table 1 (continued)

32		-H	-H	1.9 ± 0.7	6.2 ± 0.3	0.2 ± 0.0
33			-H	2 ± 0.1	12 ± 1	0.23 ± 0.02
34		-H	-H	2 ± 0.3	14 ± 0.4	0.29 ± 0.04
35			-H	2.1 ± 0.2	11 ± 0.3	0.67 ± 0.09
36		-H	-H	2.2 ± 0.4	2.6 ± 0.3	0.087 ± 0.008
37			-H	2.4 ± 0.5	0.7 ± 0.3	0.28 ± 0.03
38		-H	-H	2.4 ± 0.2	12 ± 1.4	0.23 ± 0.03

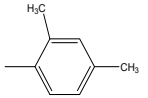
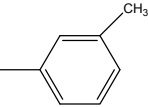
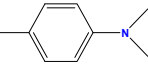
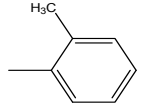
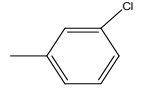
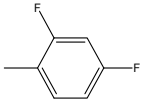
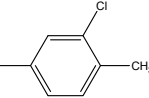
APPENDIX A

Supplementary Table 1 (continued)

39			-H	2.7 ± 0.01	4.6 ± 0.9	0.43 ± 0.1
40		-H	-H	2.83 ± 0.5	14 ± 0.4	>25
41		-H		3 ± 0.2	>25	0.16 ± 0.02
42		-H	-H	3.7 ± 0.5	>25	>25
43			-H	3.7 ± 0.4	5 ± 0.4	0.12 ± 0.02
44			-H	4.4 ± 0.3	8.2 ± 0.7	1.4 ± 0.2
45		-H	-H	4.4 ± 0.6	>25	0.27 ± 0.008
46		-H	-H	4.7 ± 0.2	>25	0.33 ± 0.04

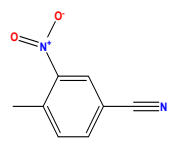
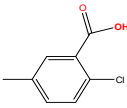
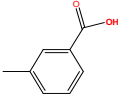
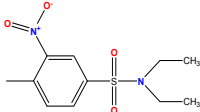
APPENDIX A

Supplementary Table 1 (continued)

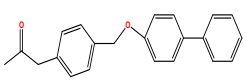
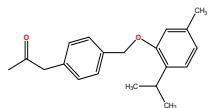
47		-H	-H	4.8 ± 1.6	>25	0.24 ± 0.03
48		-H	-H	6.1 ± 0.2	>25	0.26 ± 0.07
49		-H	-H	6.2 ± 0.4	>25	0.56 ± 0.08
50		-H	-H	7.7 ± 0.9	>25	0.4 ± 0.05
51		-H	-H	10 ± 2	>25	0.28 ± 0.08
52		-H	-H	11 ± 0.7	>25	0.54 ± 0.04
53		-H	-H	11 ± 2	>25	0.064 ± 0.005

APPENDIX A

Supplementary Table 1 (continued)

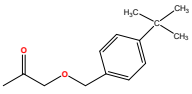
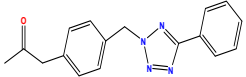
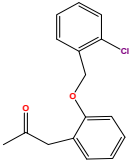
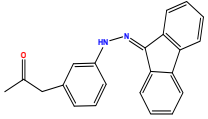
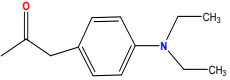
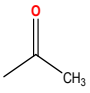
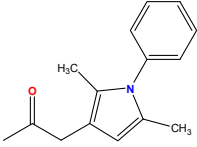
54		-H	-H	>25	>25	>25
55		-H	-H	>25	>25	3.6 ± 0.3
56		-H	-H	>25	>25	4.2 ± 0.1
57		-H	-H	>25	>25	0.09 ± 0.06

D. *N'*-(9*H*-fluoren-9-ylidene)benzohydrazide

58		-H	-H	1.3 ± 0.2	2.3 ± 0.2	0.018 ± 0.001
59		-H	-H	1.5 ± 0.2	3.6 ± 0.7	0.26 ± 0.03

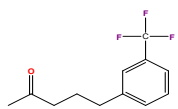
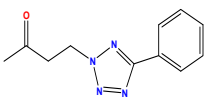
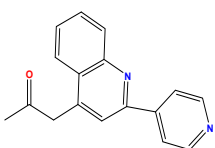
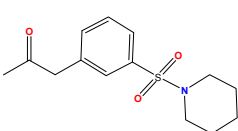
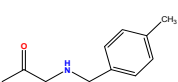
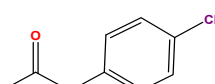
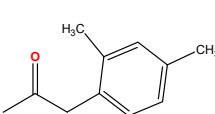
APPENDIX A

Supplementary Table 1 (continued)

60		-H	-H	2.1 ± 0.2	>25	0.26 ± 0.06
61		-H	-H	2.3 ± 0.2	14 ± 0.4	0.37 ± 0.06
62		-H	-H	2.6 ± 0.02	>25	0.52 ± 0.03
63		-H	-H	2.6 ± 0.8	1.0 ± 0.2	0.063 ± 0.02
64		-H	-H	2.8 ± 0.3	13 ± 0.4	0.36 ± 0.09
65		-H	-H	3.1 ± 0.4	>25	0.41 ± 0.06
66		-H	-H	3.1 ± 0.2	>25	0.45 ± 0.05

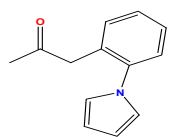
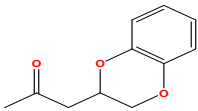
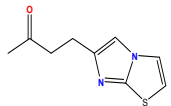
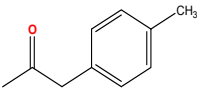
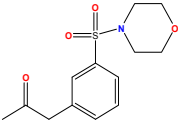
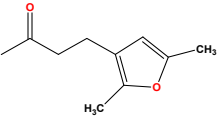
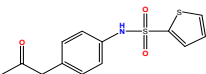
APPENDIX A

Supplementary Table 1 (continued)

67		-H	-H	3.5 ± 0.8	>25	0.77 ± 0.03
68		-H	-H	4.3 ± 0.8	>25	0.84 ± 0.1
69		-H	-H	4.5 ± 0.4	>25	2.2 ± 0.2
70		-H	-H	4.9 ± 0.5	21 ± 0.2	2.2 ± 0.2
71		-H	-H	5.8 ± 0.2	>25	3.9 ± 0.1
72		-H	-H	6.5 ± 0.3	>25	2.5 ± 0.3
73		-H	-H	8 ± 0.02	17 ± 3	4.4 ± 0.5

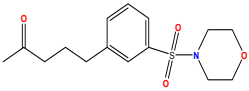
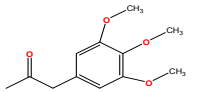
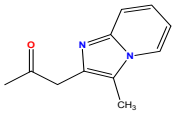
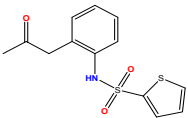
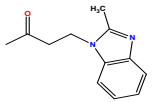
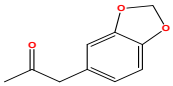
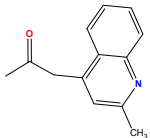
APPENDIX A

Supplementary Table 1 (continued)

74		-H	-H	9 ± 1	>25	4 ± 0.3
75		-H	-H	10 ± 0.3	>25	5.4 ± 0.3
76		-H	-H	12 ± 2	>25	2.4 ± 0.04
77		-H	-H	14 ± 0.6	>25	7.2 ± 0.6
78		-H	-H	15 ± 2	>25	3.4 ± 0.2
79		-H	-H	15 ± 1	>25	7.5 ± 0.3
80		-H	-H	15 ± 2	>25	3.5 ± 0.9

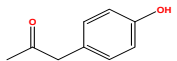
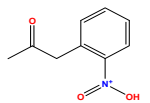
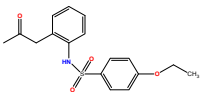
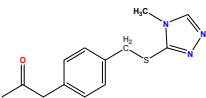
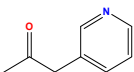
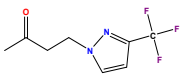
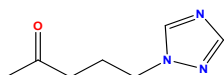
APPENDIX A

Supplementary Table 1 (continued)

81		-H	-H	16 ± 0.5	>25	8.2 ± 0.2
82		-H	-H	17 ± 0.6	>25	5.6 ± 2
83		-H	-H	18 ± 0.2	>25	14 ± 0.8
84		-H	-H	18 ± 2	>25	6.8 ± 0.8
85		-H	-H	19 ± 2	>25	14 ± 0.4
86		-H	-H	22 ± 2	>25	11 ± 0.5
87		-H	-H	22 ± 4	>25	4.8 ± 0.06

APPENDIX A

Supplementary Table 1 (continued)

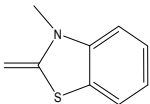
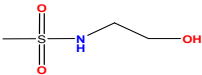
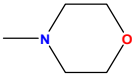
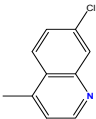
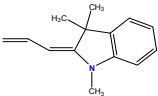
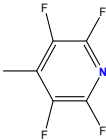
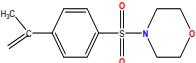
88		-H	-H	>25	>25	>25
89		-H	-H	>25	>25	>25
90		-H	-H	>25	>25	4.5 ± 0.9
91		-H	-H	>25	>25	>25
92		-H	-H	>25	>25	>25
93		-H	-H	>25	>25	2.2 ± 0.2
94		-H	-H	>25	>25	>25

APPENDIX A

Supplementary Table 1 (continued)

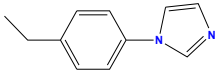
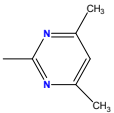
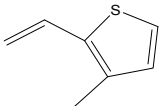
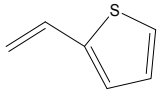
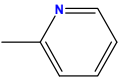
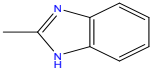
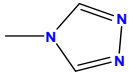
95		-H	-H	>25	>25	0.23 ± 0.05
----	---	----	----	-----	-----	-----------------

E. Other

96			-H	0.5 ± 0.06	1.7 ± 0.1	0.5 ± 0.03
97		-H	-H	1.7 ± 0.2	>25	0.3 ± 0.02
98		-H	-H	1.8 ± 0.1	9.4 ± 1.6	0.33 ± 0.06
99		-H	-H	2.2 ± 0.2	13 ± 3	0.11 ± 0.01
100		-H	-H	2.5 ± 0.3	11 ± 0.5	0.31 ± 0.04
101		-H	-H	3.3 ± 0.2	>25	0.33 ± 0.07

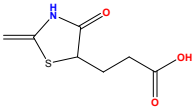
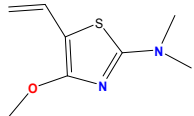
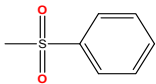
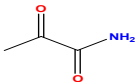
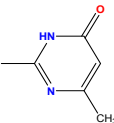
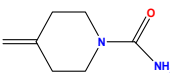
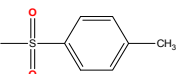
APPENDIX A

Supplementary Table 1 (continued)

102		-H	-H	3.3 ± 0.5	>25	1.4 ± 0.09
103		-H	-H	3.7 ± 0.3	13 ± 1	3.8 ± 0.1
104		-H	-H	6 ± 0.4	>25	0.24 ± 0.01
105		-H	-H	11 ± 2	>25	2.3 ± 0.2
106		-H	-H	14 ± 2	>25	>25
107		-H	-H	14 ± 3	>25	2.6 ± 0.6
108		-H	-H	21 ± 4	>25	0.71 ± 0.2

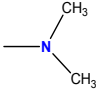
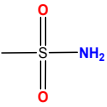
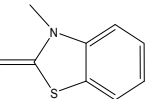
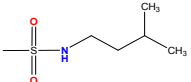
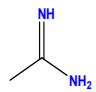
APPENDIX A

Supplementary Table 1 (continued)

109		-H	-H	>25	>25	1.7 ± 0.2
110		-H	-H	>25	>25	1.7 ± 0.2
111		-H	-H	>25	>25	4.3 ± 0.5
112		-H	-H	>25	>25	5.3 ± 0.02
113		-H	-H	>25	>25	>25
114		-H	-H	>25	>25	>25
115		-H	-H	>25	>25	>25

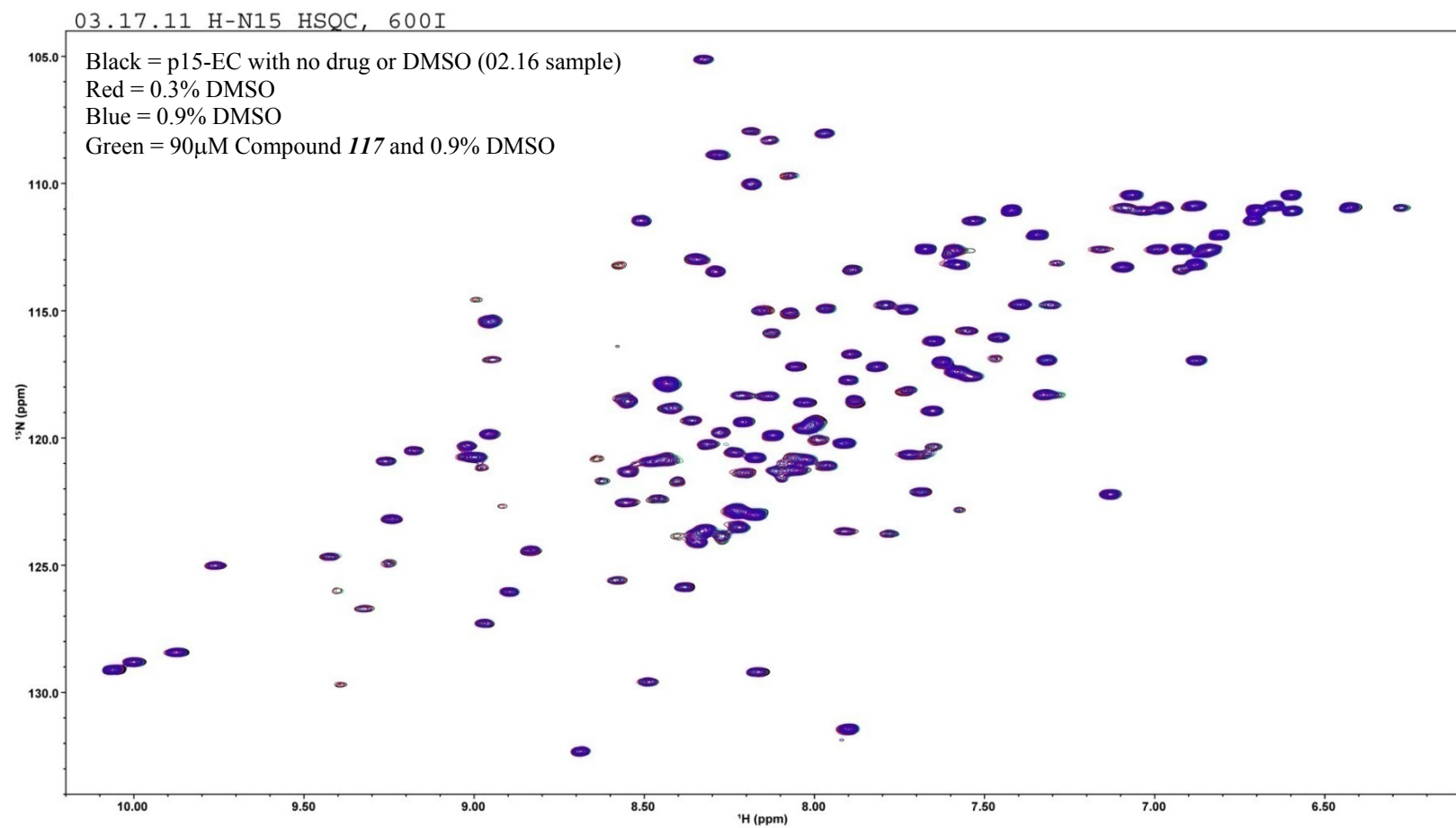
APPENDIX A

Supplementary Table 1 (continued)

116			-H	>25	>25	>25
117			-H	>25	5.7 ± 1.5	>25
118		-H	-H	>25	>25	>25

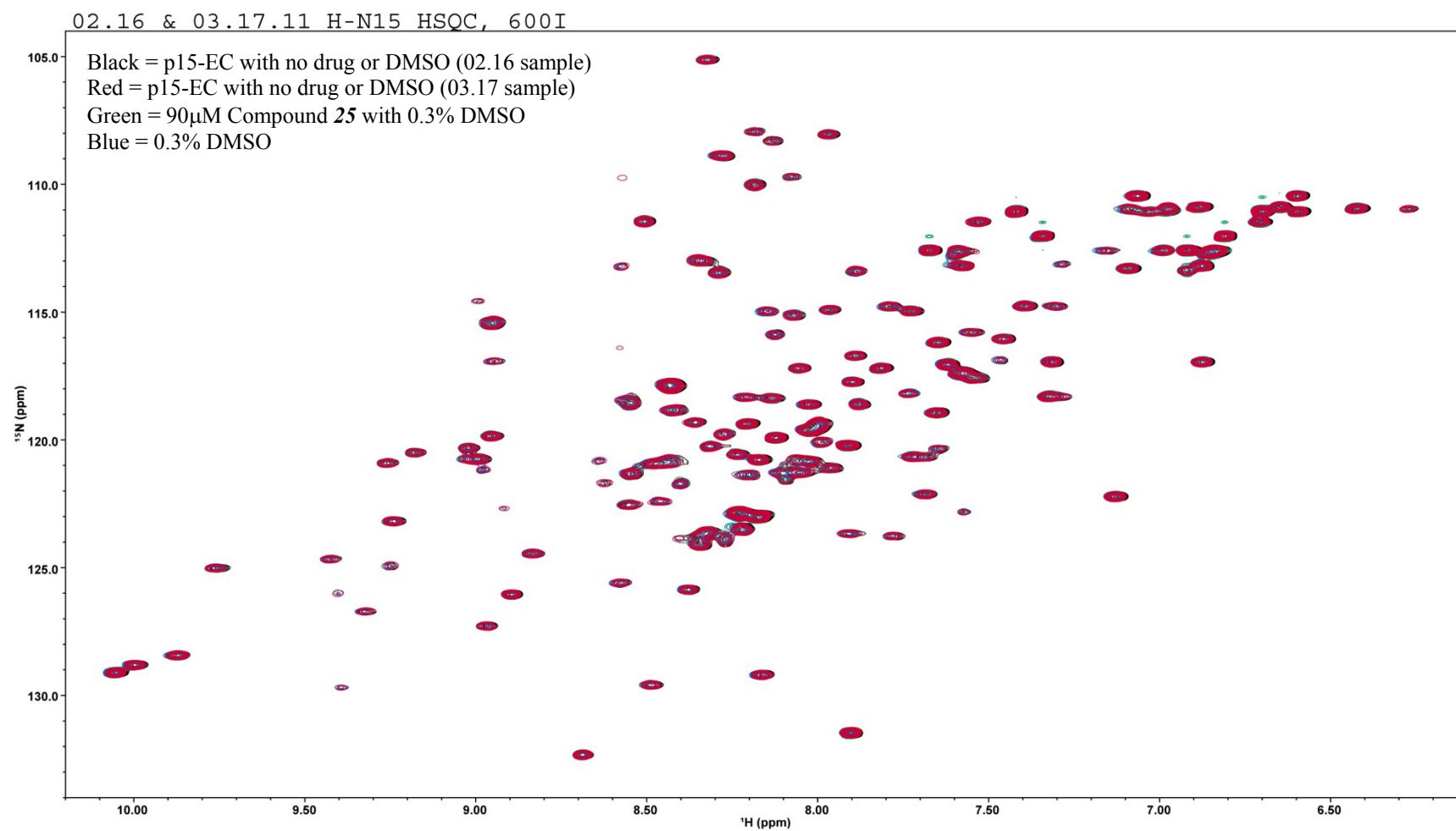
APPENDIX B

Supplementary Figure 1: Overlay of ^1H - ^{15}N HSQC of p15-EC RT RNH Domain Fragment with Compound *117* and DMSO Spectra



APPENDIX B

Supplementary Figure 2: Overlay of ^1H - ^{15}N HSQC p15-EC RT RNH Domain Fragment Compound 25 and DMSO Spectra



APPENDIX C

ABBREVIATIONS

AIDS - acquired immunodeficiency syndrome

AMV - alfalfa mosaic virus (or lucerne mosaic virus)

BBNH - *N*-(4-tert-Butylbenzoyl)-2-hydroxy-1-naphthaldehyde hydrazone

BTDBA - 4-[5-(Benzoylamino)thien-2-yl]-2,4-dioxobutanoic acid

CC₅₀ -half-maximal cytotoxicity concentration

CPHM - 4-chlorophenylhydrazone of mesoxalic acid

DDDP - DNA dependent DNA polymerase

DHBNH - dihydroxy benzoyl naphthyl hydrazone

DKA - diketo acids

dsDNA - double stranded DNA

dsRNA - double stranded RNA

E - enzyme is not pre-incubated

EC₅₀ - half-maximal effective concentration

EI - enzyme pre-incubated with an inhibitor

ES - enzyme pre-incubated with the RNA/DNA substrate

ESI - enzyme pre-incubated with RNA/DNA substrate and an inhibitor

HIV - human immunodeficiency virus

HSQC - heteronuclear single quantum coherence

HTS - high-throughput substrate (refer to *Table 2*, subsection 2.3.4)

IC₅₀ - half-maximal inhibitor concentration

IN - integrase

K_{cat} - catalytic rate of an enzyme

K_d - dissociation constant

K_m - Michaelis-Menton constant

APPENDIX C

ABBREVIATIONS (*continued*)

MLV - murine leukemia virus

NCME - 5-nitro-furan-2-carboxylic carbamoylmethyl ester

NEM - *N*-ethylmaleimide

NMR - nuclear magnetic resonance

NNRTI - non-nucleoside reverse transcriptase inhibitor

NNRTIBP - non-nucleoside reverse transcriptase inhibitor binding pocket

PBS - primer binding site

PDB - protein data bank

pol - polymerase

PR - protease

p15-EC - RT RNH domain fragment

p51 - 51 kDa subunit of HIV-1 reverse transcriptase

p66 - 66 kDa subunit of HIV-1 reverse transcriptase

RDDP - RNA dependent DNA polymerase

RFU - relative fluorescence units

RDS-1643 - 6-[1-(4-Fluorophenyl)methyl-1H-pyrrol-2-yl)]-2,4-dioxo-5-hexenoic acid ethyl ester

RNH - ribonuclease H domain

RNHI - ribonuclease H inhibitor

RT - reverse transcriptase

9-AN - photoactive analogue of nevirapine

BIBLIOGRAPHY

1. Abram, M.E. and Parniak M.A. 2005. Virion Instability of Human Immunodeficiency Virus Type 1 Reverse Transcriptase (RT) Mutated in the Protease Cleavage Site between RT p51 and the RT RNase H Domain. *J. Virol.* **79**:11952-11961.
2. Amacker, M. and Hubscher, U. 1998. Chimeric HIV-1 and feline immunodeficiency virus reverse transcriptases: critical role of the p51 subunit in the structural integrity of heterodimeric lentiviral DNA polymerases. *J. Mol. Biol.* **278**:757-765.
3. Arion, D., Sluis-Cremer, N., Min, K.L., Abram, M.E., Fletcher, R.S. and Parniak, M.A. 2002. Mutational analysis of Tyr-501 of HIV-1 reverse transcriptase. Effects on ribonuclease H activity and inhibition of this activity by *N*-acylhydrazones. *J. Biol. Chem.* **277**:1370-1374.
4. Arnold, E., Jacobo-Molina, A., Nanni, R.G., Williams, R.L., Lu, X., Ding, J., Clark Jr., A.D., Zhang, A., Ferris, A.L. and Clark, P. 1992. Structure of HIV-1 reverse transcriptase/DNA complex at 7 Å resolution showing active site locations. *Nature.* **357**:85-89.
5. Beilhartz, G.L., Wendeler, M., Baichoo, N., Rausch, J., Le Grice, S. and Matthias, G. 2009. HIV-1 Reverse Transcriptase Can Simultaneously Engage Its DNA/RNA Substrate at Both DNA Polymerase and RNase H Active Sites: Implications for RNase H Inhibition. *J. Mol. Biol.* **388**:462-474.
6. Bilamboz, M., Bailly, F., Barreca, M.L., De Luca, L., Mouscadet, J.F., Calmels, C., Andreola, M.L., Witvrouw, M., Christ, F., Debyser, Z. and Cotellet, P. 2008. Design, synthesis, and biological evaluation of a series of 2-hydroxyisoquinoline-1,3(2H,4H)-diones as dual inhibitors of human immunodeficiency virus type 1 integrase and the reverse transcriptase RNase H domain. *J. Med. Chem.* **51**:7717-7730.

7. Billamboz, M., Bailly, F., Lion, C., Touati, N., Vezin, H., Calmels, C., Androla, M-L., Christ, F., Debyser, Z. and Cotelle, P. 2011. Magnesium Chelating 2-Hydroxyisoquinoline-1,3(2H,4H)-diones, as Inhibitors of HIV-1 Integrase and/or the HIV-1 Reverse Transcriptase Ribonuclease H Domain: Discovery of a Novel Selective Inhibitor of the Ribonuclease H Function. *J. Med. Chem.* **54**:1812-1824.
8. Bokesch, H.R., Wamiru, A., Le Grice, S.F., Beutler, J.A., McKee, T.C. and McMahon, J.B. 2008. HIV-1 Ribonuclease H Inhibitory Phenolic Glycosides from *Eugenia hyemalis*. *J. Nat. Prod.* **7**:1634–1636.
9. Borkow, G., Fletcher, R.S., Barnard, J., Arion, D., Motakis, D., Dmitrienko, G.I. and Parniak, M.A. 1997. Inhibition of the Ribonuclease H and DNA Polymerase Activities of HIV-1 Reverse Transcriptase by N-(4-tert-Butylbenzoyl)-2-hydroxy-1-naphthaldehyde Hydrazone. *Biochem.* **36**:3179-3185.
10. Budihas, S.R., Gorshkova, I., Gaidamakov, S., Wamiru, A., Bona, M.K., Parniak, M.A., Crouch, R.J., McMahon, J.B., Beutler, J.A., and Le Grice, S.F.J. 2005. Selective inhibition of HIV-1 reverse transcriptase-associated ribonuclease H activity by hydroxylated tropolones. *Nucleic Acids Res.* **33**:1249-1256.
11. Cavanagh J., Fairbrother W.J., Palmer A.G.I. and Skelton N.J. 1996. Protein NMR Spectroscopy. San Diego: Academic Press.
12. Champoux, J.J. 1993. Roles of ribonuclease H in reverse transcription. In: Skalka, A.M., Goff, S.P. (Eds.), *Reverse Transcriptase*. Cold Spring Harbor Press, Plainview, New York, pp. 103–118.
13. Chattopadhyay, D., Evans, D.B., Deibel, M.R. Jr., Vosters, A.F., Eckenrode, F.M., Einspahr, H.M., Hui, J.O., Tomasselli, A.G., Zurcher-Neely, H.A. and Heinrikson, R.L. 1992. Purification and characterization of heterodimeric human immunodeficiency virus type 1 (HIV-1) reverse transcriptase produced by in vitro processing of p66 with recombinant HIV-1 protease. *J. Biol. Chem.* **267**:14227–14232.
14. Cirino, N.M., Cameron, C.E., Smith, J.S., Rausch, J.W., Roth, M.J., Benkovic, S.J., and Le Grice, S.F. 1995. Divalent cation modulation of the ribonuclease functions of human immunodeficiency virus reverse transcriptase. *Biochemistry.* **34**:9936–9943.

15. Chung, S., Wendeler, M., Rausch, J.W., Beilhartz, G., Gotte, M., O'Keefe, B.R., Bermingham, A., Beutler, J.A., Liu, S., Zhuang, X. and Le Grice, S.F.J. 2010. Structure-Activity Analysis of Vinylogous Urea Inhibitors of Human Immunodeficiency Virus-Encoded Ribonuclease H. *Antimicrobial Agents and Chemotherapy*. **54**:3913-3921.
16. Davies, J.F., Hostomska, Z., Hostomsky, Z., Jordan, S.R., and Matthews, D.A. 1991. Crystal Structure of the Ribonuclease H Domain of HIV- I Reverse Transcriptase. *Science*. **252**:88-95.
17. Davis, W.R., Tomsho, J., Nikam, S., Cook, E.M., Somand, D. and Peliska, J.A. 2000. Inhibition of HIV-1 Reverse Transcriptase-Catalyzed DNA Strand Transfer Reactions by 4-Chlorophenylhydrazones of Mesoxalic Acid. *Biochem*. **39**:14279-14291.
18. Delaglio F., Grzesiek S., Vuister G.W., Zhu G., Pfeifer J. and Bax A. 1995. Nmrpipe - a multidimensional spectral processing system based on unix pipes. *J Biomol NMR* **6**:277–293.
19. DeStefano, J.J., Buiser, R.G., Mallaber, L.M., Bambara, R.A. and Fay, P.J. 1991. Human immunodeficiency virus reverse transcriptase displays a partially processive 3- to 5-endonuclease activity. *J. Biol. Chem*. **266**:24295–24301.
20. DeStefano, J.J., Mallaber, L.M., Fay, P.J. and Bambara, R.A. 1993. Determinants of the RNase H cleavage specificity of human immunodeficiency virus reverse transcriptase. *Nucleic Acids Res*. **21**:4330–4338.
21. DeStefano, J.J., Mallaber, L.M., Fay, P.J. and Bambara, R.A. 1994. Quantitative analysis of RNA cleavage during RNA-directed DNA synthesis by human immunodeficiency and avian myeloblastosis virus reverse transcriptases. *Nucleic Acids Res*. **22**:3793–3800.
22. Evans, D.B., Brawn, K., Deibel Jr., M.R., Tarpley, W.G. and Sharma, S.K. 1991. A recombinant ribonuclease H domain of HIV-1 reverse transcriptase that is enzymatically active. *J. Biol. Chem*. **266**:20583–20585.
23. Fan, N., Rank, K.B., Leone, J.W., Heinrikson, R.L., Bannow, C.A., Smith, C.W., Evans, D.B., Poppe, S.M., Tarpley, W.G. and Rothrock, D.J. 1995. The differential processing of homodimers of reverse transcriptases from human immunodeficiency viruses type 1 and 2 is a consequence of the distinct specificities of the viral proteases. *J. Biol. Chem*. **270**:13573–13579.

24. Farnet, C.M., Wang, B., Lipford, J.R. and Bushman, F.D. 1996. Differential inhibition of HIV-1 preintegration complexes and purified integrase protein by small molecules. *Proc. Natl. Acad. Sci. USA* **93**:9742–9747.
25. Finston, W.I. and Champoux, J.J. 1984. RNA-primed initiation of Moloney murine leukemia virus plus strands by reverse transcriptase in vitro. *J. Virol.* **51**:26–33.
26. Fisher, A. G., Collalti, E., Ratner, L., Gallo, R. C. and Wong-Staal, F. 1985. A molecular clone of HTLV-III with biological activity. *Nature.* **316**:262-265.
27. Fletcher R.S., Holleschak G., Nagy E., Arion D., Borkow G., Gu Z., Wainberg M.A. and Parniak M.A. 1996. Single-step purification of recombinant wild-type and mutant HIV-1 reverse transcriptase. *Protein Expr Purif.* **7**:27–32.
28. Fuentes, G.M., Rodriguez-Rodriguez, L., Fay, P.J. and Bambara, R.A. 1995. Use of an oligoribonucleotide containing the polypurine tract sequence as a primer by HIV reverse transcriptase. *J. Biol. Chem.* **270**:28169–28176.
29. Fuji, H., Urano, E., Futahashi, Y., Hamatake, M., Tatsumi, J., Hoshino, T., Morikawa, Y., Yamamoto, N. and Komano, J. 2009. Derivatives of 5-nitro-furan-2-carboxylic acid carbamoylmethyl ester inhibit RNase H activity associated with HIV-1 reverse transcriptase. *J. Med. Chem.* **52**:1380-1387.
30. Furfine, E.S. and Reardon, J.E. 1991. Reverse transcriptase. RNase H from the human immunodeficiency virus. Relationship of the DNA polymerase and RNA hydrolysis activities. *J. Biol. Chem.* **266**:406–412.
31. Fu, T.B. and Taylor, J. 1992. When retroviral reverse transcriptases reach the end of their RNA templates. *J. Virol.* **66**:4271–4278.
32. Gabbara, S., Davis, W.R., Hupe, L., Hupe, D. and Peliska, J.A. 1999. Inhibitors of DNA Strand Transfer Reactions Catalyzed by HIV-1 Reverse Transcriptase. *Biochem.* **38**:13070-13076.
33. Gao, G., Orlova, M., Georgiadis, M.M., Hendrickson, W.A. and Goff, S.P. 1997. Conferring RNA polymerase activity to a DNA polymerase: a single residue in reverse transcriptase controls substrate selection. *Proc. Natl. Acad. Sci. U.S.A.* **94**:407–411.

34. Gao, G. and Goff, S.P. 1998. Replication defect of Moloney murine leukemia virus with a mutant reverse transcriptase that can incorporate ribonucleotides and deoxyribonucleotides. *J. Virol.* **72**:5905–5911.
35. Gong, Q., Menon, L., Ilina, T., Miller, L.G., Ahn, J., Parniak, M.A. and Ishima, R. 2011. Interaction of HIV-1 Reverse Transcriptase Ribonuclease H with an Acylhydrazide Inhibitor. *Chem. Biol. Drug. Des.* **77**:39-47.
36. Gopalakrishnan, V., Peliska, J.A., and Benkovic, S.J. 1992. Human immunodeficiency virus type 1 reverse transcriptase: spatial and temporal relationship between the polymerase and RNase H activities. *Proc. Natl. Acad. Sci. U.S.A.* **89**:10763–10767.
37. Gotte, M., Fackler, S., Hermann, T., Perola, E., Cellai, L., Gross, H.J., Le Grice, S.F., Heumann, H. (1995) HIV-1 reverse transcriptase-associated RNase H cleaves RNA/RNA in arrested complexes: implications for the mechanism by which RNase H discriminates between RNA/RNA and RNA/DNA. *EMBO J.* **14**:833–841.
38. Grobler, J. A., Stillmock, K., Hu, B., Witmer, M., Felock, P., Espeseth, A., Wolfe, A., Egbertson, M., Bourgeois, M., Melamed, J., Wai, J. S., Young, S., Vacca, J., and Hazuda, D. 2002. Diketo acid inhibitor mechanism and HIV-1 integrase: implications for metal binding in the active site of phosphotransferase enzymes. *Proc. Natl. Acad. Sci. U. S. A.* **99**:6661–6666.
39. Hafkemeyer, P., Neftel, K., Hobi, R., Pfaltz, A., Lutz, H., Luthi, K., Focher, F., Spadari, S. and Hubscher, U. 1991. HP 0.35, a cephalosporin degradation product is a specific inhibitor of lentiviral RNases H. *Nucleic Acids Research.* **19**:4059-4065.
40. Hang, J.Q., Rajendran, S., Yang, Y., Li, Y., Wong Kai In, P., Overton, H., Parkes, K.E.B., Cammack, N., Martin, J.A. and Klumpp, K. 2004. Activity of the isolated HIV RNase H domain and specific inhibition by *N*-hydroxyimides. *Biochem. Biophys. Res. Comm.* **317**:321-329.
41. Hazuda, D. J., Felock, P., Witmer, M., Wolfe, A., Stillmock, K., Grobler, J. A., Espeseth, A., Gabryelski, L., Schleif, W., Blau, C., and Miller, M. D. 2000. Inhibitors of strand transfer that prevent integration and inhibit HIV-1 replication in cells. *Science.* **287**:646–650.

42. Hazuda, D. J., Anthony, N.J., Gomez, R.P., Jolly, S.M., Wai, J.S., Zhuang, L., Fisher, T.E. , Embrey, M., Guare, Jr. J.P., Egbertson, M.S., Vacca, J.P., Huff, J.R., Felock, P.J., Witmer, M.V., Stillmock, K.A., Danovich, R., Grobler, J., Miller, M.D., Espeseth, A.S., Jin, L., Chen, I.W., Lin, J.H., Kassahun, K., Ellis, J.D., Wong, B.K., Xu, W., Pearson, P.G., Schleif, W.A., Cortese, R., Emini, E., Summa, V., Holloway, M.K. and Young, S.D. 2004. A naphthyridine carboxamide provides evidence for discordant resistance between mechanistically identical inhibitors of HIV-1 integrase. *Proc. Natl. Acad. Sci. U. S. A.* **101**:11233–11238.

43. Himmel, D.M., Sarafianos, S.G., Dharmasena, S., Hossain, M.M., McCoy-Simandle, K., Ilna, T., Clark, A.D. Jr., Knight, J.L., Julias, J.G., Clark, P.K., Krogh-Jespersen, K., Levy, R.M., Hughes, S.H., Parniak, M.A. and Arnold, E. 2006. HIV-1 Reverse Transcriptase Structure with RNase H Inhibitor Dihydroxy Benzoyl Naphthyl Hydrazone Bound at a Novel Site. *ACS Chem. Biol.* **1**:702-712.

44. Himmel, D.M., Meagley, K.A., Pauly, T.A., Bauman, J.D., Das, K., Dharia, C., Clark, A.D. Jr., Ryan, K., Hickey, M.J., Love, R.A., Hughes, S.H., Bergqvist, S. and Arnold, E. 2009. Structure of HIV-1 Reverse Transcriptase with the Inhibitor β -Thujaplicinol Bound at the RNase H Active Site. *Structure.* **17**:1625-1635.

45. Hnatyszyn, O., Broussalis, A., Herrera, G., Muschietti, L., Coussio, J., Martino, V., Ferraro, G., Font, M., Monge, A., Marti nez-Irujo, J., Sanroma, M., Cuevas, M.T., Santiago, E. and Lasarte, J.J. 1999. Argentine Plant Extracts Active Against Polymerase and Ribonuclease H Activities of HIV-1 Reverse Transcriptase. *Phyther. Res.* **13**:206-209.

46. Hostomska, Z., D., Matthews, A., Davies, J.F., Nodes, B.R. and Hostomsky, Z. 1991. Proteolytic release and crystallization of the RNase H domain of human immunodeficiency virus type 1 reverse transcriptase. *J. Biol. Chem.* **266**:14697–14702.

47. Hostomsky, Z., Hostomska, Z., Hudson, G.O., Moomaw, E.W. and Nodes, B.R. 1991. Reconstitution in vitro of RNase H activity by using purified *N*-terminal and *C*-terminal domains of human immunodeficiency virus type 1 reverse transcriptase. *Proc. Natl. Acad. Sci. U.S.A.* **88**:1148–1152.

48. Huang, H., Chopra, R., Verdine, G.L. and Harrison, S.C. 1998. Structure of a covalently trapped catalytic complex of HIV-1 reverse transcriptase: implications for drug resistance. *Science.* **282**:1669–1675.

49. Jacobo-Molina, A., Ding, J., Nanni, R.G., Clark Jr., A.D., Lu, X., Tantillo, C., Williams, R.L., Kamer, G., Ferris, A.L., Clark, P., Hizi, A., Hughes, S.H. and Arnold, E. 1993. Crystal structure of human immunodeficiency virus type 1 reverse transcriptase complexed with double-stranded DNA at 3.0 Å resolution shows bent DNA. *Proc. Natl. Acad. Sci. U.S.A.* **90**:6320–6324.
50. Johnson B.A. 2004. Using NMRView to visualize and analyze the NMR spectra of macromolecules. *Methods Mol Biol.* **278**: 313–352.
51. Julias, J.G., McWilliams, M.J., Sarafianos, S.G., Arnold, E. and Hughes, S.H. 2002. Mutations in the RNase H domain of HIV-1 reverse transcriptase affect the initiation of DNA synthesis and the specificity of RNase H cleavage in vivo. *Proc. Natl. Acad. Sci. U.S.A.* **99**:9515–9520.
52. Julias, J.G., McWilliams, M.J., Sarafianos, S.G., Alvord, W.G., Arnold, E. and Hughes, S.H. 2003. Mutation of amino acids in the connection domain of human immunodeficiency virus type 1 reverse transcriptase that contact the template-primer affects RNase H activity. *J. Virol.* **77**:8548–8554.
53. Kati, W.M., Johnson, K.A., Jerva, L.F. and Anderson, K.S. 1992. Mechanism and fidelity of HIV reverse transcriptase. *J. Biol. Chem.* **267**:25988–25997.
54. Keck, J.L. and Marqusee, S. 1995. Substitution of a highly basic helix/loop sequence into the RNase H domain of human immunodeficiency virus reverse transcriptase restores its Mn(2+)-dependent RNase H activity. *Proc. Natl. Acad. Sci. U.S.A.* **92**:2740–2744.
55. Kharlamova, T., Esposito, F., Zinzula, L., Floris, G., Cheng, Y.-C., Dutschman, G.E., and Tramontano, E. 2009. Inhibition of HIV-1 ribonuclease H activity by novel frangula-emodine derivatives. *Med. Chem.* **5**: 398–410.
56. Kirschberg, T.A., Balakrishnan, M., Squires, N.H., Barnes, T., Brendza, K.M., Chen, X., Eisenberg, E.J., Jin, W., Kutty, N., Leavitt, S., Liclican, A., Liu, Q., Liu X., Mak, J., Perry, J.K., Wang, M., Watkins, W.J. and Lansdon, E.B. 2009. RNase H Active Site Inhibitors of Human Immunodeficiency Virus Type 1 Reverse Transcriptase: Design, Biochemical Activity, and Structural Information. *J. Med. Chem. Lett.* **52**:5781-5784.

57. Klumpp, K., Hang, J.Q., Rajendran, S., Yang, Y., Derosier, A., Wong Kai In, P., Overton, H., Parkes, K.E.B., Cammack, N. and Martin, J.A. 2003. Two-metal ion mechanism of RNA cleavage by HIV RNase H and mechanism-based design of selective HIV RNase H inhibitors. *Nucleic Acids Research*. **31**:6852-6859.
58. Kohlstaedt, L.A., Wang, J., Friedman, J.M., Rice, P.A. and Steitz, T.A. 1992. Crystal structure at 3.5 Å resolution of HIV-1 reverse transcriptase complexed with an inhibitor. *Science*. **256**:1783–1790.
59. Krug, M.S. and Berger, S.L. 1989. Ribonuclease H activities associated with viral reverse transcriptases are endonucleases. *Proc. Natl. Acad. Sci. U.S.A.* **86**:3539–3543.
60. Le Grice S.F. and Gruninger-Leitch F. 1990. Rapid purification of homodimer and heterodimer HIV-1 reverse transcriptase by metal chelate affinity chromatography. *Eur J Biochem*. **187**:307–314.
61. Lim, D., Gregorio, G.G., Bingman, C., Martinez-Hackert, E., Hendrickson, W.A. and Goff, S.P. 2006. Crystal structure of the Moloney murine leukemia virus RNase H domain. *J. Virol*. **80**:8379–8389.
62. Loya, S., Tal, R., Kashman, Y. and Hizi, A. 1990. Illimaquinone, a Selective Inhibitor of the RNase H Activity of Human Immunodeficiency Virus Type 1 Reverse Transcriptase. *Antimicrobial agents and chemotherapy*. **34**:2009-2012.
63. Loya, S. and Hizi, A. 1993. The Interaction of Illimaquinone, a Selective Inhibitor of the RNase H Activity, with the Reverse Transcriptase of Human Immunodeficiency and Murine Leukemia Retroviruses. *J. Biol. Chem*. **268**:9323-9328.
64. Loya, S., Gao, H.Q., Avidan, O., Boyer, P.L., Hughes, S.H. and Hizi, A. 1997. Subunit-Specific Mutagenesis of the Cysteine 280 Residue of the Reverse Transcriptase of Human Immunodeficiency Virus Type 1: Effects on Sensitivity to a Specific Inhibitor of the RNase H Activity. *J. Virol*. **71**:5668-5672.
65. Marchand, C., Beutler, J.A., Wamiru, A., Budihas, S., Ilmann, U.M., Heinisch, L., Mellors, J.W., Le Grice, S.F. and Pommier, Y. 2008. Madurahydroxylactone Derivatives as Dual Inhibitors of Human Immunodeficiency Virus Type 1 Integrase and RNase H. *Antimicrobial agents and chemotherapy*. **52**:361-364.

66. McWilliams, M.J., Julias, J.G., Sarafianos, S.G., Alvord, W.G., Arnold, E. and Hughes, S.H. 2006. Combining mutations in HIV-1 reverse transcriptase with mutations in the HIV-1 polypurine tract affects RNase H cleavages involved in PPT utilization. *Virology*. **348**:378–388.
67. Min, B.S., Nakamura, N., Miyashiro, H., Kim, Y-H. and Hattori, M. 2000. Inhibition of Human Immunodeficiency Virus Type 1 Reverse Transcriptase and Ribonuclease H Activities by Constituents of *Juglans mandshurica*. *Chem. Pharm. Bull.* **48**:194-200.
68. Mohan, P., Loya, S., Avidan, O., Verma, S., Dhindsa, G.S., Wong, M.F., Huang, P.P., Yashiro, M., Baba, M. and Hizil, A. 1994. Synthesis of Naphthalenesulfonic Acid Small Molecules as Selective Inhibitors of the DNA Polymerase and Ribonuclease H Activities of HIV-1 Reverse Transcriptase. *J. Med Chem.* **37**:2513-2519.
69. Munk, C., Brandt, S. M., Lucero, G., and Landau, N. R. 2002. A dominant block to HIV-1 replication at reverse transcription in simian cells. *Proc. Natl. Acad. Sci. U. S.A.* **99**:13843-13848.
70. Nowotny M., Gaidamakov, S.A., Crouch, R.J. and Yang W. 2005. Crystal Structures of RNase H Bound to an RNA/DNA Hybrid: Substrate Specificity and Metal-Dependent Catalysis. *Cell*. **121**:1005-1016.
71. Palaniappan, C., Fuentes, G.M., Rodriguez-Rodriguez, L., Fay, P.J. and Bambara, R.A. 1996. Helix structure and ends of RNA/DNA hybrids direct the cleavage specificity of HIV-1 reverse transcriptase RNase H. *J. Biol. Chem.* **271**:2063–2070.
72. Rausch, J.W., Lener, D., Miller, J.T., Julias, J.G., Hughes, S.H. and Le Grice, S.F. 2002. Altering the RNase H primer grip of human immunodeficiency virus reverse transcriptase modifies cleavage specificity. *Biochemistry*. **41**:4856–4865.
73. Restle, T., Muller, B. and Goody, R.S. 1990. Dimerization of human immunodeficiency virus type 1 reverse transcriptase. A target for chemotherapeutic intervention. *J. Biol. Chem.* **265**:8986–8988.
74. Richter, S.N., Frasson, I. and Palu, G. 2009. Strategies for Inhibiting Function of HIV-1 Accessory Proteins: A Necessary Route to AIDS Therapy? *Curr. Med. Chem.* **16**:267-286.

75. Sarafianos, S.G., Das, K., Tantillo, C., Clark Jr., A.D., Ding, J., Whitcomb, J.M., Boyer, P.L., Hughes, S.H. and Arnold, E. 2001. Crystal structure of HIV-1 reverse transcriptase in complex with a polypurine tract RNA:DNA. *EMBO J.* **20**:1449–1461.
76. Sarafianos, S.G., Marchand, B., Das, K., Himmel, D.H., Parniak, M.A., Hughes, S.H. and Arnold, E. 2009. Structure and Function of HIV-1 Reverse Transcriptase: Molecular Mechanism of Polymerization Inhibition. *J. Mol. Biol.* **385**:693-713.
77. Schatz, O., Mous, J. and Le Grice, S.F. 1990. HIV-1 RT-associated ribonuclease H displays both endonuclease and 3' - 5'-exonuclease activity. *EMBO J.* **9**:1171–1176.
78. Schultz, S.J., Zhang, M., Kelleher, C.D. and Champoux, J.J. 2000. Analysis of plus-strand primer selection, removal, and reutilization by retroviral reverse transcriptases. *J. Biol. Chem.* **275**:32299–32309.
79. Schultz, S.J., Zhang, M. and Champoux, J.J. 2003. Specific cleavages by RNase H facilitate initiation of plus-strand RNA synthesis by Moloney murine leukemia virus. *J. Virol.* **77**:5275–5285.
80. Schultz, S.J., Zhang, M. and Champoux, J.J. 2004. Recognition of internal cleavage sites by retroviral RNases H. *J. Mol. Biol.* **344**:635–652.
81. Schultz, S.J., Zhang, M. and Champoux, J.J. 2006. Sequence, distance, and accessibility are determinants of 5'-end-directed cleavages by retroviral RNases H. *J. Biol. Chem.* **281**:1943–1955.
82. Schultz, S.J. and Champoux, J.J. 2008. RNase H activity: Structure, specificity, and function in reverse transcription. *Virus. Res.* **134**:86-103.
83. Shaw-Reid, C.A., Munshi, V., Graham, P., Wolfe, A., Witmer, M., Danzeisen, R., Olsen, D.B., Carroll, S.S., Embrey, M., Wai, J.S., Miller, M.D., Cole, J.L. and Hazuda, D.J. 2003. Inhibition of HIV-1 Ribonuclease H by a Novel Diketo Acid, 4-[5-(Benzoylamino)thien-2-yl]-2,4-dioxobutanoic Acid. *J. Biol. Chem.* **278**: 2777:2780.
84. Sluis-Cremer, N., Arion, D. and Parniak, M.A. 2002. Destabilization of the HIV-1 Reverse Transcriptase dimer upon interaction with N-acyl hydrazone inhibitors. *Mol. Pharmacol.* **62**:398-405.

85. Smith, C.M., Potts III, W.B., Smith, J.S. and Roth, M.J. 1997. RNase H cleavage of tRNA_{Pro} mediated by M-MuLV and HIV-1 reverse transcriptases. *Virology*. **229**:437–446.
86. Smith, C.M., Leon, O., Smith, J.S. and Roth, M.J. 1998. Sequence requirements for removal of tRNA by an isolated human immunodeficiency virus type 1 RNase H domain. *J. Virol.* **72**:6805–6812.
87. Smith, J.S. and Roth, M.J. 1992. Specificity of human immunodeficiency virus-1 reverse transcriptase-associated ribonuclease H in removal of the minus strand primer, tRNA(Lys3). *J. Biol. Chem.* **267**:15071–15079.
88. Smith, J.S., Gritsman, K. and Roth, M.J. 1994. Contributions of DNA polymerase subdomains to the RNase H activity of human immunodeficiency virus type 1 reverse transcriptase. *J. Virol.* **68**:5721–5729.
89. Stahl, S.J., Kaufman, J.D., Vikic-Topic, S., Crouch, R.J. and Wingfield, P.T. 1994. Construction of an enzymatically active ribonuclease H domain of human immunodeficiency virus type 1 reverse transcriptase. *Protein Eng.* **7**:1103–1108.
90. Su, H.-P., Yan, Y., Prasad, S., Smith, R.F., Daniels, C.L., Abeywickrema, P.D., Reid, J.C., Loughran, H.M., Kornienko, M., Sharma, S., Grobler, J.A., Xu, B., Sardana, V., Allison, T.J., Williams, P.D., Darke, P.L., Hazuda, D.J. and Munshi, S. 2010. Structural Basis for the Inhibition of RNase H Activity of HIV-1 Reverse Transcriptase by RNase H Active Site-Directed Inhibitors. *J. Virol.* **84**:7625-7633.
91. Suo, Z. and Johnson, K.A. 1997. Effect of RNA secondary structure on the kinetics of DNA synthesis catalyzed by HIV-1 reverse transcriptase. *Biochemistry*. **36**:12459–12467.
92. Suo, Z. and Johnson, K.A. 1997. Effect of RNA secondary structure on RNA cleavage catalyzed by HIV-1 reverse transcriptase. *Biochemistry*. **36**:12468–12476.
93. Takada, K., Bermingham, A., O'Keefe, B.R., Warmiru, A., Beutler, J.A., Le Grice, S.F., Lloyd, J., Gustafson, K.R. and McMahon, J.B. 2007. An HIV RNase H Inhibitory 1,3,4,5-Tetragalloylapiitol from the African Plant *Hylodendron gabunensis*. *J. Nat. Prod.* **70**:1647-1649.

94. Tien Dat, N., Bae, K., Wamiru, A., McMahon, J.B., Le Grice, S.F., Bona, M., Beutler, J.A. and Kim, Y.H. 2007. A Dimeric Lactone from *Ardisia japonica* with Inhibitory Activity for HIV-1 and HIV-2 Ribonuclease H. *J. Nat. Prod.* **70**:839-841.

95. Tisdale, M., Schulze, T., Larder, B.A. and Moelling, K. 1991. Mutations within the RNase H domain of human immunodeficiency virus type 1 reverse transcriptase abolish virus infectivity. *J. Gen Virol.* **72**:59-66.

96. Tomasselli, A. G., Sarcich, J.L., Barrett, L.J., Reardon, I.M., Howe, W.J., Evans, D.B., Sharma, S.K. and Heinrikson, R.L. 1993. Human immunodeficiency virus type-1 reverse transcriptase and ribonuclease H as substrates of the viral protease. *Protein Sci.* **2**:2167–2176.

97. Tramontano, E., Esposito, F., Badasa, R., Di Santob, R., Costib, R. and La Collaa, P. 2005. 6-[1-(4-Fluorophenyl)methyl-1H-pyrrol-2-yl]-2,4-dioxo-5-hexenoic acid ethyl ester a novel diketo acid derivative which selectively inhibits the HIV-1 viral replication in cell culture and the ribonuclease H activity in vitro. *Antiv. Res.* **65**:117-124.

98. UNAIDS. Report on the global AIDS epidemic, Joint United Nations Programme on AIDS. <http://www.unaids.org>. 2008.

99. Wendeler, M., Lee, H-F., Bermingham, A., Miller, J.T., Chertov, O., Bona, M.K., Baichoo, N.S., Ehteshami, M., Beutler, J., O'Keefe, B.R., Gotte, M., Kvaratskhelia, M. and Le Grice, S. 2008. Vinylogous Ureas as a Novel Class of Inhibitors of Reverse Transcriptase-Associated Ribonuclease H *Activity*. *ACS Chem. Biol.* **3**:635-644.

100. Williams, P.D., Staas, D.D., Venkatraman, S., Loughran, H.M., Ruzek, R.D., Booth, T.M., Lyle, T.A., Wai, J.S., Vacca, J.P., Feuston, B.P., Ecto, L.T., Flynn, J.A., DiStefano, D.J., Hazuda, D.J., Bahnck, C.M., Himmelberger, A.L., Dornadula, G., Hrin, R.C., Stillmock, K.A., Witmer, M.V., Miller, M.D. and Grobler, J.A. 2010. Potent and selective HIV-1 ribonuclease H inhibitors based on a 1-hydroxy-1,8-naphthyridin-2(1H)-one scaffold. *Bioorganic & Med. Chem. Lett.* **20**:6754-6757.

101. Wohrl, B.M. and Molling, K. 1990. Interaction of HIV-1 ribonuclease H with polypurine tract containing RNA–DNA hybrids. *Biochemistry*. **29**:10141–10147.
102. Yanagita, H., Urano, E., Matsumoto, K., Ichikawa, R., Takaesu, Y., Ogata, M., Murakami, T., Wu, H., Chiba, J., Komano, J. and Hoshino, T. 2011. Structural and biochemical study on the inhibitory activity of derivatives of 5-nitro-furan-2-carboxylic acid for RNase H function of HIV-1 reverse transcriptase. *Bioorgo. & Med. Chem.* **19**:816-825.
103. Yang, W. 2008. An equivalent metal ion in one- and two-metal-ion catalysis. *Nature Struct. Mol. Biol.* **15**:1228–1231.
104. Zhang, W.H., Svarovskaia, E.S., Barr, R. and Pathak, V.K. 2002. Y586F mutation in murine leukemia virus reverse transcriptase decreases fidelity of DNA synthesis in regions associated with adenine- thymine tracts. *Proc. Natl. Acad. Sci. U.S.A.* **99**:10090–10095.